The role of Apelin signaling and endocardial protrusions during cardiac development in zebrafish

---

Dissertation

zur Erlangung des Doktorgrades

der Naturwissenschaften

vorgelegt beim Fachbereich 15

der Johann Wolfgang Goethe-Universität

in Frankfurt am Main

von

Jialing Qi

aus Jiangsu, China

Frankfurt 2023

(D30)

vom Fachbereich Biowissenschaften (FB15) der Johann Wolfgang Goethe - Universität als Dissertation angenommen.

Dekan: Prof. Dr. Sven Klimpel

Gutachter: Prof. Dr. Didier Y. R. Stainier

Prof. Dr. Virginie Lecaudey

Datum der Disputation:

Supervisors

Prof. Dr. Didier Y. R. Stainier, Ph.D.

Department of Developmental Genetics

Max Planck Institute for Heart and Lung Research

Bad Nauheim, Germany

&

Prof. Dr. Christian S. M. Helker, Ph.D.

Faculty of Biology, Cell Signaling and Dynamics

Philipps-University Marburg

Marburg, Germany

Reviewers

Prof. Dr. Didier Y. R. Stainier, Ph.D.

Department of Developmental Genetics

Max Planck Institute for Heart and Lung Research

Bad Nauheim, Germany

&

Prof. Dr. Virginie Lecaudey, Ph.D.

Department of Developmental Biology of Vertebrates

Institute of Cell biology and Neuroscience

Johann Wolfgang Goethe University

Frankfurt am Main, Germany

Erklärung

Ich erkläre hiermit, dass ich mich bisher keiner Doktorprüfung im Mathematisch-Naturwissenschaftlichen Bereich unterzogen habe.

Frankfurt am Main, den .....

(Unterschrift)

Versicherung

Ich erkläre hiermit, dass ich die vorgelegte Dissertation über

The role of Apelin signaling and endocardial protrusions during cardiac development in zebrafish

selbständig angefertigt und mich anderer Hilfsmittel als der in ihr angegebenen nicht bedient habe, insbesondere, dass alle Entlehnungen aus anderen Schriften mit Angabe der betreffenden Schrift gekennzeichnet sind.
Ich versichere, die Grundsätze der guten wissenschaftlichen Praxis beachtet, und nicht die Hilfe einer kommerziellen Promotionsvermittlung in Anspruch genommen zu haben.

Einen Teil der vorliegende Ergebnisse der Arbeit sind in folgendem Publikationsorgan veröffentlicht:

Jialing Qi, et al. eLife 2022; 11: e73231. DOI: https://doi.org/10.7554/eLife.73231. Apelin signaling dependent endocardial protrusions promote cardiac trabeculation in zebrafish.

Frankfurt am Main, den .....

(Unterschrift)

- *If you're wrong, admit it.*
- *If you're confused, ask questions.*
- *If you're stuck, seek for help.*
- *If you make mistake, learn from it.*
- *If you learn something, teach others.*

Table of Contents

Abstract

During cardiac development, cardiomyocytes (CMs) are delaminated from the compact muscle wall to increase the muscle mass of the heart. This process is also known as cardiac trabeculation. It has been shown that growth factors produced by endocardial cells (EdCs) are required for myocardial morphogenesis and growth. In particular, Neuregulin produced by EdCs promotes myocardial trabeculation. The deficiency of Neuregulin signaling leads to hypotrabeculation. Endocardial protrusions project from the endocardium to the myocardium are also essential for the trabeculae onset. Yet current studies only introduce the function of endocardial sprouts descriptively. This article first reports the mechanisms of endocardial sprouting during myocardial trabeculation. By living imaging, we first demonstrate that EdCs interact with CMs through membrane protrusions in zebrafish embryos. More interestingly, these protrusions stay in close contact with their target CMs in spite of the cardiac contraction. We utilize loss-of-function strategies to report the importance of myocardial *apelin*, which induces endocardial protrusion formation. Zebrafish lacking Apelin signaling exhibit defects in endocardial protrusion formation as well as excessive deposition of cardiac jelly and hypotrabeculation. Notably, we also present data that blocking protrusion formation in endocardial cells phenocopies the trabeculation defects in *apelin* mutants. Mechanistically, endocardial-derived Neuregulin requires Apelin signaling mediated endocardial protrusions, and Neuregulin dependent pERK expression is attenuated in the condition of reduced endocardial protrusion formation. Together, our data suggest that endocardial-myocardial communication through endocardial protrusions acts as an underlying principle allowing myocardial growth.

Abbreviations

Commonly used abbreviations in the thesis

Abbreviation	Description
A	Atrium
apln	Apelin
aplnra	Apelin receptor a
aplnrb	Apelin receptor b
ASP	Air sac primodium
AVC	Atrio-ventricular canal
BFP	Blue fluorescent protein
BSA	Bovine serum albumin
CDC42	Cell division control protein 42 homolog
cdh5	Cadherin 5
cDNA	Complementary DNA
CJ	Cardiac jelly
CL	Compact layer
CM(s)	Cardiomyocyte(s)
CVD(s)	Cardiovascular disease(s)
daf	Days after fertilization
de CMs	Delaminating cardiomyocytes
DMSO	Dimethyl sulfoxide
DNA	Deoxyribonucleic acid
dpf	Days post fertilization
Dpp	Decapentaplegic
E.Coli	Escherichia coli
EC(s)	Endothelial cell(s)
ECM	Extra cellular matrix

Abbreviations

EdC(s)	Endocardial cell(s)
EdU	5-ethynyl-2´-deoxyuridine
EGF	Epidermal growth factor
EGFP	Enhanced green fluorescent protein
ErbB	Receptor tyrosine kinase ErbB
Erk	Extracellular signal-related kinase
F-actin	Filamentous actin
FGF	Fibroblast growth factor
Gal4	Gal4 transcription factor
gDNA	Genomic DNA
GFP	Green fluorescent protein
GPCR	Orphan G protein-couple receptor
hpf	Hours post fertilization
HRMA	High resolution melt analysis
irsp53	Insulin receptor substrate p53
ISV	Intersegmental vessel
kdrl	Kinase insert domain receptor like
KTR	Kinase translocation reporter
mRNA	Messenger RNA
myl7	Myosin light chain 7
Nrg	Neuregulin
p2a	2A self-cleaving peptides
PBS	Phosphated-buffer saline
PCR	Polymerase chain reaction
PFA	Paraformaldehyde
RFP	Red fluorescent protein
RNA	Ribonucleic acid
SEM	Standard error of mean

Abbreviations

TBE	Tris-borate-EDTA
Tg	Transgenic line
TL CMs	Trabecular layer CMs
UAS	Upstream activation sequence
V	Ventricle
WT	Wild type

1 Introduction

This thesis focuses on the early steps of cardiac development – the formation of endocardial protrusion, myocardial trabeculation, and some key signaling pathways contributing to these two steps.

The introduction provides an overview on the heart development in different species, and the crosstalk between EdCs and CMs.

1.1 The cardiovascular system

The cardiovascular system is one of the first organ systems that functions in the vertebrate embryo, and it consists of the heart, blood, and blood vessels. The heart is a muscular engine device that constantly pumps blood. The blood, a body fluid that transports oxygen, nutrients, hormones, and waste products, is carried by blood vessels to the various organs. A crucial role of the cardiovascular system is to maintain the body's homeostasis, and numerous mechanisms are involved in this maintenance. Cardiovascular disease (CVD) is a class of disorders of the cardiovascular system and is the leading cause of death globally. There are many risk factors of CVDs, including genetics.

1.2 Heart development in vertebrates

1.2.1 Human heart development

Introduction

The human heart has four chambers- two atria that collect the blood into the heart and two ventricles that receive the blood from the atria and then expel it to other organs in the body. The heart does not develop from a tiny four-chambered structure, but rather an intricate process of heart maturation takes place. The cardiovascular system arises from the mesoderm and the heart starts to develop in a region called the cardiogenic area (Figure 1A). About 21 days after fertilization (daf), two endocardial tubes fused to form a primitive heart tube (Figure 1B-1C). Blood is collected by the primitive atrium and pumped out of the heart by the primitive ventricle (Figure 1D). Around 23 daf, the primitive heart tube begins to fold and twist, which is known as cardiac looping (Figure 1E). The alignment of cardiac chambers resembles that of the adult heart at 35 daf (Figure 1G). Towards the end of 4^{th} week, the single atrium and single ventricle gradually start to septate and it eventually forms the final four-chambered organ at 8^{th} week (Figure 1H-1I). The heart wall contains of three layers: the epicardium is the outer layer, the myocardium is in the middle, and the endocardium is the inner layer (Figure 1I).

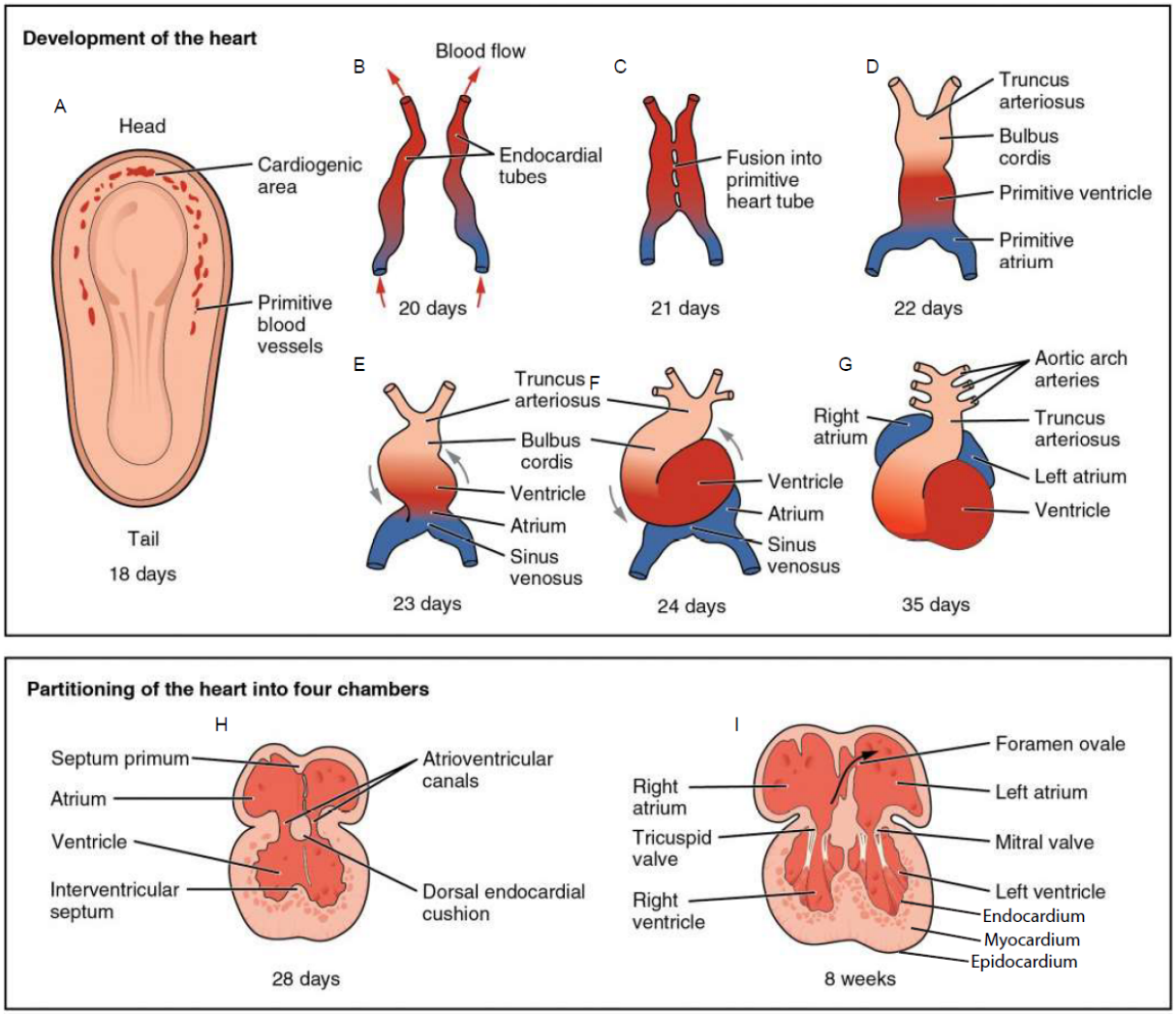

Figure 1. Human heart development during the first eight weeks.

Figure adapted from Betts et al., 2013. https://openstax.org/books/anatomy-and-physiology/pages/19-5-development-of-the-heart

1.2.2 Mouse heart development

The development of the mouse heart is similar to that of the human heart. A four-chambered heart is developed from a linear heart tube after a series of

developmental processes, such as cardiac looping and chamber formation (Epstein et al., 2015).

1.2.3 Zebrafish heart development

Unlike humans and mice, zebrafish have only one bicameral heart, one ventricle and one atrium. During the development of zebrafish heart, there are heart tube stage, and the stages of cardiac looping and cardiac chamber formation. In zebrafish, the CM progenitors migrate to the midline and form a heart disc at 22 hours post fertilization (hpf) (Figure 2A-2B). A contracting heart tube can be observed at around 24 hpf (Figure 2C). Cardiac looping, a process that allows cardiac chambers to align properly, begins at around 28 hpf (Figure 2D). At 48 hpf, the looped heart is divided by the atrio-ventricular canal (AVC) into a heart with two chambers. The immature heart consists of the inflow tract sinus venosus, atrium, ventricle, and outflow tract bulbous arteriosus. Compared to other animal models such as mouse and chick, zebrafish is an ideal model for studying heart development because its transparency allows imaging with single-cell resolution and high-speed of the beating heart.

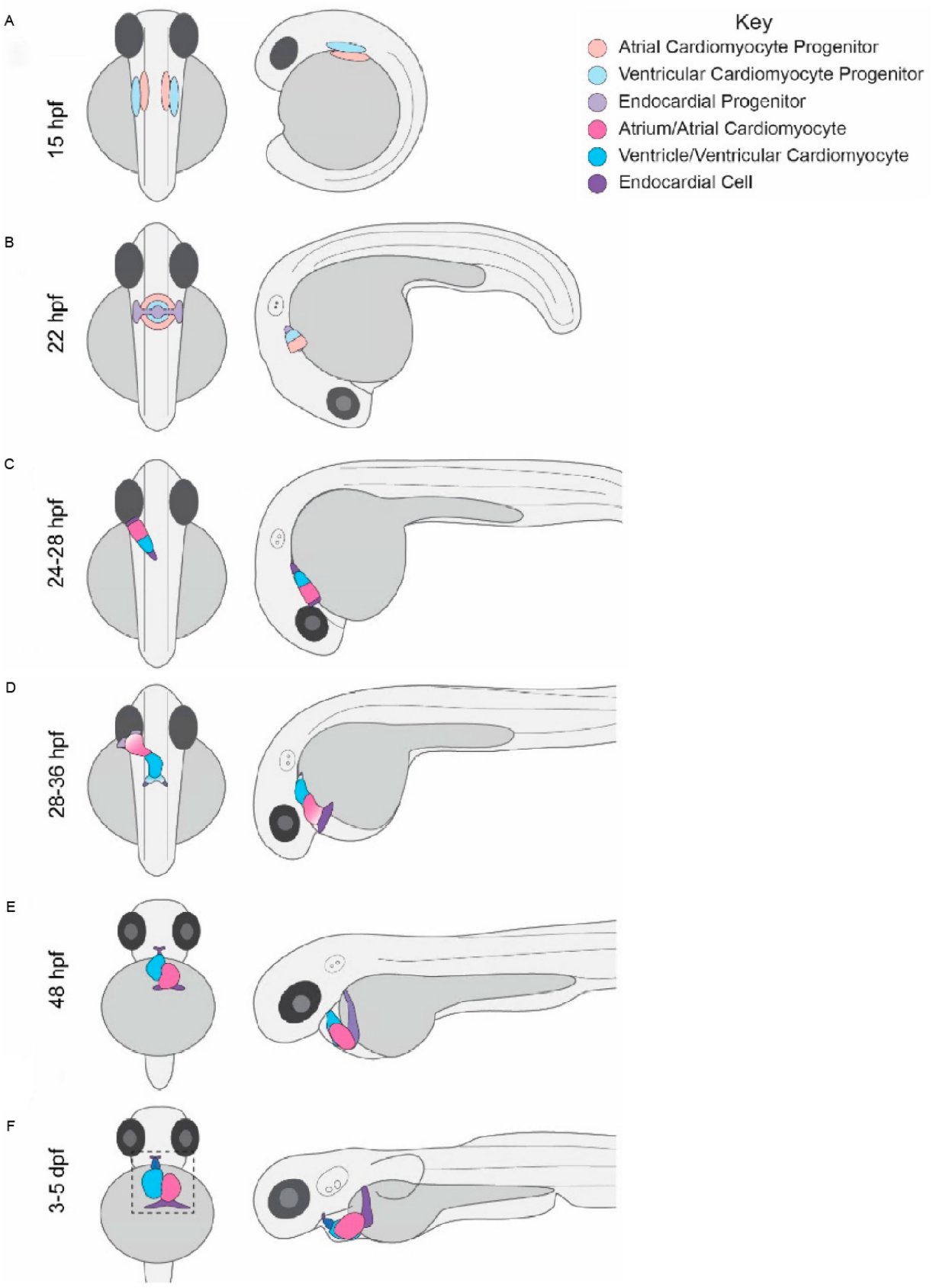
A
15 hpf
B
22 hpf
C
24-28 hpf
D
28-36 hpf
E
48 hpf
F
3-5 dpf
Key
Atrial Cardiomyocyte Progenitor
Ventricular Cardiomyocyte Progenitor
Endocardial Progenitor
Atrium/Atrial Cardiomyocyte
Ventricle/Ventricular Cardiomyocyte
Endocardial Cell

Figure 2. Development of the zebrafish heart in the first five days after fertilization. Left row, dorsal view; right row, lateral view. **(A-B)** CM and EdC progenitors migrate towards the midline and fuse into a heart disc. **(C)** The heart disc elongates to form a linear heart tube. **(D)** The linear heart tube starts looping. **(E-F)** A two-chambered heart is formed. Figure adapted from Brown et al., *J Cardiovasc Dev Dis*. (Brown et al., 2016).

1.2.4 Cardiac trabeculation in mouse and zebrafish

The vertebrate heart undergoes a series of morphogenetic events in order to meet the needs of growth, from a linear heart tube to a mature organ. Two important cell types of the heart are cardiomyocyte (CM) and endocardial cell (EdC), the former forming the myocardium, and the latter forming the endocardium. The myocardium consists of the compact layer and trabecular layer. In mice, cardiac trabeculation has been defined into six distinct stages: endocardial sprouting, endocardial touchdown, ingression, assembly, trabecular extension, and termination (del Monte-Nieto et al., 2018). At embryonic day 8 (E8.0), the endocardium starts to sprout, and the endocardial sprouts appear to be cellular. These sprouts reach the compact myocardium and form touchdowns at around E8.5. Interestingly, the endocardial sprouts extend beneath the laminar trabeculae. However, the function of endocardial sprouts during cardiac trabeculation is unclear. The trabecular CMs exist prior to sprouting and continue to rearrange, assemble, extend, and develop into trabeculae, finger-like multicellular protrusions. During this process, the cardiac jelly (CJ), a special extracellular matrix (ECM) that separates the endocardium from the myocardium, is progressively degraded.

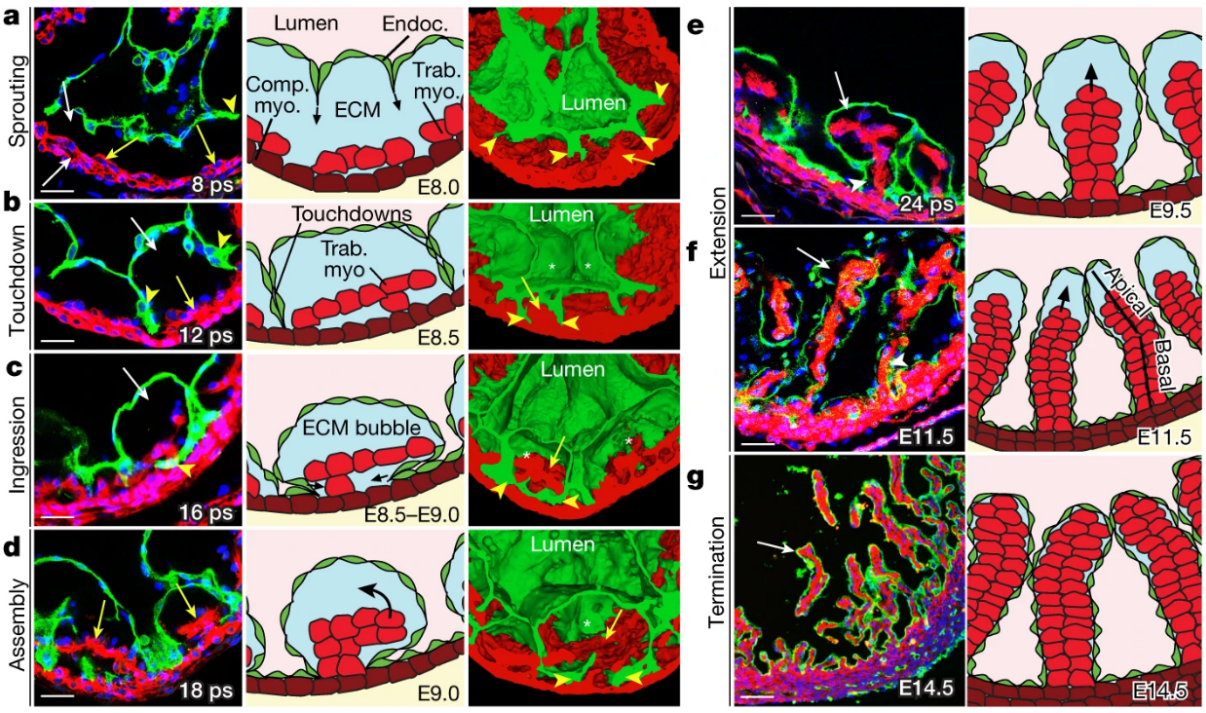

Figure 3. Cardiac trabeculation stages in mouse.

Cardiac trabeculation is divided into six stages from E8.0 to E14.5: sprouting, touchdown, ingression, assembly, extension, and termination. Figure from Del Monte-Nieto et al., *Nature*. (del Monte-Nieto et al., 2018). License number: 5507701328843.

The cardiac trabeculation process in mouse and zebrafish shares many similarities, but there are also some distinctive features during cardiac trabeculation in zebrafish. In contrast to the multilayered compact myocardium of the mouse, the compact myocardium of zebrafish is mono-layered at early stages of development (Figure 4) (Liu et al., 2010; Priya et al., 2020). At around 60 hpf, CMs delaminate from the compact myocardial wall towards the heart chamber to seed the trabeculae in a stochastic manner, and the trabeculae can be observed at 3 days post fertilization (dpf) (Liu et al., 2010; Priya et al., 2020; Staudt et al., 2014). Endocardial morphogenesis has not been described in cardiac trabeculation in zebrafish.

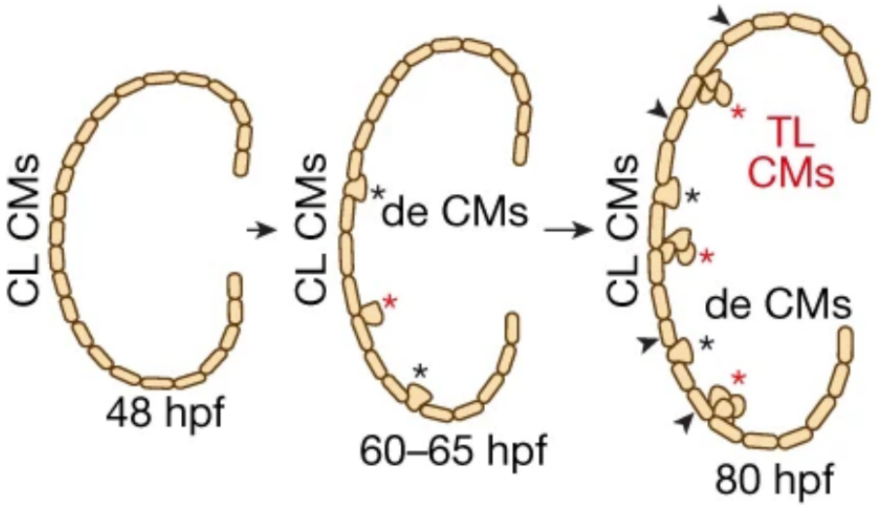

Figure 4. Schematic model showing the mid-sagittal sections of the zebrafish heart from 48 – 80 hpf.

The myocardium is a monolayer at 48 hpf. At around 60 hpf, several CMs delaminate from the compact layer (CL). At 80 hpf, multiple trabeculae are formed at 80 hpf. CL, compact layer; de CMs, delaminating CMs; TL CMs, trabecular layer CMs. Figure from Priya et al., *Nature*. (Priya et al., 2020). License number: 5507710443669.

Cardiac trabeculae are important for achieving incresed cardiac contractility and also for the formation of cardiac conduction system. Impaired cardiac trabeculation often leads to heart failure and lethality in embryos (Gassmann et al., 1995; Lai et al., 2010; Lee et al., 1995; Liu et al., 2010; Rasouli & Stainier, 2017), left ventricular noncompaction (Claudia & Josef, 2004; Oechslin et al., 2000a), and cardiomyopathy in human (Jenni et al., 1999).

1.2.5 Neuregulin signaling pathway plays an important role in cardiac trabeculation in mouse and zebrafish

Several signaling pathways are involved in cardiac trabeculation, and one of the most important is neuregulin (Nrg)/ErbB signaling pathway. In mice, the ligand Nrg1 is expressed in the endocardium, whereas the receptors ErbB2 and ErbB4 are expressed in the myocardium (Figure 5) (Gassmann et al., 1995; Grego-Bessa et al., 2007; Lee et al., 1995; Odiete et al., 2012). Disruption of Nrg1, ErbB2, or ErbB4 results in cardiac trabeculation defects (Gassmann et al., 1995; Lai et al., 2010; Lee et al., 1995). Nrg1 consists of an extracellular receptor-binding domain, cleavage site, a transmembrane domain, and a cytoplasmic domain (Kamezaki et al., 2016). After proteolytic cleavage, the extracellular domain including an epidermal growth factor-like (EGF-like) domain of Nrg1 is released and binds to ErbB4, allowing the ligand actives the ErbB4 receptor. Remarkably, the soluble form of Nrg1 does not bind directly to ErbB2. Instead, ErbB2 dimerises with ErbB4 when Nrg1 binds to ErbB4 (Figure 5) (GrausPorta et al., 1997).

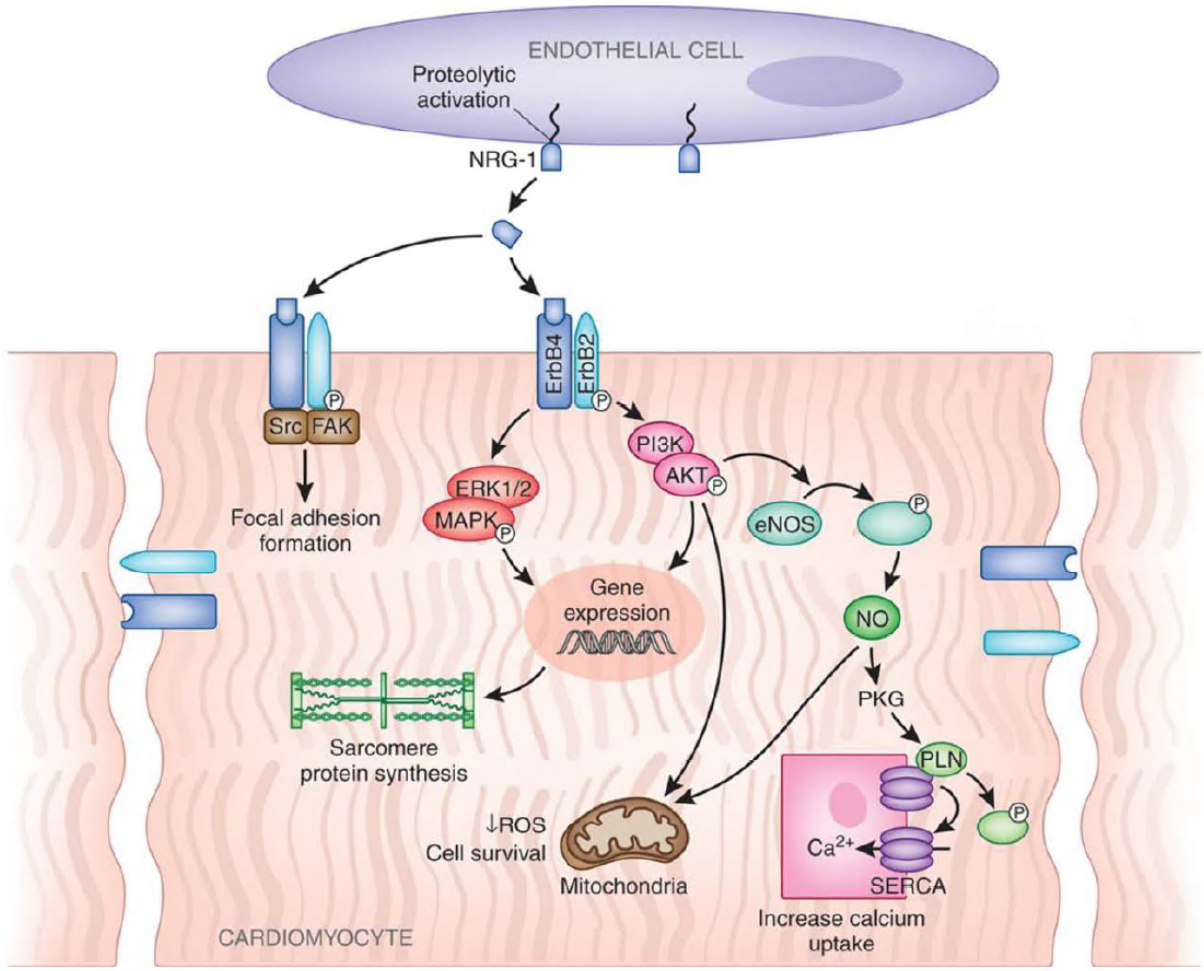

Figure 5. Schematic model showing Nrg1/ErbB2/ErbB4 signaling in ECs and CMs. Nrg1 is expressed in the ECs, whereas ErbB2 and ErbB4 are expressed in the CMs. The released soluble form of Nrg1 actives ErbB, and also interacts with several signaling cascades, including Erk 1/2. Figure adapted from Odiete et al., *Circ Res*. (Odiete et al., 2012).

Although Nrg1 is essential for cardiac trabeculation in mice, it is dispensable for cardiac trabeculation in zebrafish (Rasouli & Stainier, 2017; Samsa et al., 2016). Interestingly, Nrg2 is dispensable during cardiac development in mouse (Britto et al., 2004), but it is required for cardiac trabeculation in zebrafish (Figure 6) (Rasouli &

Stainier, 2017). All these discoveries suggest that it will be interesting to study the selection of neuregulin ligand during evolution.

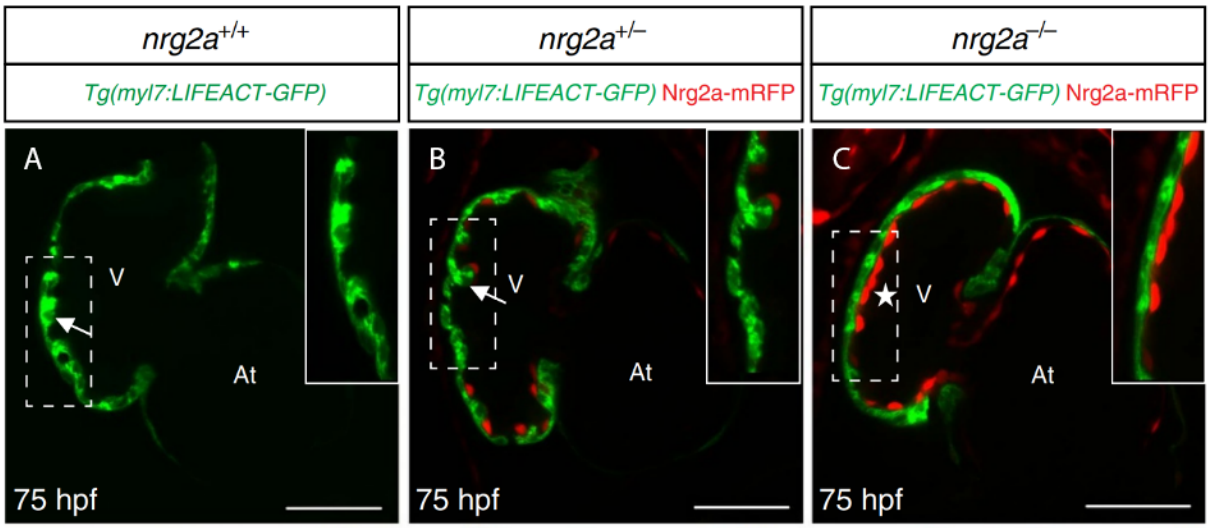

Figure 6. Nrg2a deficiency imparis cardiac trabeculation.
Compared with wild-type and heterzygous siblings **(A-B)**, the *nrg2a* mutant **(C)** exhibits defects in cardiac trabeculation. Figure adapted from Rasouli and Stainier, *Nat Commun*. (Rasouli & Stainier, 2017).

1.2.6 The endocardium is important for myocardial development

More interestingly, several endocardial signaling pathways are required for myocardial trabeculation. Genetic deletion of endocardium expressed Notch1, a Notch receptor, results in cardiac trabeculation defects (D'Amato et al., 2016; del Monte-Nieto et al., 2018; Grego-Bessa et al., 2007). Angiopoietin 1/Tie2 signaling is another known pathway involved in cardiac development. The absence of the myocardium-expressed ligand angiopoietin 1, or the endocardium-expressed receptor Tie2 leads to severe deficits in cardiac trabeculation (Qu et al., 2019; Suri et al., 1996; Tachibana et al., 2005). Furthermore, specific deletion of PlexinD1 (Plxnd1), the receptor of semaphorin 3E, in the endocardium results in hypertrabeculation and noncompaction of ventricular myocardium (Sandireddy et al., 2019). All these data

indicate that the endocardium plays an essential role during myocardial development.

1.3 Cell-cell communication

Cell-cell communication, also known as cell-cell signaling, is a process by which cells transmit and receive signals from other cells; intercellular communication allows cells to have an impact on each other's fate and behavior. Cells need to communicate and interact with each other in order to modulate cellular stimulation, proliferation, differentiation, and migration. A typical cell-cell communication model is diffusion-based paracrine signaling, in which the donor cells produce ligands that bind to the corresponding receptors on the recipient cells. When two cells are connected, e.g., by gap junctions, signals can be transmitted via gap junctions. In many cases, however, the ligands have to travel across the ECM of which separates the donor cells and recipient cells. An interesting question here is whether the large molecules diffuse freely between cells. Recently, an increasing number of studies have shown a novel mechanism of cell-cell communication in which molecules actively pass through actin enriched filopodia-like protrusions, also knowns as cytonemes, in various animal models including *Drosophila* (Huang et al., 2019; Ramirez-Weber & Kornberg, 1999; Roy et al., 2011), chick (Sanders et al., 2013), zebrafish (Stanganello et al., 2015), and mouse (Fierro-Gonzalez et al., 2013).

1.3.1 Filopodia-mediated cell-cell communication

Filopodia, which facilitate signaling exchanges between cells, were first designated as cytonemes in *Drosophila* in 1999 (Ramirez-Weber & Kornberg, 1999). There is growing evidence demonstrates that cytonemes also present in many vertebrate organisms, i.e., mouse, chick, and zebrafish (Fierro-Gonzalez et al., 2013; Sanders et al., 2013; Stanganello et al., 2015). These cytonemes not only bring ligands to the receptor-expressing target cells (Roy et al., 2011, 2014), but also transport the corresponding receptors to the ligand-producing cells (Sagar et al., 2015) (Figure 7).

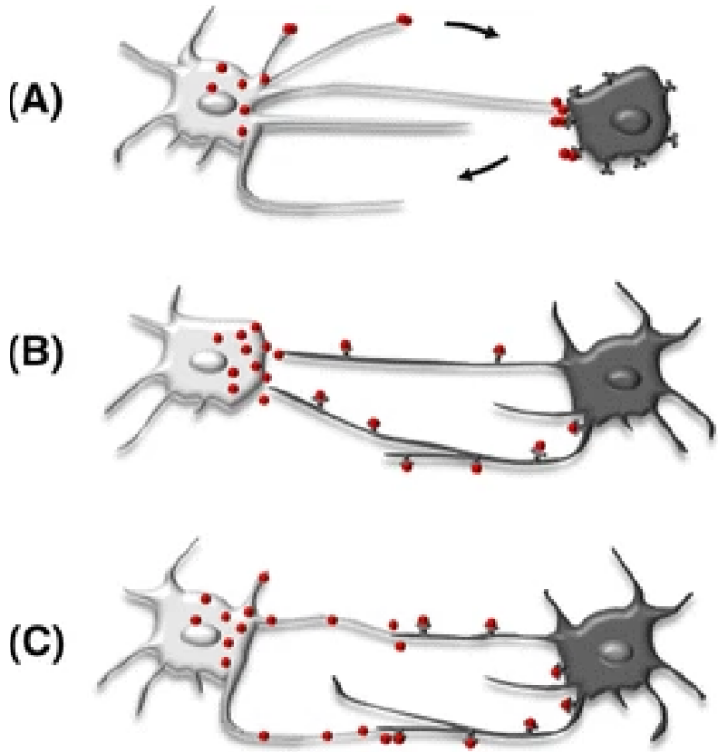

Figure 7. Schematic model showing three types of filopodia-mediated cell-cell communication.

(A) Ligand-producing cells bring ligand to the receptor-present cells. **(B)** Receptor-present cells bring the receptor to the ligand-producing cells. **(C)** Both (A) and (B) occur. Figure from Prols et al., *Cell Mol Life Sci*. (Prols et al., 2016). License number: 5507720168865.

In *Drosophila*, previous work has shown that decapentaplegic (Dpp) and fibroblast growth factor (FGF) are transported by cytonemes. Dpp and FGF, required for air sac primordium (ASP) development, are expressed in the wing imaginal disc. ASP cytonemes take up Dpp and FGF from the disc and bring them to the ASP (Roy et al., 2014).

In zebrafish, Wnt8a is located in the tips of signaling filopodia of the producing cells. The signaling filopodia transport Wnt8a to the recipient cells and bind to its receptors (Stanganello et al., 2015).

1.3.2 Regulators of filopodia formation

The formation of filopodia depends on the precise polymerization of actin filaments. CDC42, a small GTPase, is one of the best-studied factors that induce filopodia formation (Nobes & Hall, 1995). It has been reported that the insulin-receptor substrate p53 (IRSp53) acts as a downstream of CDC42 in filopodia formation (Krugmann et al., 2001; Lim et al., 2008). Previous studies also suggest that IRSp53 directly affects filopodia formation by activating F-actin bundling (Yamagishi et al., 2004).

1.3.3 Animal models for the study of cell-cell communication

As mentioned in section **1.3.1**, cytonemes were shown to transport molecules in the late 20th century (Ramirez-Weber & Kornberg, 1999). These findings expand the understanding of paracrine signaling. In the classical model of paracrine signaling, the molecule disperses passively from the producing cells across the target fields. However, the discovery of cytonemes gives us a new insight that protein moves along

the signaling filopodia from the producing cells to the target cells instead of freely moving in the extracellular fluid. As mentioned above, signaling filopodia exist in multiple animal models, including zebrafish, chick, mouse, as well as a non-vertebrate model *Drosophila*. Many challenges prevent scientists to understand cell-cell communication via signaling filopodia in vertebrates *in vivo*. These challenges include the ability to track and visualize cell behavior at a single-cell level, and the ability to manipulate cells. The zebrafish becomes an ideal model for studying cell-cell communication because its transparency allows single-cell resolution and high-speed imaging.

1.4 Apelin signaling pathway

1.4.1 Core pathway

Apelin is a peptide hormone characterized as an endogenous ligand for the orphan G protein-couple receptor (GPCR) Apelin receptor (Aplnr/APJ) in 1998 (Tatemoto et al., 1998). Serene Chng and her colleagues identified another ligand of Aplnr, Apela (Elabela), in zebrafish (Chng et al., 2013). In mammals, the Apelin signaling pathway consists of two ligands, *Apelin* and *Apela*, and one receptor *Aplnr*. Due to genome duplication, there are two receptors for Apelin signaling pathway, *aplnra* and *aplnrb*, in zebrafish.

1.4.2 Role of Apelin signaling in the cardiovascular system

Apelin signaling pathway has been shown to regulate the cardiovascular system in different organisms, such as *Xenopus* (Inui et al., 2006), zebrafish (Chng et al., 2013; Helker et al., 2015, 2020), and mouse (Charo et al., 2009). These data suggest that the function of Apelin signaling pathway is evolutionary conserved. In mice, *Aplnr* has been shown expressed in the retinal vessels during vascular formation (Saint-Geniez et al., 2002). Interestingly, *Apln* is tip cell-enriched in the retinal vessels (del Toro et al., 2010). Consistent with the findings in mice, the expression of *apln* was detected in the endothelial tip cells whereas the expression of *aplnrb* expression was detected in all sprouting endothelial cells (ECs) during intersegmental vessel (ISV) formation in zebrafish (Helker et al., 2020). Lacking Apln or Aplnr function resulted in a reduction of angiogenesis (Cox et al., 2006; Helker et al., 2020; Kalin et al., 2007), EC proliferation (del Toro et al., 2010), and also impaired filopodia formation of endothelial tip cells (Helker et al., 2020). In contrast to the requirement of *apln* during angiogenesis, *apela* is required for vasculogenesis, a process in which a primitive vascular network formed *de novo* (Helker et al., 2015). Furthermore, loss of Apela also resulted in cardiac malformation (Chng et al., 2013; Ho et al., 2017; Pauli et al., 2014).

Apelin signaling is not only involved in cardiovascular development, but also in several cardiovascular diseases, for instance, tumor angiogenesis (Kidoya et al., 2012; Uribesalgo et al., 2019; Zhao et al., 2018), pulmonary hypertension (Alastalo et al., 2011; Chandra et al., 2011; Goetze et al., 2006), atherosclerosis (Chun et al., 2008; Hashimoto et al., 2007; Kojima et al., 2010; Pitkin et al., 2010), cardiac hypertrophy (Scimia et al., 2012).

2 Aims

As mentioned in the introduction, cardiac trabeculation is a critical process during heart maturation and its defects lead to severe heart dysfunctions. In recent years, many mechanisms related to cardiac trabeculation maturation have been addressed. These mechanisms occur in either the myocardium or the endocardium. Priya et al. have shown that the crowd of CMs is a key to the onset of cardiac trabeculation (Priya et al., 2020). However, the contribution of the endocardium to the onset of myocardial trabeculation is not well studied. Inspired by Del Monte-Nieto et al, who reported that the endocardium protrudes sprouts in the early phase of cardiac trabeculation (del Monte-Nieto et al., 2018), I started the project with the aims to:

1. **Investigate the role of endocardial protrusions during cardiac trabeculation.**

   I will generate a transgenic fish line that specifically blocks the formation of endothelial protrusion and study the cardiac trabeculation in this transgenic line.

2. **Identify the signaling pathway(s) that drive(s) the formation of endocardial protrusions.**

   I will identify the genes that mediate the formation of endocardial protrusion by analyzing the corresponding mutants. Moreover, I will also examine the cardiac trabeculation in these mutants.

3. **Understand how endocardial protrusions regulate cardiac trabeculation.**

   Nrg/ErbB signaling is a well-known myocardial pathway in which the ligand is expressed in the endocardium whereas the receptor is expressed in the myocardium. I will study whether the function of Nrg/ErbB signaling is affected to inhibit the endocardial protrusion formation.

To achieve these aims, I choose to use zebrafish as the animal model because its embryos a) survive for a week even with a malfunctioned cardiovascular system; b) develop externally and are transparent, allowing high-resolution live imaging of cellular behavior.

3 Materials and Methods

3.1 Materials

3.1.1 Antibiotic

Table 1: Antibiotic used and its working concentration.

Antibiotic	Working concentration
Ampicillin	100 µg/mL

3.1.2 Antibodies

Table 2: List of antibodies used, and their respective supplier and dilution.

Antibody	Isotype	Supplier	Catalog #	Dilution
Anti-mCherry	Mouse monoclonal	Takara Bio Clontech	632543	1:500
Anti-EGFP	Chicken polyclonal	Aves Lab	GFP-1020	1:500
MF 20	Mouse monoclonal	Developmental Studies Hybridoma Bank		Supernatant 1.0 ml. 1:50
Alexa Fluor 488 anti-Chicken	Goat IgG	Life Technologies	A11039	1:500

Alexa Fluor 568 anti-Mouse	Goat IgG	Life Technologies	A11004	1:500
Alexa Fluor 647 anti-Rabbit	Goat IgG	Life Technologies	A21244	1:500

3.1.3 Bacterial strain

Table 3: Bacterial strain used and its working purpose.

Bacterial strain	Purpose
DH5α	Competent cells for transformation

3.1.4 Buffers and solutions

Table 4: List of buffers and solutions used, and their composition.

Buffer / Solution	Composition
0.1% PBST	0.1% Tween-20 dissolved in 1X PBS
0.1% PBSTx	0.1% Triton-X100 dissolved in 1X PBS
4% PFA	4 g PFA dissolved in 100 ml PBS, adjust pH to 7 by HCl/NaOH
1X MBS	dilute 5X MBS and autoclave
1X PBDX	0.5% Triton X-100 + 1% DMSO + 1% BSA dissolved in 1X PBS

5X MBS	88mM NaCl + 5mM HEPES + 2.4mM $NaHCO_3$ + 1mM KCl + 0.82mM $MgSO_4 \cdot 7\ H_2O$ + 0.41mM $CaCl_2 \cdot 2\ H_2O$ + 0.33mM $Ca(NO_3)_2 \cdot 4\ H_2O$, adjusted pH to 7.4
10X PBS	10 PBS tablets in 200 ml distilled water
10X TBE	121 g Tris + 62 g Boric Acid + 7.4 g EDTA dissolved in 1 L distilled water
Alkaline Tris buffer	100 mM Tris-HCl pH 9.5 + 100 mM NaCl + 0.1% Tween 20 dissolved in distilled water
Bleaching solution	1.5% H_20_2 + 1% KOH
Blocking buffer (immunostaining)	1X PBDX + 10% goat serum
Blocking buffer (*in situ*)	2 mg/mL BSA + 2% sheep serum in 0.1% PBST
Egg water	3 g Instant Ocean + 0.75 g Calcium sulfate dissolved in 10 L distilled water
Lysis buffer (zebrafish embryos and larva)	50 mM NaOH

3.1.5 Kits

Table 5: List of kits used, and their respective supplier.

Kit	**Supplier**	**Catalog #**
Click-iT™ EdU Alexa Fluor™ 647 Imaging Kit	Invitrogen	C10340

Cold Fusion cloning kit	System Biosciences	MC101A-1
GeneJET gel extraction kit	Thermo Fisher Scientific	K0691
GeneJET PCR purification kit	Thermo Fisher Scientific	K0701
GeneJET plasmid miniprep kit	Thermo Fisher Scientific	K0502
In-Fusion HD cloning kit	Takara	639650
Maxima First Strand cDNA Synthesis	Thermo Fisher Scientific	K1672
miRNeasy micro kit	Qiagen	217084
QiaQuick nucleotide removal kit	Qiagen	28304
RNA clean and concentrator	Zymo Research	R1016
T4 DNA ligase	Promega	M1804

3.1.6 Chemicals

Table 6: List of chemicals used, and their respective supplier.

Chemical	**Supplier**	**Catalog #**
10X NEBuffer 2.1	NEB	B7202S
1-Phenyl-2-thiourea (PTU)	Sigma	P7629
5-ethynyl-2´-deoxyuridine (EdU)	Invitrogen	C10340
Agarose	Peqlab	35-1020
Agarose, low gelling temperature	Sigma	A9414

Alexa Fluor 568 Phalloidin	Thermo Fisher Scientific	A12380
Bovine serum albumin (BSA)	Sigma	A2153
Calcium Chloride ($CaCl_2$)	Merck Millipore	10035-04-8
Chloroform	Merck	102445
Citric acid	Sigma	27109
CutSmart buffer	NEB	B7204S
DAPI	Sigma	D9542
Dimethylsulfoxide (DMSO)	Sigma	D4540
DNA ladder (1 kb)	Thermo Scientific	SM0311
DNA ladder (100 bp)	Thermo Scientific	SM0241
Ethanol	Roth	K928.3
Gel loading dye	Thermo Scientific	R0611
Goat serum	Sigma	
Heparin	Sigma	136098-10-7
HEPES	Sigma	H3375
Hydrochloridic acid (HCl)	Sigma	H1758
Hydrogen peroxide (H_2O_2)	Sigma	7722-84-1

Isopropanol	Roth	6752,4
Methanol	Roth	4627.5
Methylene blue	Sigma	M9140
Mineral oil	Sigma	M8410
Nuclease-free water	Ambion	AM9938
Paraformaldehyde (PFA)	Sigma	P6148
Phenol red	Sigma	P0290
Phosphate-buffered saline (PBS) tablets	Sigma	P4417
Pronase	Roche	10165921001
Proteinase K	Roche	1092766
Sheep serum	Sigma	ABIN925265
Sodium Chloride (NaCl)	Sigma	S3014
Sodium hydroxide (NaOH)	Sigma	221465
Sucrose	Sigma	S0389
SYBR safe	Invitrogen	S33102
Tricaine (ethyl-m-aminobenzoate methanesulfonate)	Pharmaq	NA
Tris	Sigma	5429.2
Tris hydrochloride (Tris-HCl)	Sigma	RES3098T-B701X
Triton X-100	Sigma	RES3103T-A101X

Trizol	Ambion	15596018
Tween-20	Sigma	P1379

3.1.7 Drugs

Table 7: List of drugs used.

Drug	Supplier	Concentration
ErbB2 inhibitor PD168393	Sigma	10 µM
MEK inhibitor PD0325901	Sigma	1 µM
Notch inhibitor RO 4929097	MedChemExpress	1 µM

3.1.8 Enzymes

Table 8: List of enzymes used, and their respective supplier.

Enzyme	Supplier
MluI-HF	NEB
SalI-HF	NEB
KAPA2G Fast ReadyMix polymerase	Roche
PrimeSTAR max DNA polymerase	Takara
SYBR Green PCR master mix	Thermo Scientific

3.1.9 Growth media

Table 9: List of growth media used.

Growth medium	Composition
SOC medium	Tryptone 2% + Yeast extract 0.5% + NaCl 0.05% + KCl 0.0186% dissolve in distilled water and adjust pH to 7, add $MgCl_2$ 10mM + D-glucose 20 mM, then autoclave
LB agar	Roth
LB medium	Roth

3.1.10 Centrifuges

Table 10: List of centrifuges used, and their respective supplier.

Centrifuge	Supplier
Centrifuge (1.5-2 mL tubes) 5424	Eppendorf
Centrifuge (15 mL, 50 mL tubes) 5810 Rf	Eppendorf
MiniStar 1205-0713	VWR

3.1.11 Microscopes

Table 11: List of microscopes used, and their respective supplier.

Microscope	Supplier
Stereomicroscope SMZ18	Nikon
Stereomicroscope SMZ25	Nikon
Stereomicroscope Stemi 2000	Zeiss
Confocal microscope LSM800 Examiner	Zeiss

Confocal microscope LSM880	Zeiss
Spinning Disk microscope, cell observer SD	Zeiss

3.1.12 Miscellaneous laboratory equipment

Table 12: List of miscellaneous laboratory equipment used, and respective supplier.

Equipment	**Supplier**
Bacterial incubator	Heraeus
Bacterial incubator shaker	Infors HAT
Bullet Blender	Next Advance
CFX connect real time PCR detection system	Bio Rad
Dark reader transilluminator	Clare chemical
Eco Real-Time PCR System	Illumina
Electrophoresis power supply	Bio Rad
Gel Doc EZ system	Bio Rad
Heating block	VWR
Injection micromanipulator	World precision instruments
Micropipette puller P-1000	Sutter instruments
Microscale	Novex
Microwave	Bosh

Nanodrop 2000c	Thermo Scientific
NextSeq500 instrument	Illumina
PCR mastercycler Pro	Eppendorf
Pipetboy	Integra
Printer P95	Mitsubishi
Sunflower mini shaker PS-3D	BioSan
Vortex Genie 2	Scientific Insdustries
Weighing balance	Sartorius
Zebrafish aqua culture system	Tecniplast
Zebrafish breeding tanks	Tecniplast
Zebrafish incubator	Binder

3.1.13 Laboratory supplies

Table 13: List of laboratory supplies used, and their respective supplier.

Laboratory supply	**Supplier**
Bacterial culture tube	Sarstedt
Beakers	VWR
Centrifuge tubes (1.5 mL, 2 mL)	Sarstedt
Conical flasks (100 mL, 500 mL)	VWR
Falcons (15 mL, 50 mL)	Greiner bio-one

Forceps	Dumont
Glass bottles (50 mL, 100 mL, 250 mL, 500 mL, 1000 mL)	Duran
Glass bottom dish	MatTek
Insulin Syringes	Terumo
Laboratory film	Parafilm
Latex gloves	Roth
Microloader pipette tips	Eppendorf
Nitrile gloves	VWR
PCR tubes (200 µL)	Sarstedt
Petri dish (90 mm, 60 mm, 35 mm)	Grainer bio-one
Pipetboy	Integra
Pipette filter tips	Grainer bio-one
Pipette tips	Grainer bio-one
Pipettes (2 µL, 20 µL, 200 µL, 1000 µL)	Gilson
Scalpel	Braun
Serum pipette	Grainer bio-one

3.1.14 Oligonucleotides

Table 14: List of oligonucleotides used, and their sequence and purpose.

Primer name	Sequence 5´-3´	Purpose
irsp53^{dn} fwd	TTCGAATTAGATCTGTCGACCGCCACCA TGTCTCGCACCGACGAGGT	Cloning
irsp53^{dn} rev	GTAGCTCCGCTTCCACGCGTCTGTGCAA AGCCTGCCATGC	Cloning
apln mut fwd	GGAGGGGAGAGCAGAAATGA	Genotyping
apln mut rev	AAACCACCAGCACAATCACC	Genotyping
aplnrb mut fwd	TGCTCTACATGCTCATCTTCA	Genotyping
aplnrb mut rev	ATTCCCAGTGAGTCCCAGGA	Genotyping
aplnra mut fwd	GAAGGACTCAAAGCCAACGC	Genotyping
aplnra mut rev	GAAGATAACCACGCCGTTCC	Genotyping

3.1.15 Plasmids

Table 15: List of plasmids used in the thesis with their respective resistance, source, and purpose.

Plasmid	Resistance	Source	Purpose
5XUAS-p2a-tagRFP	Ampicillin	This study	Expressing *irsp53^{dn}*

3.1.16 Software

Table 16: List of software used in the thesis with their respective purpose.

Software	Purpose

Adobe Photoshop, Illustrator	Image formatting
Fiji Image J	Image processing
Gitools	Bioinformatics analysis
GraphPad Prism 8	Data analysis
GSEA	Bioinformatics analysis
Imaris	Image processing
Microsoft Office (Word, Excel)	Writing, data analysis, image formatting
PerlPrimer	Primer design
Primer 3	Primer design
SnapGene	Sequence analysis
Zen Digital Imaging	Image processing

3.1.17 Zebrafish food

Table 17: List of zebrafish food used for different developmental stages.

Food	**Developmental stage**
Brine Shrimp	5 dpf – 12 dpf
SDS100	12 dpf – 1 month
SDS 200	1 month – 2 months
SDS 300	2 months – 3 months
Tropical Breeder Mix and SDS 400	Adult fish

3.1.18 Zebrafish lines

This section (**3.1.18 Zebrafish lines**) is quoted from the article published in the journal *eLife* (Qi et al. eLife 2022; 11: e73231. DOI: https://doi.org/10.7554/eLife.73231) (Qi et al., 2022).

Table 18: List of zebrafish lines used, and the sources where they were first described.

Line	Details	Source	Identifier
AB	Wild type		
TgBAC(apln:EGFP)^{bns157}	*apln* reporter	(Helker et al., 2020)	ZFIN: *bns157*
TgBAC(cdh5:Gal4ff)^{mu101}	Endothelium reporter for UAS driver lines	(Bussmann & Schulte-Merker, 2011)	ZFIN: *mu101*
Tg(UAS:LIFEACT-GFP)^{mu271}	Cytoskeleton reporter for Gal4 driver lines	(Helker et al., 2013)	ZFIN: *mu271*
Tg(fli1a:nrg2a-p2a-tdTomato)^{bns199}	Overexpress *nrg2a* in the endothelium	(Rasouli & Stainier, 2017)	ZFIN: *bns199*
Tg(myl7:mCherry-CAAX)^{bns7}	Membrane myocardial reporter	(Uribe et al., 2018)	ZFIN: *bns7*
Tg(myl7:BFP-CAAX)^{bns193}	Membrane myocardial reporter	(Guerra et al., 2018)	ZFIN: *bns193*

Tg(myl7:MKATE-CAAX)^{sd11}	Membrane myocardial reporter	(Lin et al., 2012)	ZFIN: *sd11*
Tg(kdrl:HsHRAS-mCherry)^{s896}	Membrane vascular reporter	(Chi et al., 2008)	ZFIN: *s896*
Tg(myl7:HRAS-EGFP)^{s883}	Membrane myocardial reporter	(D'Amico et al., 2007)	ZFIN: *s883*
Tg(tp1-MmHbb:EGFP)^{um14}	Notch reporter	(Parsons et al., 2009)	ZFIN: *um14*
Tg(myl7:mVenus-gmnn)^{ncv43Tg}	Proliferating CM reporter	(Jimenez-Amilburu et al., 2016)	ZFIN: *ncv43Tg*
Tg(UAS: irsp53^{dn}-p2a-tagRFP)^{bns440}	Overexpress *irsp53dn* for Gal4 driver lines	(Qi et al., 2022)	*bns440*
TgBAC(aplnrb:VenusPEST)^{mr13}	*aplnrb* reporter	(Qi et al., 2022)	*mr13*
Tg(-0.8myl7:ERK-KTR-Clover-p2a-Hsa.H2B-tagBFP)	Erk reporter	(Qi et al., 2022)	
Tg(-0.8myl7:ERK-KTR-Clover-p2a-Hsa.H2B-mScarlet)^{bns565}	Erk reporter	(Qi et al., 2022)	*bns565*
apln^{mu267} mutant	*apln* mutant	(Helker et al., 2015)	ZFIN: *mu267*

aplnrb^{mu281} mutant	*aplnrb* mutant	(Helker et al., 2015)	ZFIN: *mu281*
aplnra^{mu296} mutant	*aplnra* mutant	(Helker et al., 2015)	ZFIN: *mu296*
apela^{br13} mutant	*apela* mutant	(Chng et al., 2013)	ZFIN: *br13*

3.2 Methods

Parts of this chapter (**3.2 Methods**) are quoted from the article published in the journal *eLife* (Qi et al. eLife 2022; 11: e73231. DOI: https://doi.org/10.7554/eLife.73231) (Qi et al., 2022).

3.2.1 Zebrafish methods

3.2.1.1 Zebrafish maintenance and breeding

Zebrafish were housed and maintained under standard conditions. To mimic the natural environment, zebrafish older than 5 dpf are maintained in an aquaculture system (Tecniplast) with a 14 hours/10 hours light-dark cycle, with water temperature maintained at 28°C and the room temperature at 29°C.

For breeding, 3-4 pairs of male and female fish were placed in a mating tank, with males and females separated by a divider in the evening. In the morning of the following day, the dividers were removed to allow mating. After 20-30 minutes, embryos at the bottom of the mating tanks were collected by a mesh tea strainer and were rinsed into 9cm Petri dishes with egg water. Later in the afternoon, fertilized embryos were picked out under a stereomicroscope and placed into new Petri dishes at a density of 50 embryos per dish.

The embryos were maintained in 40 ml fresh egg water until 5 dpf. For imaging, embryos and larvae were staged by hours post fertilization at 28.5°C (Kimmel et al., 1995), and 0.003% Phenylthiourea (PTU) was added into egg water at 22 to 24 hpf to avoid pigmentation. Removal of chorion was necessary if the experiments were to be performed at 24 or 48 hpf. Two methods were applied to remove chorion: using two forceps or by adding 200 µl of 10mg/ml pronase per Petri dish for 10 minutes. The egg water containing PTU was replaced with fresh egg water after the removal of the chorion.

3.2.1.2 Microinjection

3.2.1.2.1 Preparation of the microinjection plates

2% agarose was dissolved in egg water. 30-40 ml solution was poured into 90 mm Petri dishes. A mold provided with stripes was carefully placed on the solution until it solidified at room temperature. After removing the mold, the agarose plates were kept at 4°C and covered with some fresh egg water to avoid the plates from drying out.

3.2.1.2.2 Preparation of microinjection needles

A glass capillary was inserted into the micropipette puller device under tension. A platinum filament heated the center of the capillary and then the capillary was pulled into two parts with thin tips. A forceps was used to break off the thin tips to open a small hole through which the injection solution could be injected into the embryos.

3.2.1.2.3 Microinjection

10 µl of the injection mix was filled into the injection needles with microloader pipette tips. One-cell stage embryos were aligned along the strips of the microinjection plates with the cell facing injection needle. Plasmids were injected into the cell.

3.2.1.2.4 Zebrafish screening

The injected embryos were dechorionated at 24 hpf using the above-mentioned methods. PTU was added after dechorionation to avoid pigment formation. At 48 hpf, embryos with positive fluorescence were selected and grown to adulthood.

For founder screening, raised adult fish were outcrossed with wild-type fish, and only those fish whose offspring showed positive fluorescence were categorized as

founders. One founder fish was outcrossed with one wild-type fish respectively to obtain the F1 generation.

3.2.1.3 Embryonic zebrafish heart isolation and RNA extraction

48 hpf *apln* mutant and wild-type embryos with *Tg(myl7:mCherry-CAAX)* background were placed into 60 mm Petri dishes containing 10 ml cold 1X MBS to reduce tissue stickiness. Insulin syringes were used to isolate the heart. To avoid the movement of embryos, one syringe was used to fix the embryo; the other syringe was used to cut the outflow tract and inflow tract, and then the heart was carefully detached from the body. The isolated hearts were placed in a 1.5 mL tube with 20 µL filter tips, and the tube was always kept on ice. After collecting 25 hearts per tube, the tubes were centrifuged at 5000 rpm. After carefully removing the remaining MBS, 60 µl Trizol was added. Then the collected zebrafish hearts were homogenized in Trizol using a bullet blender homogenizer. A miRNA micro kit was used to extract the total RNA of the heart. RNA was preserved at -80°C prior to RNA-sequencing.

3.2.1.4 Anesthesia of adult zebrafish

For anesthetization, adult zebrafish were placed into egg water containing 0.01% tricaine. When the movement of the gill slowed down to one beat per second, the fish were taken out for further experiments.

After the experiments were completed, the fish were placed in a container with fresh water to allow them to recover from anesthesia.

3.2.1.5 Genotyping of zebrafish

For genotyping of fish younger than 120 hpf (5dpf), the individual anesthetized fish was placed in a 200 µl tube. Then, the genomic DNA was extracted (see **3.2.2.1**) to perform genotyping via HRMA or PCR.

For genotyping adult fish, the caudal fin tip was cut from the anesthetized fish and placed into a 200 µl tube. Genomic DNA was then extracted (see **3.2.2.1**) for genotyping via HRMA or PCR.

3.2.1.6 Killing of zebrafish

A maximum of five fish were killed in one-liter of system water containing 0.01% tricaine.

3.2.2 Molecular biology

3.2.2.1 Genomic DNA (gDNA) extraction

The individual embryo, larva, or fin was placed into a 200 µl tube. 80 µl 50 mM NaOH was added, and the tube was stored at 95°C for 10 min to lyse the biological material. 8 µl 1M Tris-HCl (pH8) was added to the solution and mixed well.

3.2.2.2 cDNA synthesis

At least 500 ng RNA was used for first-strand cDNA synthesis via the Maxima cDNA synthesis kit. The steps are shown below:

Step	Reagent	Amount for reaction (total 20 µl)
1	10X dsDNase Buffer	1 µl
	dsDNase	1 µl
	Template RNA	1 pg to 5 µg
	Nuclease-free Water	To 10 µl

2	2 min at 37°C	
3	5X Reaction Mix	4 µl
	Maxima Enzyme Mix	2 µl
	Nuclease-free Water	4 µl
4	**10** in at 25°C, 15 min at 50 °C, 5 min at 85°C	

Table 19: Protocol for cDNA synthesis.

3.2.2.3 Real-time polymerase chain reaction (PCR)

The primers were designed by Primer 3 software. Amplification of desired sequences was performed by KAPA2G Fast ReadyMix (Roche) or PrimeSTAR Max Premix (Takara Clontech) polymerase. The following conditions were used in the thermocycler for each polymerase:

Temperature	Time	Cycle (s)	Description
95°C	5 min	1	Initial denaturation
95°C	30 sec	35	Denaturation
58°C	30 sec		Annealing
72°C	1 min/kb		Extension
72°C	5 min	1	Final extension
4°C	Indefinite time		Hold

Table 20: Standard thermal cycler conditions for KAPA2G Fast polymerase.

Temperature	Time	Cycle (s)	Description

98°C	2 min	1	Initial denaturation
98°C	15 sec	35	Denaturation
58°C	30 sec		Annealing
72°C	1 min/kb		Extension
72°C	5 min	1	Final extension
4°C	Indefinite time		Hold

Table 21: Standard thermal cycler conditions for PrimeSTAR Max polymerase.

3.2.2.4 Agarose gel electrophoresis

To prepare agarose gels, 1% agarose was added in 1X TBE buffer, and the agarose powder was mixed with the TBE buffer by manually rotating the conical flask. The agarose powder was dissolved by heating up the buffer in the microwave. 5 µl SYBR was added into 100 ml dissolved buffer. Gel loading dye was mixed with the PCR product and load on the 1% agarose. The gels were run for 30 min with a constant voltage of 160 V. The gels were checked with a blue-light transilluminator, and an image was taken with a gel-imaging device.

3.2.2.5 DNA purification from agarose gel

The desired band was cut off from the agarose gel and the DNA was purified by a GeneJET gel extraction kit according to the manufacturer's instructions. The purified DNA was eluted in 12 µl of nuclease-free water.

3.2.2.6 DNA restriction digest

DNA samples were mixed with the desired restriction enzymes and reaction buffer. The reaction is shown below:

Component	50 µl Reaction

DNA	1 µg
10x CutSmart buffer	5 µl
Restriction enzyme	1 µl
Nuclease-free water	to 50 µl
Incubation temperature	37°C
Incubation time	1-2 hours

Table 22: Standard conditions for restriction digest.

3.2.2.7 DNA ligation reaction

The DNA insert and vector were digested as described in section **3.2.2.6**. After gel purification as described in section **3.2.2.5**, the insert and vector were ligated with Cold Fusion, In-Fusion, or T4 DNA ligase.

A Cold Fusion or In-Fusion reaction is shown below:

Component	2.5 µl Reaction
Insert DNA	200 ng
Vector DNA	100 ng
5x Master Mix	0.5 µl
Nuclease-free water	to 2.5 µl
Incubation temperature	50°C
Incubation time	15 minutes

Table 23: Standard conditions for Cold Fusion or In-Fusion.

A T4 DNA ligase reaction is shown below:

Component	10 µl Reaction
Molar ratio insert DNA/ vector DNA	3:1
Ligase 10X buffer	1 µl
T4 DNA ligase	0.5 µl
Nuclease-free water	to 10 µl
Incubation temperature	Room temperature
Incubation time	1 hours

Table 24: Standard conditions for T4 DNA ligase.

3.2.2.8 *E.Coli* competent cell transformation

E.Coli competent cells were thawed on ice for 5 minutes. The ligation mixture was added into the competent cells and mixed well by pipetting up and down. Then the mixture was incubated on ice for 10 minutes. A heat shock of 42°C was performed for 45 seconds, followed by a 2-minute incubation on ice. The mixture was applied onto a LB agar plate containing Ampicillin using glass beads and incubated overnight at 37°C.

3.2.2.9 Inoculation and DNA plasmid isolation

Following transformation, a single bacterial colony was inoculated into 5 ml LB medium with the desired antibiotic and incubated overnight in a bacterial shaker at 37°C. The next morning, the bacterial culture was centrifuged at 4000 rpm for 5 minutes and the supernatant was discarded. The DNA plasmid was isolated from the bacterial pellet using a GnenJET plasmid MiniPrep kit.

3.2.2.10 DNA sequencing

1 µg of DNA plasmid was mixed with 30 µM (3 µl x 10 µM) sequencing primer, and then sent to GATC Biotech for a Sanger-sequencing.

3.2.2.11 High-resolution melt analysis (HRMA)

HRMA was performed to genotype the mutants. The following reactions and conditions were used:

Component	10 µl Reaction
Sybr Green	5 µg
10 µM forward primer	1 µl
10 µM reverse primer	1 µl
gDNA	1 µl
Nuclease-free water	2 µl

Table 25: Standard reaction for HRMA.

Temperature	Time	Cycle (s)	Description
95°C	10 min	1	Polymerase activation
95°C	10 sec	40	PCR cycling
60°C	30 sec		
95°C	15 sec	1	High resolution melt curve
55°C	15 sec		

95°C	**15** ec		

Table 26: Standard conditions for HRMA.

3.2.2.12 Immunostaining (Day1, Day2)

Day 1: primary antibody incubation

Zebrafish embryos and larvae at desired stages were fixed in 4% PFA for 2 hours at room temperature. Fixed animals were washed three times for 5 minutes with PBS/1% BSA/1%DMSO/0.5% Triton X-100 (PBDT), and then blocked with PBDT/10% goat serum for 1 hour at room temperature before incubation with the primary antibody overnight at 4°C.

Day 2: secondary antibody incubation

The following day, the samples were washed four times in PBDT for 30 min and then incubated with a secondary antibody at room temperature for 2 hours. Samples were then incubated with 1 µg/ml DAPI for 10 minutes and washed three times with PBS/0.1% Tween for 5 minutes. Samples were mounted in 1.4% low-melt agarose for imaging.

1. Inhibitor treatments

Zebrafish embryos were treated with 1 µM of Notch inhibitor RO 4929097 from 24 hpf to 48 hpf. At 48 hpf, the embryos were washed twice with egg water containing 0.1% (w/v) 1-phenyl-2-thiourea (PTU) and mounted in 1.4% low-melting point agarose containing 1.6 mg/ml Tricaine prior to imaging.

Zebrafish embryos were treated with 1 µM MEK inhibitor PD 0325901 or 10 µM ErbB2 inhibitor PD 168393 for 16 hours from 56 hpf. At 72 hpf, larvae were washed twice with PTU egg water and mounted in 1.4% low-melting agarose containing 1.6 mg/ml tricaine prior to imaging.

2. EdU staining

Zebrafish embryos were treated with 1 mM EdU dissolved in 1% DMSO in PTU egg water for 24 hours (from 48 hpf to 72 hpf) or 44 hours (from 28 hpf to 72 hpf). At 72 hpf, treated larvae were washed twice with PTU egg water. Larvae were then anesthetized with 0.2% (w/v) tricaine for 5 min before being fixed in 4% PFA for 2 hours at room temperature. The CLICK-IT reaction for EdU labeling was conducted as described by the manufacturer. Samples were processed for immunostaining on Day 2 using the procedure described above and mounted in 1.4% low-melting agarose for imaging.

3.2.3 Transgenic line generation

In order to generate transgenic line *Tg(UAS:irsp53^{dn}-p2a-tagRFP)*, a dominant negative form of *irsp53* (Meyen et al., 2015; Millard et al., 2005) was first amplified with the following primers: forward, 5'-TTCGAATTAGATCTGTCGACCGCCACCATGTCTCGCACCGACGAGGT-3'; reverse, 5'-GTAGCTCCGCTTCCACGCGTCTGTGCAAAGCCTGCCATGC-3'. The amplification was then cloned into the upstream of tagRFP in a 5xUAS-p2a vector.

3.2.4 Confocal imaging

Confocal images were acquired by Zeiss LSM800 with a 40x/1.1 W objective or by LSM 880 with a 20x/1.1 W objective.

Confocal videos were acquired under a 40x objective at 100 frames/second with a Hamamatsu ORCA flash 4.0 sCMOS camera. To achieve a calculated pixel resolution of 0.7 µm, the image was binned 4x4.

3.2.4.1 Live imaging of stopped hearts

To stop the heartbeat, zebrafish embryos were mounted in 1.4% low-melt agarose containing 1.6 mg/ml tricaine on glass-bottom dishes.

3.2.4.2 Live imaging of beating hearts

Zebrafish embryos were mounted in 0.8% low-melting agarose containing 0.2 mg/ml tricaine on glass-bottom dishes. Egg water containing 0.2 mg/ml tricaine was then added to the solidified agarose.

3.2.5 Image processing and analysis

Imaris x64 was used to process the images. Images were processed using Adobe Photoshop.

3.2.6 Quantification

The number of endocardial protrusions was counted from the ventricular maximum intensity projections at 24 hpf. The number of endocardial protrusions was counted in the ventricular mid-sagittal plane at 48 hpf.

The ratio of trabecular CMs was calculated as reported previously (Jimenez-Amilburu et al., 2016). For counting the number of trabeculae in the ventricular outer curvature, the trabeculae from the mid-sagittal plane were counted, and the delaminating CMs were counted as trabeculae as well. For counting the number of trabecular CMs in the ventricular outer curvature, the trabecular CMs from the mid-sagittal plane were counted. The number of multilayered CMs in the ventricular outer curvature was also counted from the mid-sagittal plane.

EdU-positive and Gmnn-positive cells were counted in the whole ventricle.

For measuring the volume of CJ, the paintbrush, the drawing tool in Fiji, was utilized to mark the space between the endocardium and myocardium in the ventricular outer curvature of the ventricle, and then a function of 3D surface reconstruction in Imaris was applied.

To determine the heart rate, the number of the heartbeat was counted in one minute. To calculate the ejection fraction, the systolic and diastolic ventricular areas were measured, and the following formula was used:

$$ejection\ fraction\ (\%) = \frac{diastole - systole}{diastole} \times 100$$

3.2.7 Statistical analysis

The sample size is indicated in each figure, one spot corresponds to one sample. The Student's *t*-test (two-tailed) was used to analyze all quantifications in GraphPad Prism 8. Statistically significant changes are considered when $p<0.05$. Exact *P* values are given in each figure.

4 Results

Parts of this chapter (**4 Results**) have been published as an article in the journal *eLife* (Qi et al. eLife 2022; 11: e73231. DOI: https://doi.org/10.7554/eLife.73231) (Qi et al., 2022).

The authors' contribution was described in the paper as follows:

Jialing Qi, Conceptualization, Data curation, Investigation, Methodology, Project administration, Vali-dation, Visualization, Writing – original draft; Annegret Rittershaus, Rashmi Priya, Shivani Mansingh, Resources; Didier YR Stainier, Conceptualization, Funding acquisition, Resources, Software, Super-vision, Writing - review and editing; Christian SM Helker, Conceptualization, Funding acquisition, Project administration, Resources, Supervision, Writing - original draft, Writing - review and editing.

4.1 Endocardial-myocardial interactions during trabeculation in zebrafish

4.1.1 Phases of endocardial-myocardial interaction during trabeculation

The trabeculation stages in mouse have been defined as endocardial sprouting, touchdown formation, endocardial ingression, trabecular extension, and termination (del Monte-Nieto et al., 2018). To investigate whether these stages are evolutionary conserved, I examined the endocardial-myocardial interactions in zebrafish. The early embryonic zebrafish heart consists of two cell types: endocardial cells and myocardial cells (Figure 8A-D). Endocardial cells form the endocardium and myocardial cells form the myocardium. The initial myocardium (Figure 8A and B) and the compact myocardium at 60 and 72 hpf (Figure 8C and D) are monolayers. To investigate the possible interactions between the endocardium and myocardium, I used the *TgBAC(cdh5:Gal4ff); Tg(UAS:LIFEACT-GFP)* lines to label the actin

cytoskeleton of EdCs, and the *Tg(myl7:mCherry-CAAX)* line to label the membrane of CMs. I found endocardial protrusions extending towards the myocardium at 24 (Figure 8A-A'') and 48 hpf (Figure 8B-B''). Subsequently, these ventricular endocardial protrusions form anchor points with the myocardium and are consistent with the observations in mouse (del Monte-Nieto et al., 2018), I also named these anchor points as touchdowns (Figure 8B-B''). Remarkably, these touchdowns are stable during cardiac contractions (Figure 8E-H). Approximately at 60 hpf, the CMs start to delaminate from the compact myocardium towards the lumen to seed the trabecular layer (Figure 8C, C', and C''''), consistent with the previous report (Priya et al., 2020). After this step, the trabecular CMs begin to assemble into "finger-like" multicellular projections, as known as trabeculae, at 72 hpf (Figure 8D, D', and D'''').

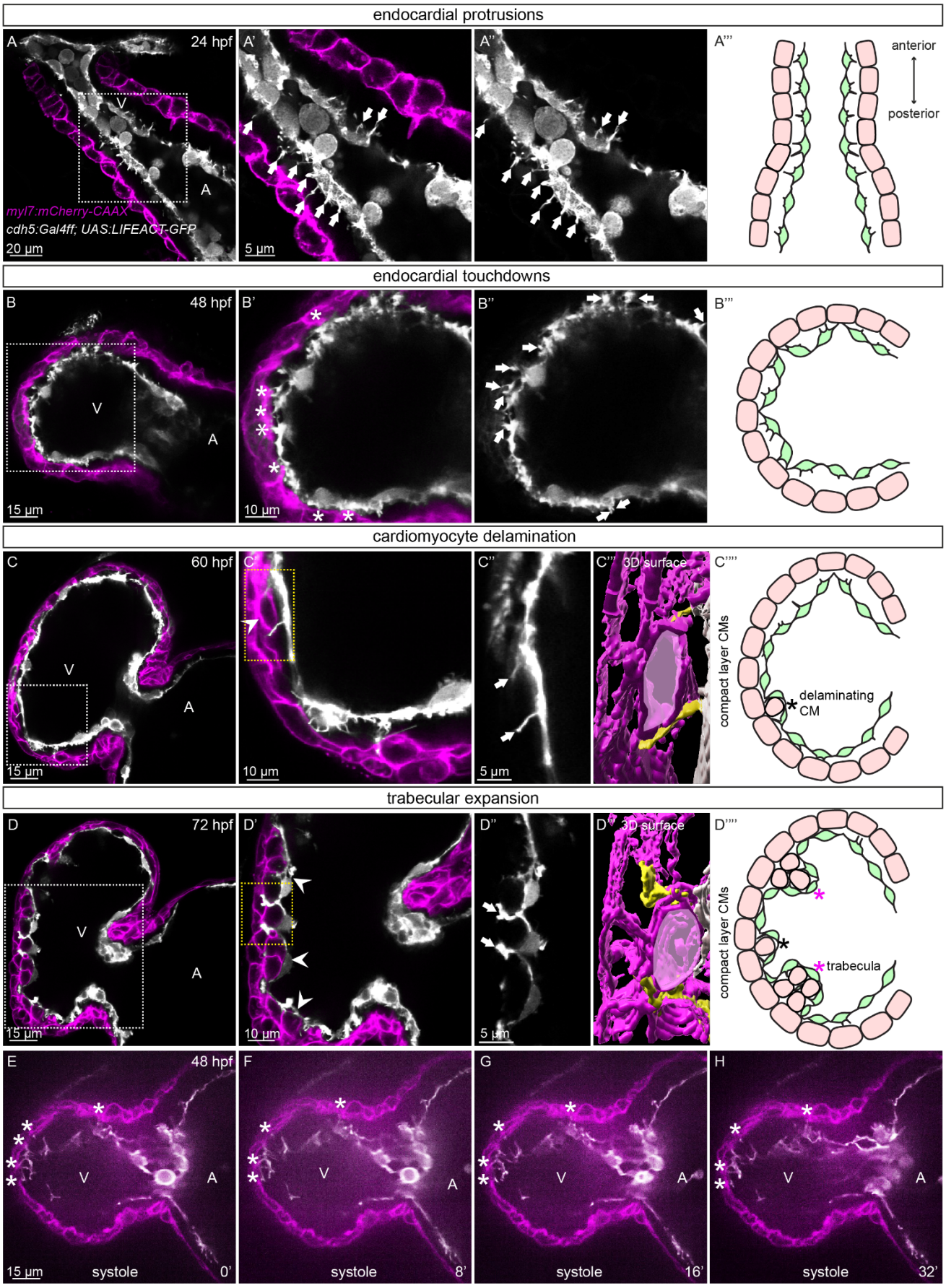
endocardial protrusions
A
24 hpf
V
A
myl7:mCherry-CAAX
cdh5:Gal4ff; UAS:LIFEACT-GFP
20 µm
A'
5 µm
A''
A'''
anterior
posterior
endocardial touchdowns
B
48 hpf
V
A
15 µm
B'
10 µm
B''
B'''
cardiomyocyte delamination
C
60 hpf
V
A
15 µm
C'
10 µm
C''
5 µm
C'''
3D surface
C''''
compact layer CMs
delaminating CM
trabecular expansion
D
72 hpf
V
A
15 µm
D'
10 µm
D''
5 µm
D'''
3D surface
D''''
compact layer CMs
trabecula
E
48 hpf
V
A
15 µm
systole
0'
F
V
A
systole
8'
G
V
A
systole
16'
H
V
A
systole
32'

Figure 8. Phases of endocardial-myocardial interactions during heart development in zebrafish.

(A-D) Confocal images of the heart of *Tg(myl7:mCherry-CAAX)*; *Tg(cdh5:Gal4ff)*; *Tg(UAS:LIFEACT-GFP)* zebrafish at 24 **(A)**, 48 **(B)**, 60 **(C)** and 72 **(D)** hpf. **(A-A'')** Area in white box shown in **(A'-A'').** Endocardial protrusions extend towards the myocardium at 24 hpf. **(B-B'')** Area in white box shown in **(B'-B'')**. Endocardial protrusions and touchdowns can be detected between the endocardium and the myocardium at 48 hpf. **(C-C''')** Area in white box shown in **(C')**. Area in yellow box shown in **(C''-C''')**. CMs delaminate from the myocardial compact layer at 60 hpf. **(C''')** 3D surface rendering of the boxed area in **C'.** **(D-D''')** Area in white box shown in **(D')**. Area in yellow box shown in **(D''-D''')**. CMs form cardiac trabeculae at 72 hpf. **(D''')** 3D surface rendering of the boxed area in **D'**. **(A''''-D'''')** Schematic representations of endocardial protrusions, endocardial touchdowns, CM delamination, and trabecular expansion. **(E-H)** Still images from a spinning disk time-lapse of the heart of *Tg(myl7:mCherry-CAAX)*; *Tg(cdh5:Gal4ff)*; *Tg(UAS:LIFEACT-GFP)* at 48 hpf. Arrows point to endocardial protrusions; arrowheads point to delaminating CMs or trabeculae; white asterisks indicate touchdowns; black asterisks indicate delaminating CMs; purple asterisks indicate trabeculae; numbers in the bottom right corner refer to seconds. All images are ventral views, anterior to the top. V, ventricle; A, atrium.

4.1.2 Direction and distribution of endocardial protrusions

Next, I studied the direction as well as the distribution of endocardial protrusions. At 48, 60, and 72 hpf, I found that most of endocardial protrusions extend in the direction of the myocardium (Figure 9A) and more endocardial protrusions in the ventricle than in the atrium (Figure 9B). A very interesting finding is the observation that endocardial protrusions extend along, and sometimes around the delaminating and trabecular CMs at 60 and 72 hpf (Figure 9D and E).

I then analyzed the correlation between the endocardial protrusions and delaminating/ trabecular CMs. In zebrafish, cardiac trabeculae are mainly observed in the outer curvature of the ventricle (Liu et al., 2010). Interestingly, the endocardial protrusions are mostly located in the outer curvature of the ventricle at 48, 60, and 72 hpf (Figure 9C-F). Furthermore, 69% of all endocardial protrusions in the outer curvature are in close proximity to delaminating CMs at 60 hpf, and 91% of all endocardial protrusions in the outer curvature are in close proximity to trabecular CMs at 72 hpf (Figure 9D, E, and G). 98% of delaminating CMs and 93% of trabecular CMs are close to endocardial protrusions at 60 and 72 hpf, respectively (Figure 9D, E, and H). The temporal and spatial correlations suggest that endocardial protrusions play a role during cardiac trabeculation.

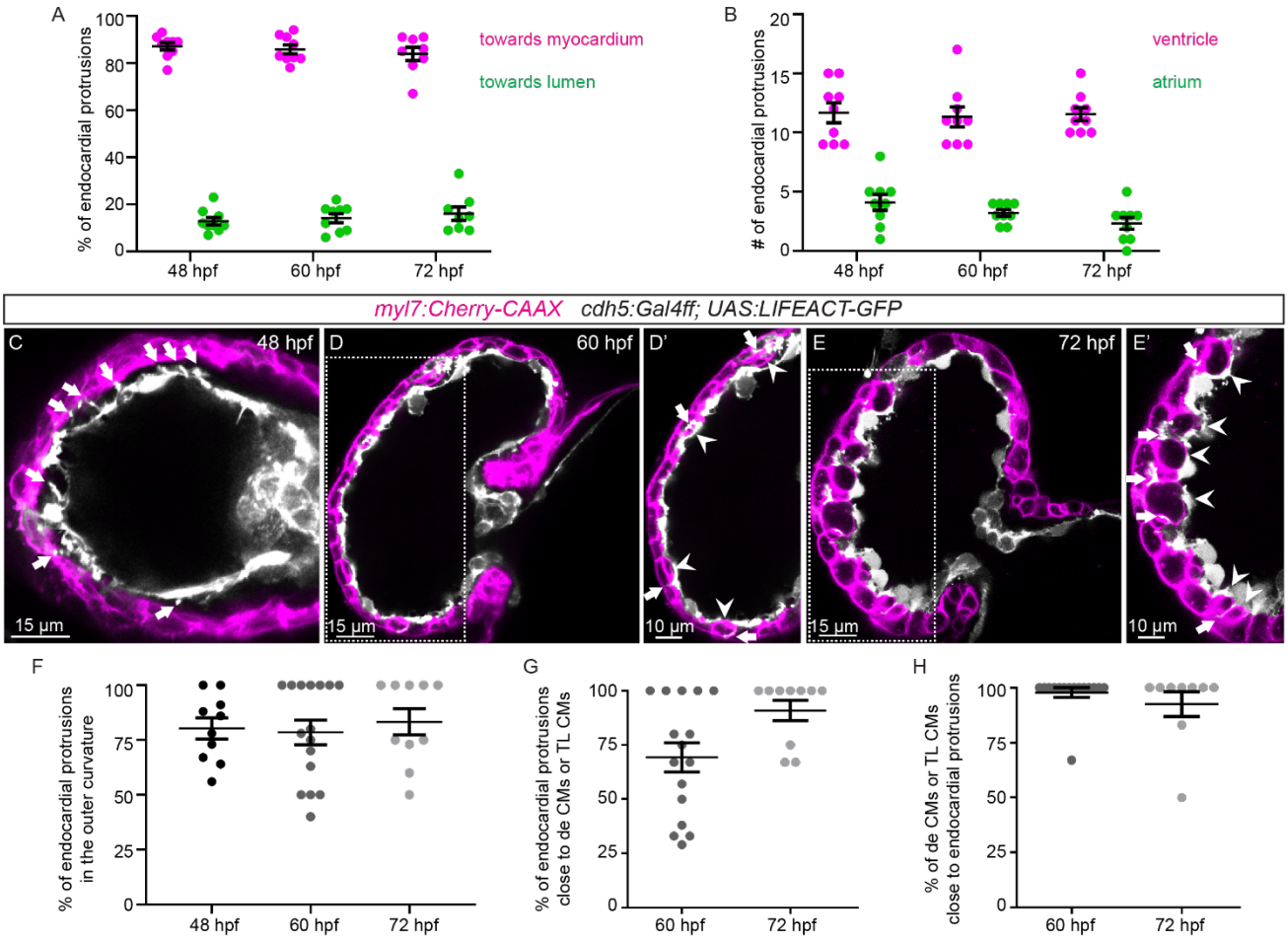

Figure 9. Most ventricular endocardial protrusions are present in the outer curvature and are close to delaminating or trabecular CMs.

(A) Graphic showing the direction of endocardial protrusions. **(B)** Graphic showing the average number of endocardial protrusions in the ventricle and atrium. **(C-E)** Confocal images of the heart of *Tg(myl7:mCherry-CAAX)*; *Tg(cdh5:Gal4ff)*; *Tg(UAS:LIFEACT-GFP)* zebrafish at 48 **(C),** 60 **(D)** and 72 **(E)** hpf. **(F)** Graphic showing the percentage of endocardial protrusions in the outer curvature of the ventricle. **(G)** Graphic showing the percentage of endocardial protrusions close to delaminating CMs or trabecular CMs. **(H)** Graphic showing the percentage of delaminating CMs or trabecular CMs close to endocardial protrusions. de CM, delaminating CM; TL CM, trabecular layer CM. Arrows point to endocardial protrusions; arrowheads point to delaminating CMs and trabecular CMs close to endocardial protrusions.

4.2 Genetically blocking endocardial protrusion formation reduces cardiac growth

4.2.1 Genetically block endocardial protrusion formation via using *Tg(UAS: irsp53dn-p2a-RFP)* line

As mentioned in **4.1.2**, I proposed that there are correlations between endocardial protrusions and myocardial trabeculation, whereupon I decided to study the role of endocardial protrusions during cardiac growth. To achieve this goal, a transgenic line, *Tg(UAS: irsp53^{dn}-p2a-RFP)* (Figure 10A), was generated to specifically block protrusion formation in the endothelium by crossing it to *TgBAC(cdh5:Gal4ff)*. IRSp53 is known to modulate the formation of different types of membrane extensions in cells via regulating the actin cytoskeleton (Millard et al., 2005; Nakagawa et al., 2003; Scita et al., 2008). Overexpressing Irsp53^{dn} specifically in endothelial cells resulted in a 70% reduction in the number of endocardial protrusions at 48 hpf (Figure 10B-D), while their distribution remained essentially unaffected (Figure 10E-E').

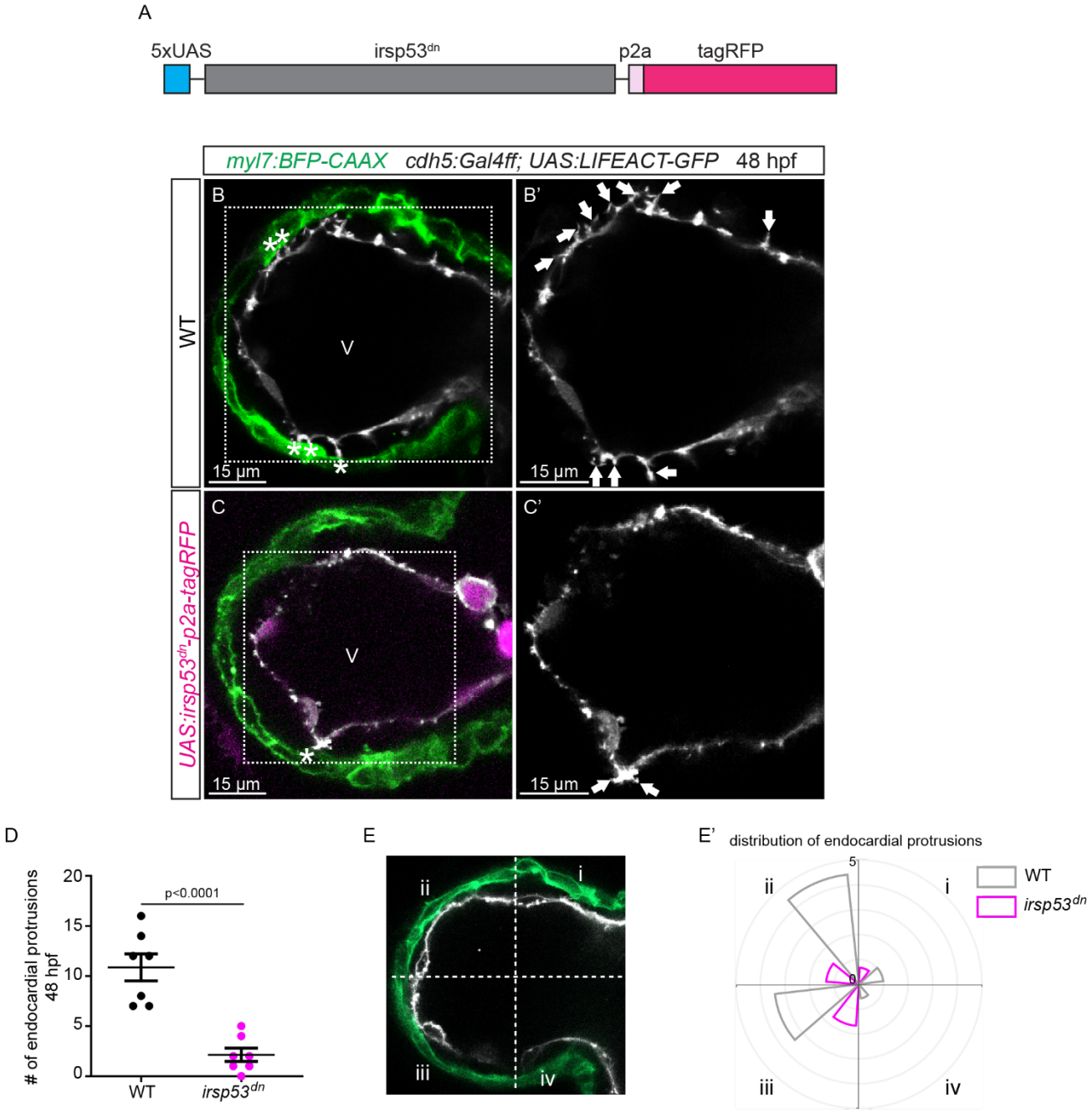
A
5xUAS
irsp53dn
p2a
tagRFP
myl7:BFP-CAAX cdh5:Gal4ff; UAS:LIFEACT-GFP 48 hpf
WT
UAS:irsp53dn-p2a-tagRFP
B
B'
C
C'
V
15 µm
D
# of endocardial protrusions 48 hpf
p<0.0001
WT
irsp53dn
E
i
ii
iii
iv
E'
distribution of endocardial protrusions
WT
irsp53dn

Figure 10. The construct for the overexpression of the dominant-negative form of *irsp53* in the endothelium inhibits the formation of endocardial protrusions.
(A) Construct used for the generation of *Tg(UAS:irsp53^{dn}-p2a-tagRFP)* line. **(B-C)** Confocal images of the heart of *Tg(myl7:BFP-CAAX)*; *Tg(cdh5:Gal4ff)*; *Tg(UAS:LIFEACT-GFP)*; +/- *Tg(UAS:irsp53^{dn}-p2a-tagRFP)* zebrafish at 48 hpf. Endocardial protrusions and touchdowns are diminished in embryos with endothelial overexpression of *irsp53^{dn}* **(C)**. **(D)** Graphic showing the number of endocardial protrusions in wild-type and *irsp53^{dn}* embryos at 48 hpf. **(E-E')** The ventricle is defined into 4 regions by individual dash line at 48 hpf **(E)**. Distribution and average number of endocardial protrusions in different regions of the ventricle in mid-sagittal sections from 48 hpf wild-type and *irsp53^{dn}* embryos **(E')**. Arrows point to endocardial protrusions; white asterisks indicate touchdowns. All images are ventral views, anterior to the top. V, ventricle; A, atrium.

4.2.2 Genetically blocking endocardial protrusion formation reduces myocardial trabeculation

To test the hypothesis that endocardial protrusions modulate myocardial trabeculation, I analyzed embryos overexpressing *irsp53*^{dn} in their EdCs in a CM membrane line (*Tg(myl7:BFP-CAAX)*). In contrast to the wild-type, the larvae with *irsp53*^{dn} overexpression in ECs exhibit a reduction in cardiac trabeculation (Figure 11).

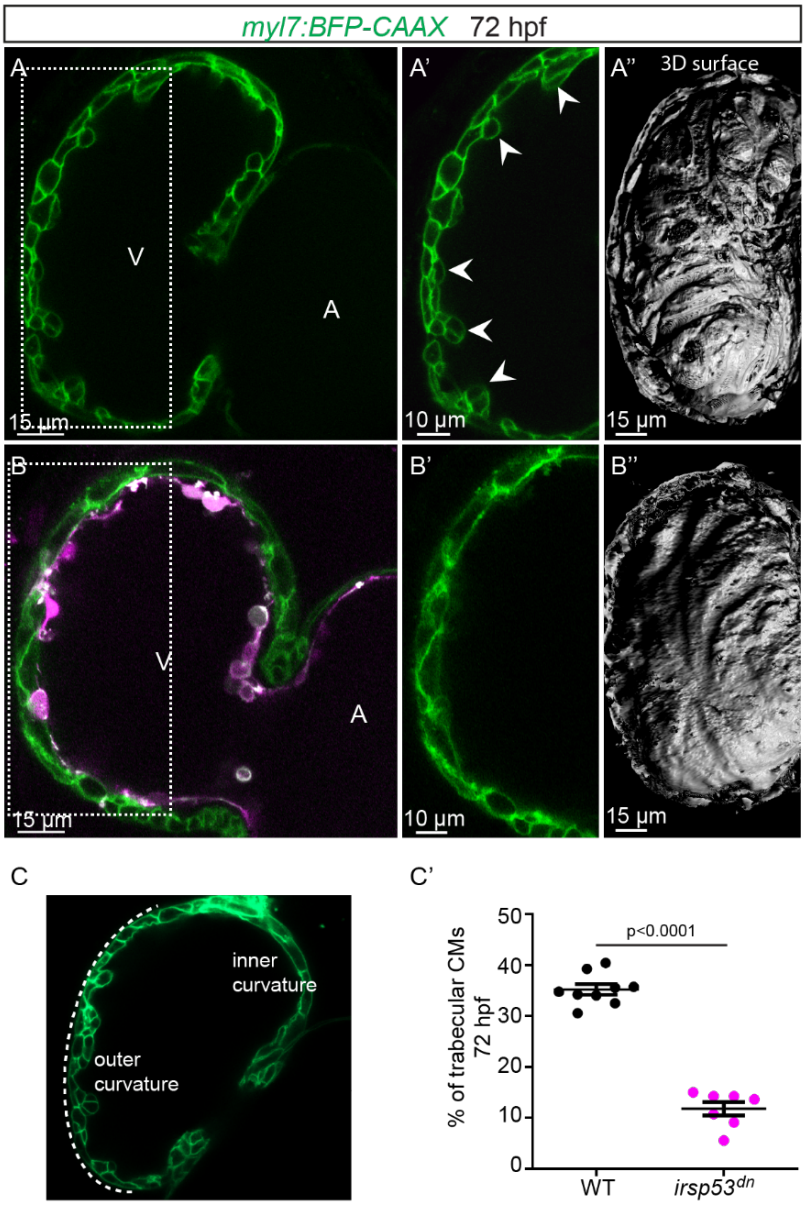

Figure 11. Blocking endocardial protrusion formation reduces cardiac trabeculation. **(A-B)** Confocal images of the heart of *Tg(myl7:BFP-CAAX)*; *Tg(cdh5:Gal4ff)*; *Tg(UAS:LIFEACT-GFP)*; +/- *Tg(UAS:irsp53^{dn}-p2a-tagRFP)* zebrafish at 72 hpf. Cardiac trabeculation is diminished in larvae with endothelial overexpression of *irsp53^{dn}*; **(A''-B'')** 3D rendering. **(C-C')** The ventricle is separated into the outer and inner curvature by dash line at 72 hpf **(C)**. Graphic showing the percentage of trabecular CMs in the outer curvature of wild-type and *irsp53^{dn}* larvae at 72 hpf **(C').** Arrowheads point to trabeculae. All images are ventral views, anterior to the top. V, ventricle; A, atrium. Data in graphs expressed as mean ± SEM.

4.2.3 Genetically blocking endocardial protrusion formation reduces CM proliferation

To further analyze a possible effect of endocardial protrusions upon CM proliferation, I overexpressed the *irsp53^{dn}* in the endothelium in the context of the *Tg(myl7:mVenus-gmnn)* reporter to visualize cycling CMs. In contrast to wild-type, larvae with *irsp53^{dn}* overexpression in the ECs show fewer mVenus-Gmnn^{+} CMs in the ventricle (Figure 12).

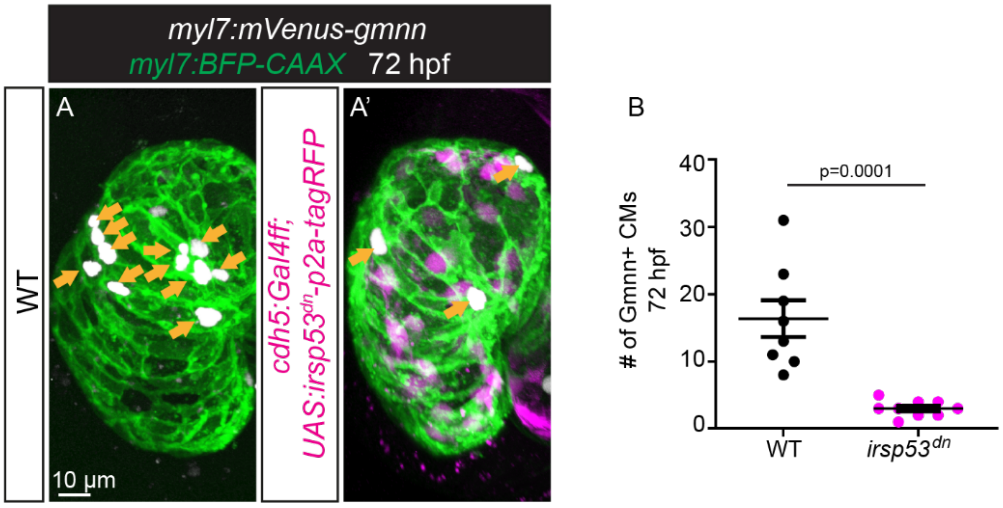

Figure 12. Blocking endocardial protrusion formation reduces CM proliferation. **(A-A')** Confocal images of the heart of *Tg(myl7:BFP-CAAX)*; *Tg(myl7:mVenus-gmnn)*; +/- *Tg(UAS:irsp53^{dn}-p2a-tagRFP)* zebrafish at 72 hpf. Fewer proliferating CMs are observed in the ventricle of the larvae with endothelial overexpression of *irsp53^{dn}*. **(B)** Graphic showing the number of mVenus-Gmnn^{+} CMs in the ventricle of wild-type and *irsp53^{dn}* larvae at 72 hpf. Yellow arrows point to mVenus-Gmnn^{+} CMs. All images are ventral views, anterior to the top. Data in graphs given as mean ± SEM.

4.3 The role of Apelin signaling during endocardial protrusion formation and myocardial trabeculation

4.3.1 The expression pattern of the components of the Apelin signaling pathway

It was recently reported that Apelin signaling pathway positively mediates the formation of endothelial protrusion during angiogenesis in the zebrafish trunk (Helker et al., 2020). Hence, I hypothesized that Apelin signaling regulates endocardial protrusion formation. The *TgBAC(apln:EGFP)* line (Helker et al., 2020) and the *Tg(aplnrb:VenusPEST)* line were used to visualize the expressions of *apln* and *aplnrb*, respectively, at single-cell resolution respectively. *apln*:EGFP expression was detected in the myocardium at 48 and 72 hpf (Figure 13A and B). Moreover, *aplnrb:*VenusPEST expression was detected in the endocardium at 48 and 72 hpf (Figure 13 C and D). These results show that *apln* is expressed in the myocardium, while *aplnrb* is expressed in EdCs. Based on these results, I hypothesized that Apelin signaling contributes to endocardial-myocardial interactions.

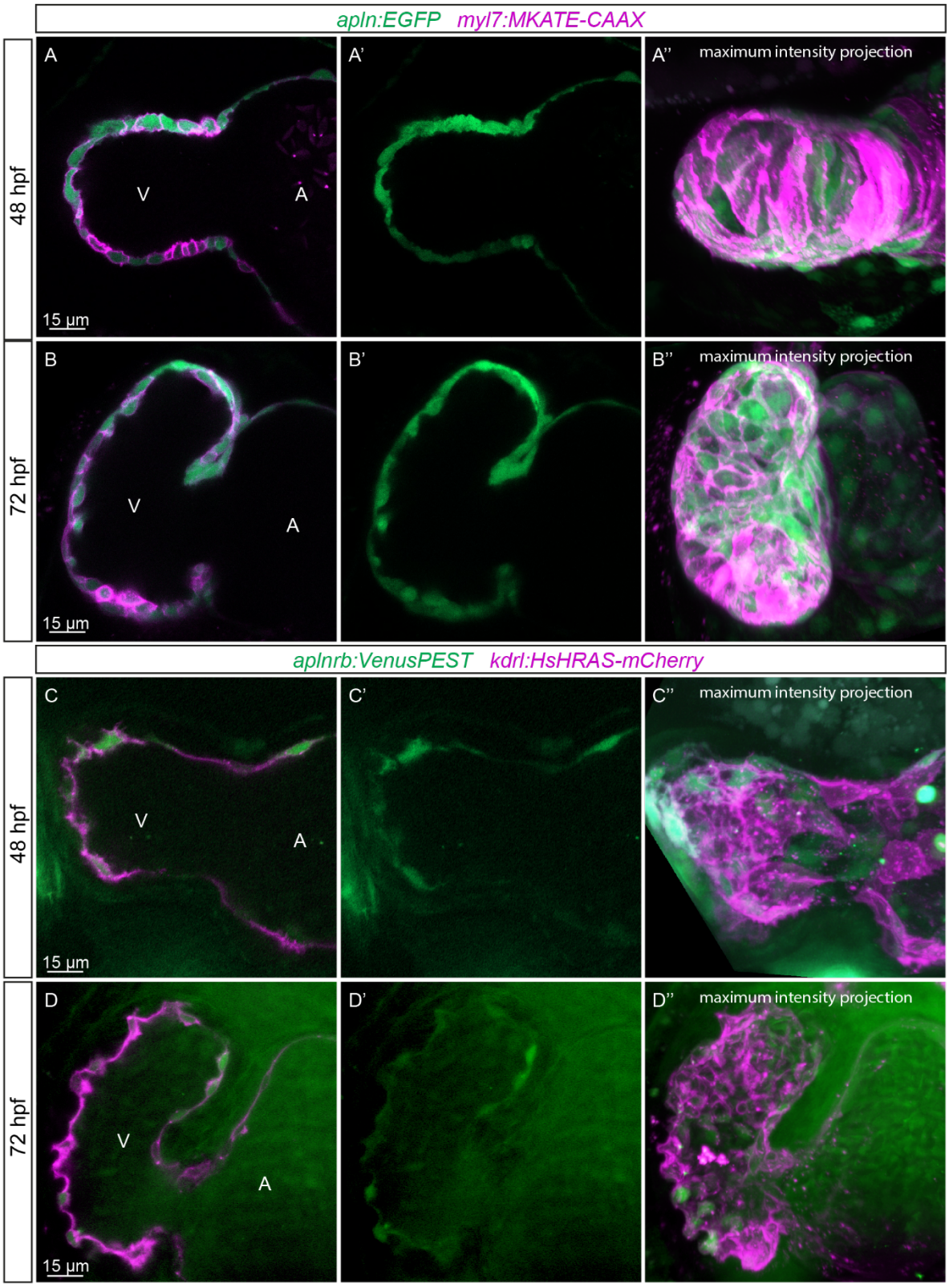
apln:EGFP myl7:MKATE-CAAX
48 hpf
A
A'
A''
maximum intensity projection
V
A
15 µm
72 hpf
B
B'
B''
maximum intensity projection
V
A
15 µm
aplnrb:VenusPEST kdrl:HsHRAS-mCherry
48 hpf
C
C'
C''
maximum intensity projection
V
A
15 µm
72 hpf
D
D'
D''
maximum intensity projection
V
A
15 µm

Figure 13. Expression pattern of Apelin signaling pathway elements.

(A-D) Confocal images of the heart of *TgBAC(apln:EGFP); Tg(myl7:MKATE-CAAX)* **(A, B)** and *TgBAC(aplnrb:VenusPEST); Tg(kdrl:HsHRAS-mCherry)* **(C, D)** zebrafish at 48 **(A, C)** and 72 **(B, D)** hpf. **(A''-D'')** Confocal images of maximum intensity projections. **(A-B)** *TgBAC(apln:EGFP)* expression is detected in the myocardium at 48 **(A)** and 72 **(B)** hpf. **(C-D)** *TgBAC(aplnrb:VenusPEST)* expression is detected in the endocardium at 48 **(C)** and 72 **(D)** hpf. All images are ventral views, anterior to the top. V, ventricle; A, atrium.

4.3.2 Apelin signaling positively regulates endocardial protrusion formation and myocardial trabeculation

4.3.2.1 The phenotypes of *aplnra*, *aplnrb*, and *apela* mutants

To test the hypothesis that Apelin signaling is required for endocardium-myocardium interactions, I used the *aplnra* mutant (Helker et al., 2015), *aplnrb* mutant (Helker et al., 2015), *apln* mutant (Helker et al., 2015), and *apela* mutant (Chng et al., 2013). I did not analyze *apela* mutants because they fail to form a heart (Chng et al., 2013). Although most *aplnrb* mutants are unable to form a heart (Scott et al., 2007; Zeng et al., 2007), a low number of them are. I analyzed *aplnrb* mutants that can form a heart and found they display a reduced number of endocardial protrusions at 48 hpf (Figure 14A and B) and a reduced number of trabeculae at 72 hpf (Figure 14C and D). In wild-type larvae, the cardiac jelly (CJ) in the outer curvature of the ventricle between the endocardium and myocardium appears to be mainly degraded at 72 hpf (Figure 14C); however, the CJ appears to be thicker at 72 hpf in *aplnrb* mutants (Figure 14D). Additionally, *aplnra* mutants display a reduced number of trabeculae at 72 hpf as well (Figure 14E and F).

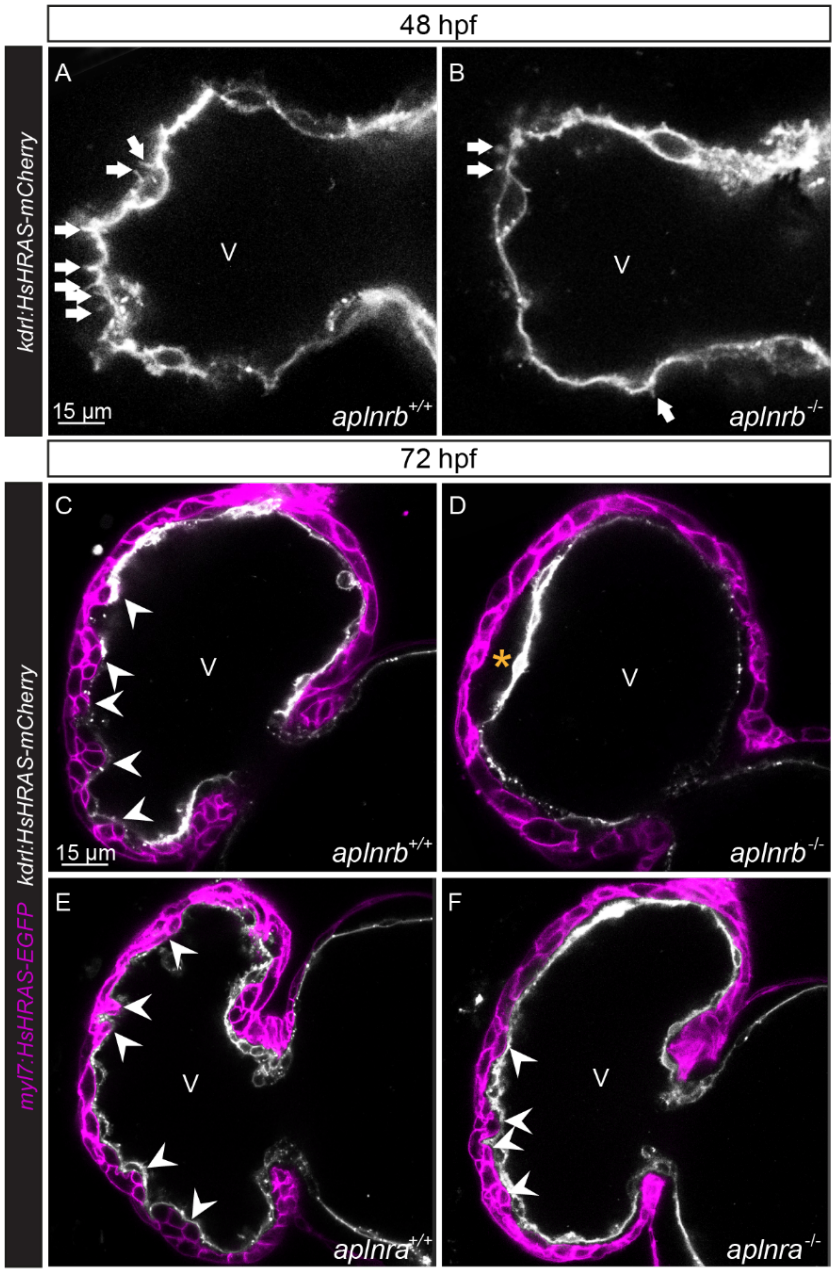

Figure 14. *aplnrb* mutants exhibit a reduction of endocardial protrusions and a reduction of trabeculae, and *aplnra* mutant exhibits a mild reduction in trabeculation.

(A–F) Confocal images of the heart of *Tg(kdrl:HsHRAS-mCherry)* **(A-B)** and *Tg(myl7:HsHRAS-EGFP); Tg(kdrl:HsHRAS-mCherry)* **(C-F)** zebrafish at 48 **(A-B)** and 72 **(C-F)** hpf. **(A–B)** Compared with *aplnrb*$^{+/+}$ siblings **(A)**, *aplnrb*$^{-/-}$ embryos **(B)** display fewer endocardial protrusions at 48 hpf. **(C-D)** Compared with *aplnrb*$^{+/+}$ siblings **(C)**, *aplnrb*$^{-/-}$ larvae **(D)** display reduced trabeculation and thicker CJ at 72 hpf. **(E-F)**

Compared with *aplnra*$^{+/+}$ siblings **(E)**, *aplnra*$^{-/-}$ larvae **(F)** display a mild reduction in trabeculation at 72 hpf. Arrows point to endocardial protrusions; arrowheads point to trabeculae; yellow asterisk indicates CJ. All images are ventral views, anterior to the top. V, ventricle.

4.3.2.2 The phenotypes of *apln* mutants

4.3.2.2.1 *apln* positively regulates the formation of endocardial protrusion

Since most of *apln* mutants form a heart, I focused the study on *apln* mutants. I examined the endocardial protrusion formation of *apln* mutants and observed a significantly reduced number of endocardial protrusions in the *apln* mutants at 24 and 48 hpf (Figure 15A-F). Consistent with the fewer number of endocardial protrusions, *apln* mutants also exhibit a reduced number of endocardial touchdowns at 48 hpf (Figure 15D, E, and G).

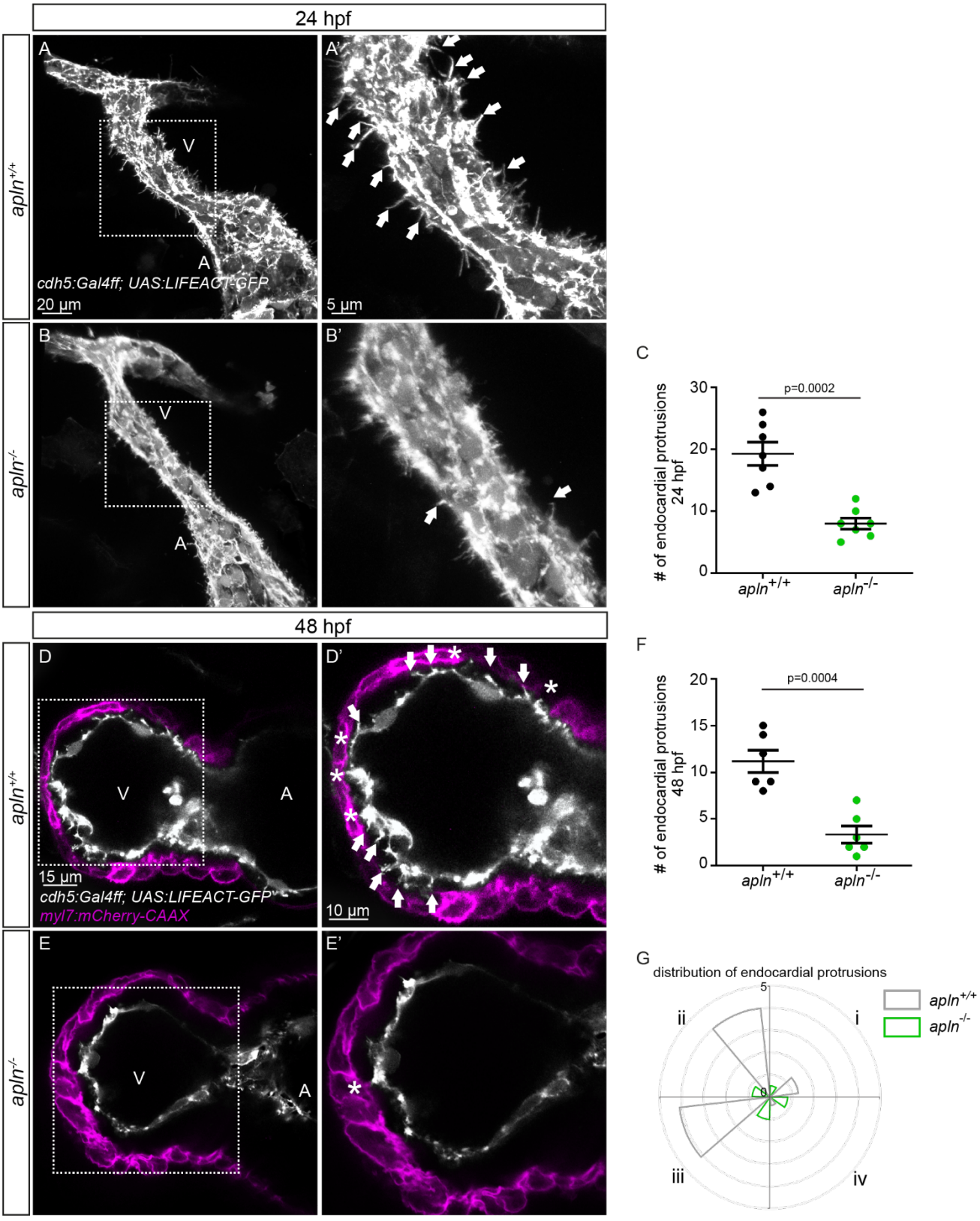
24 hpf
A
A'
V
A
cdh5:Gal4ff; UAS:LIFEACT-GFP
20 µm
5 µm
apln+/+
B
B'
V
A
apln-/-
48 hpf
D
D'
V
A
15 µm
cdh5:Gal4ff; UAS:LIFEACT-GFP
myl7:mCherry-CAAX
10 µm
E
E'
V
A
C
p=0.0002
# of endocardial protrusions 24 hpf
30
20
10
0
apln+/+
apln-/-
F
p=0.0004
# of endocardial protrusions 48 hpf
20
15
10
5
0
apln+/+
apln-/-
G
distribution of endocardial protrusions
5
ii
i
iii
iv
apln+/+
apln-/-

Figure 15. Loss of *apln* leads to a reduction of endocardial protrusions.
(A-B) Confocal maximum intensity projections of the heart of *Tg(cdh5:Gal4ff)*; *Tg(UAS:LIFEACT-GFP)* zebrafish at 24 hpf. Boxed area shown in **(A'-B')**. In contrast to $apln^{+/+}$ embryos **(A)**, the number of endocardial protrusions is reduced in $apln^{-/-}$ embryos **(B)** at 24 hpf. **(C)** Graphic showing the number of ventricular endocardial protrusions of $apln^{+/+}$ and $apln^{-/-}$ siblings at 24 hpf. **(D-E)** Confocal mid-sagittal sections of the heart of *Tg(myl7:mCherry-CAAX)*; *Tg (cdh5:Gal4ff)*; *Tg(UAS:LIFEACT-GFP)* zebrafish at 48 hpf. Boxed area shown in **(D'-E')**. In contrast to $apln^{+/+}$ embryos **(D)**, fewer endocardial protrusions and touchdowns are in $apln^{-/-}$ embryos **(E)** at 48 hpf. **(F)** Graphic showing the number of ventricular endocardial protrusions of $apln^{+/+}$ and $apln^{-/-}$ siblings at 48 hpf. **(G)** Average number and distribution of endocardial protrusions in the defined ventricular regions of mid-sagittal sections from $apln^{+/+}$ and $apln^{-/-}$ siblings at 48 hpf. Arrows point to endocardial protrusions; white asterisks indicate touchdowns. All images are ventral views, anterior to the top. V, ventricle; A, atrium. Data in graphs expressed as mean ± SEM.

4.3.2.2.2 *apln* positively regulates myocardial growth

To further investigate the role of Apelin-dependent endocardial protrusions during myocardial growth, I first decided to analyze trabeculation and found reduced cardiac trabeculation in *apln* mutants (Figure 16A-C). Next, I analyzed the proliferation of CM in *apln* mutants via the EdU labeling technique. In contrast to $apln^{+/+}$ siblings, $apln^{-/-}$ larvae display a significantly lower number of EdU^{+} CMs in their ventricle (Figure 16D-F). I also observed that $apln^{-/-}$ larvae exhibit a significantly thicker CJ in comparison with $apln^{+/+}$ siblings at 72 hpf (Figure 16G and H).

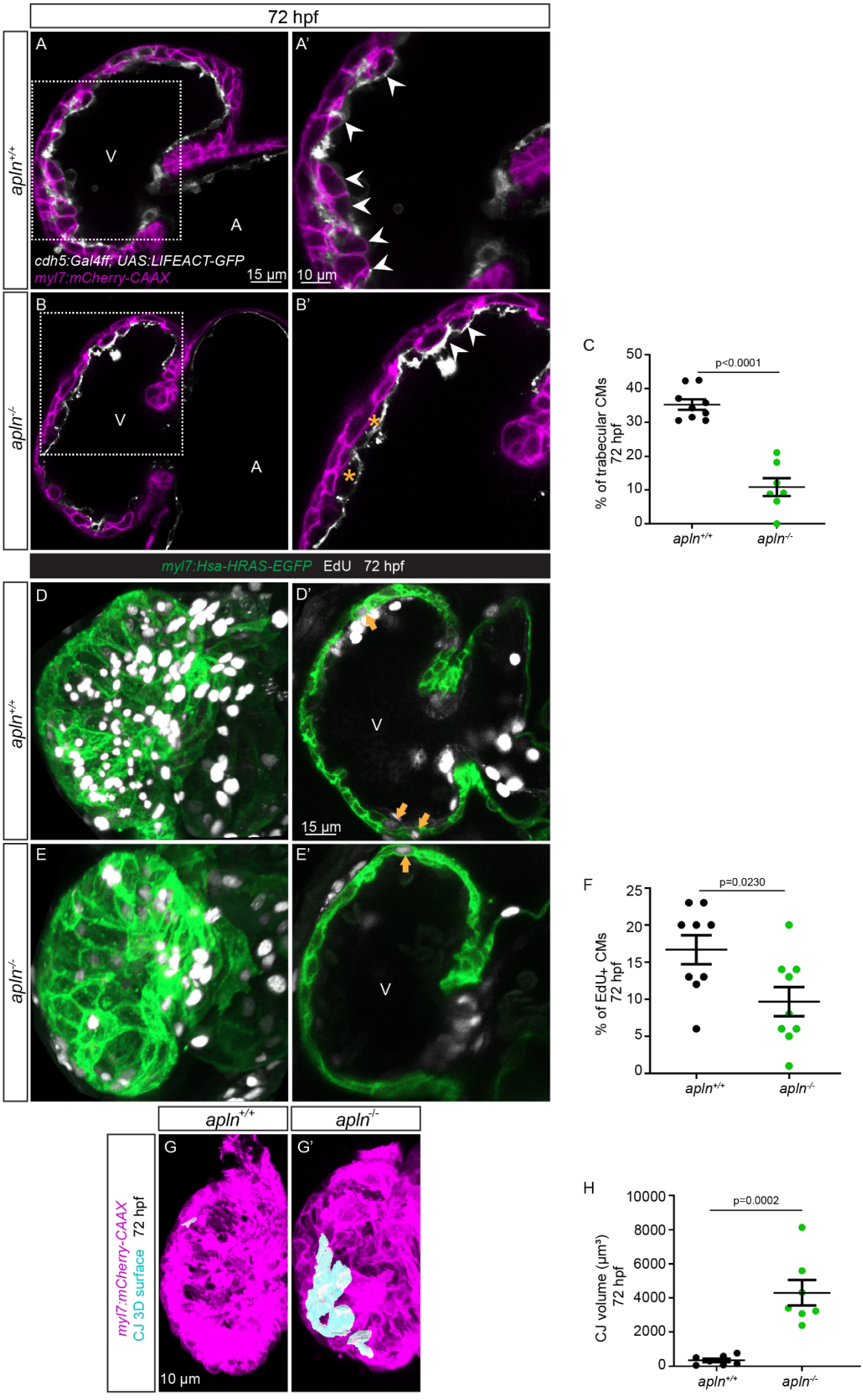
72 hpf
apln+/+
apln-/-
A
A'
B
B'
V
A
cdh5:Gal4ff; UAS:LIFEACT-GFP
myl7:mCherry-CAAX
15 µm
10 µm
myl7:Hsa-HRAS-EGFP EdU 72 hpf
D
D'
E
E'
15 µm
apln+/+
apln-/-
G
G'
myl7:mCherry-CAAX
CJ 3D surface
72 hpf
10 µm
C
% of trabecular CMs 72 hpf
p<0.0001
F
% of EdU+ CMs 72 hpf
p=0.0230
H
CJ volume (µm³) 72 hpf
p=0.0002

Figure 16. Loss of *apln* leads to reduced myocardial trabeculation and CM proliferation.

(A-B) Confocal images of the heart of *Tg(myl7:mCherry-CAAX)*; *Tg (cdh5:Gal4ff)*; *Tg(UAS:LIFEACT-GFP)* zebrafish at 72 hpf **(A-B)**. In contrast to $apln^{+/+}$ siblings **(A)**, $apln^{-/-}$ larvae **(B)** show impaired trabeculation and thicker CJ. **(C)** Graphic showing the percentage of trabecular CMs in the ventricular outer curvature of 72 hpf $apln^{+/+}$ and $apln^{-/-}$ siblings. **(D-E)** Confocal images of the heart of *Tg(myl7:HsHRAS-EGFP)* larvae at 72 hpf. **(D-E)** Confocal images of maximum intensity projections. **(D'-E')** Mid-sagittal sections of D and E, respectively. In contrast to $apln^{+/+}$ siblings **(D)**, $apln^{-/-}$ larvae **(E)** show fewer EdU^+ CMs in their ventricle. **(F)** Graphic showing the percentage of EdU^+ CMs of $apln^{+/+}$ and $apln^{-/-}$ siblings in their ventricle. **(G-G')** Maximum intensity projections. In contrast to $apln^{+/+}$ siblings **(G),** $apln^{-/-}$ larvae **(G')** show a thicker CJ at 72 hpf**. (H)** Graphic showing the CJ volume of $apln^{+/+}$ and $apln^{-/-}$ siblings in their outer curvature at 72 hpf. Arrowheads point to trabeculae; yellow asterisks indicate CJ; yellow arrows point to EdU^+ CMs. All images are ventral views, anterior to the top. V, ventricle; A, atrium. Data in graphs expressed as mean ± SEM.

4.3.2.2.3 Loss of *apln* does not impair sarcomere structure and cardiac function

To better understand the cardiac function in the context of *apln* deficiency, I performed Phalloidin Staining to label F-actin and found no obvious defects in the formation of sarcomere (Figure 17A and B). I then checked heart rate and ejection fraction in *apln* mutants and again there was no obvious difference between *apln* mutants and their wild-type littermates (Figure 17C and D). All these data indicate that the reason of myocardial trabeculation phenotype in *apln* mutants is the deficiency of endocardial protrusion formation and is not due to heart dysfunction.

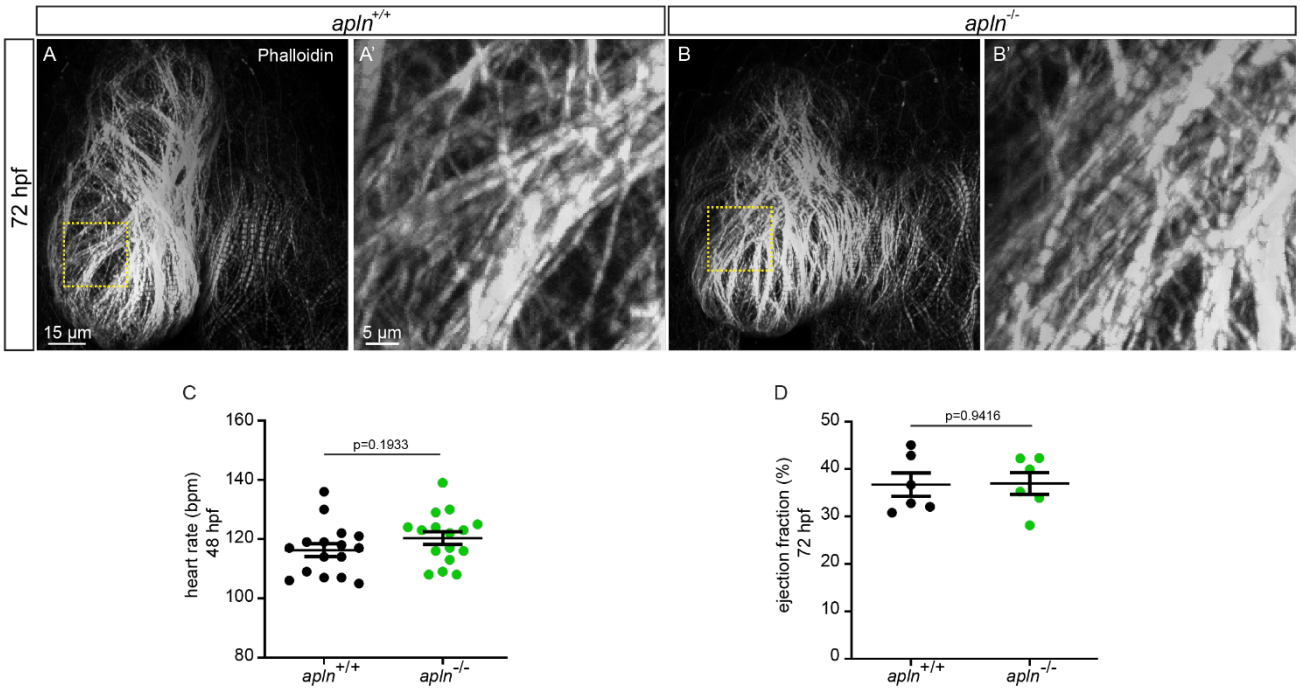

Figure 17. Wild-type like sarcomere structure and cardiac function in *apln*$^{-/-}$ larvae. **(A-B)** Confocal maximum intensity projection images of the heart of 72 hpf larvae stained with Phalloidin. Compared with *apln*$^{+/+}$ siblings **(A)**, sarcomere formation appears to be normal in *apln*$^{-/-}$ larvae **(B)** (*apln*$^{+/+}$, n=5; *apln*$^{-/-}$, n=4). **(C)** Graphic showing the heart rate of *apln*$^{+/+}$ and *apln*$^{-/-}$ siblings. **(D)** Graphic showing the ejection fraction of *apln*$^{+/+}$ and *apln*$^{-/-}$ siblings. All images are ventral views, anterior to the top. V, ventricle. Data in graphs expressed as mean ± SEM.

4.4 The role of Notch signaling during endocardial protrusion formation

Notch signaling is known to negatively regulate endothelial protrusion formation in several vascular beds in a negative manner (Hellstrom et al., 2007; Leslie et al., 2007; Siekmann & Lawson, 2007; Suchting et al., 2007). To investigate whether Notch signaling mediates endocardial protrusion formation as well, I inhibited Notch signaling by treating zebrafish embryos with the γ–secretase inhibitor RO4929097 and observed a decreased Notch expression in the endocardium (Figure 18A and B). Next, I treated *Tg(cdh5:Gal4ff)*; *Tg(UAS:LIFEACT-GFP)* embryos with the same inhibitor and observed an increased number of endocardial protrusions in the ventricle (Figure 18C, D, and G). However, the number of endocardial touchdowns is reduced in Notch inhibitor treated zebrafish embryos at 48 hpf, which is consistent with the phenotype of reduced touchdown in Notch deficient mice (Figure 18E, F, and H).

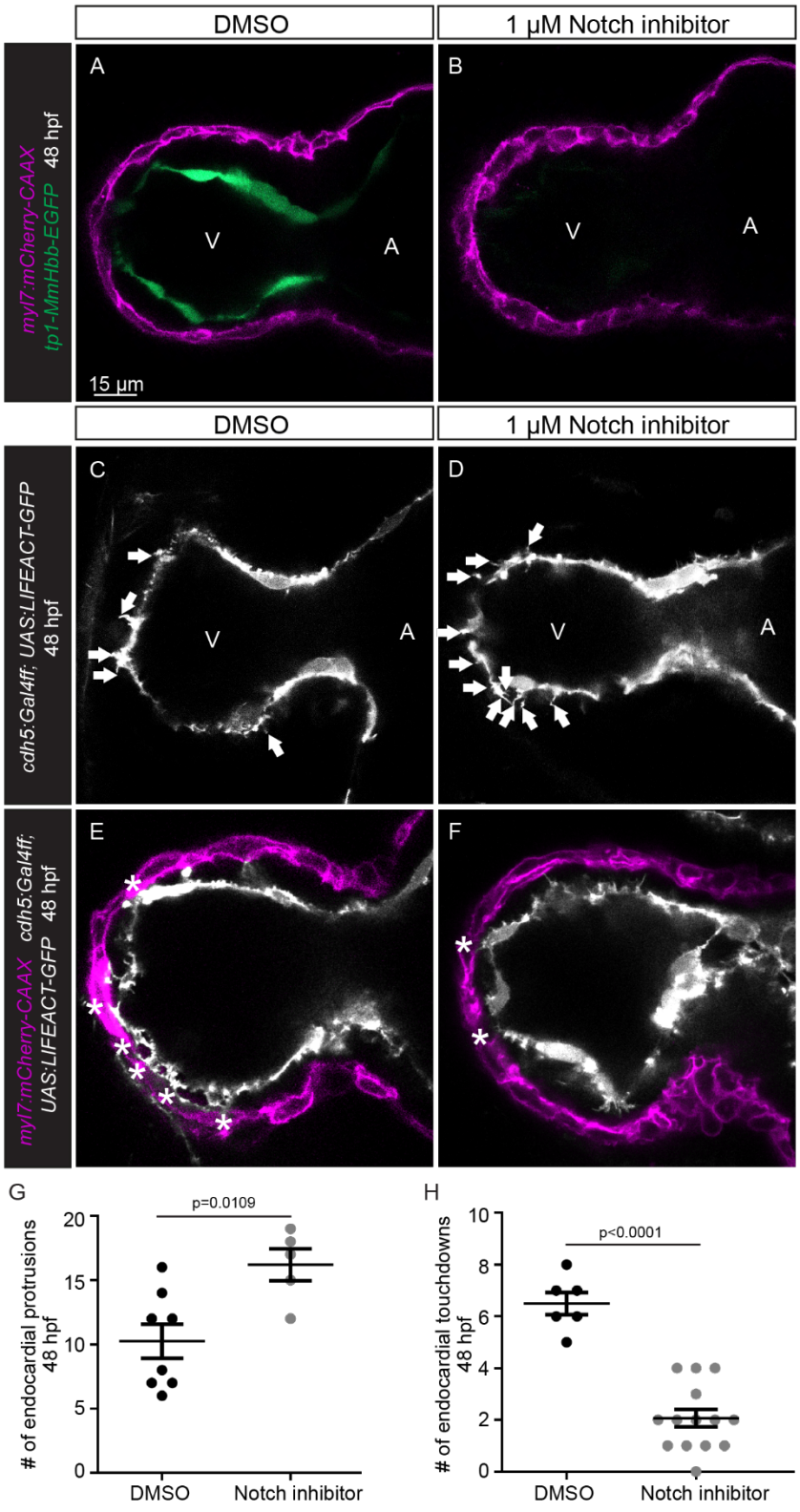
DMSO
1 µM Notch inhibitor
myl7:mCherry-CAAX
tp1-MmHbb-EGFP 48 hpf
A
B
V
A
15 µm
DMSO
1 µM Notch inhibitor
cdh5:Gal4ff; UAS:LIFEACT-GFP
48 hpf
C
D
V
A
myl7:mCherry-CAAX cdh5:Gal4ff;
UAS:LIFEACT-GFP 48 hpf
E
F
G
p=0.0109
# of endocardial protrusions
48 hpf
20
15
10
5
0
DMSO
Notch inhibitor
H
p<0.0001
# of endocardial touchdowns
48 hpf
10
8
6
4
2
0
DMSO
Notch inhibitor

Figure 18. Notch signaling suppresses endocardial protrusion formation.
(A-D) Confocal images of the heart of *Tg(myl7:mCherry-CAAX)*; *Tg(tp1-MmHbb:EGFP)* **(A-B)** and *Tg(cdh5:Gal4ff)*; *Tg(UAS:LIFEACT-GFP)* **(C-D)** embryos at 48 hpf. **(A-B)** Expression of the Notch reporter in the endocardium is blocked by the treatment of Notch inhibitor RO4929097 from 24 to 48 hpf. **(C-D)** Embryos treated with RO4929097 display more endocardial protrusions. **(E-F)** Embryos treated with RO4929097 display fewer endocardial touchdowns. **(G)** Graphic showing the number of ventricular endocardial protrusions in embryos treated with DMSO and Notch inhibitor at 48 hpf. **(H)** Graphic showing the number of ventricular endocardial touchdowns in DMSO and RO4929097 treated embryos at 48 hpf. Arrows point to endocardial protrusions; asterisks indicate touchdowns. All images are ventral views, anterior to the top. V, ventricle; A, atrium. Data in graphs are given as mean ± SEM.

4.5 Endocardial protrusions mediate the function of endocardial *nrg2a*

Nrg-ErbB signaling is one of the major signaling pathways for cardiac trabeculation in mouse and zebrafish (Gassmann et al., 1995; Lai et al., 2010; Lee et al., 1995; Liu et al., 2010; Meyer & Birchmeier, 1995; Rasouli & Stainier, 2017). Interestingly, the ligand Nrg is expressed in the endocardium (Meyer & Birchmeier, 1995; Rasouli & Stainier, 2017), while the receptor ErbB is expressed in the myocardium (Gassmann et al., 1995; Meyer & Birchmeier, 1995). To determine whether endocardial protrusions modulate Nrg-ErbB signaling, I first utilized a *Tg(fli1a:nrg2a-p2a-tdTomato)* line (Rasouli & Stainier, 2017) to overexpress *nrg2a* in the endocardium. Overexpressing *nrg2a* in the endothelium leads to hypertrabeculation as well as multilayered CMs (Figure 19A and B, 19G-I). Strikingly, overexpression of *nrg2a* in the endothelium, blocking endocardial protrusion formation by endothelial overexpression of *irsp53*^{dn}, resulting in a reduction in trabeculation and fewer multilayered CMs compared with controls (Figure 19E-E', 19G-I). Consistent with these results, overexpressing *nrg2a* in the endothelium of *apln* mutants also results in a reduction trabeculation and fewer multilayered CMs compared with controls (Figure 19F-F', 19G-I).

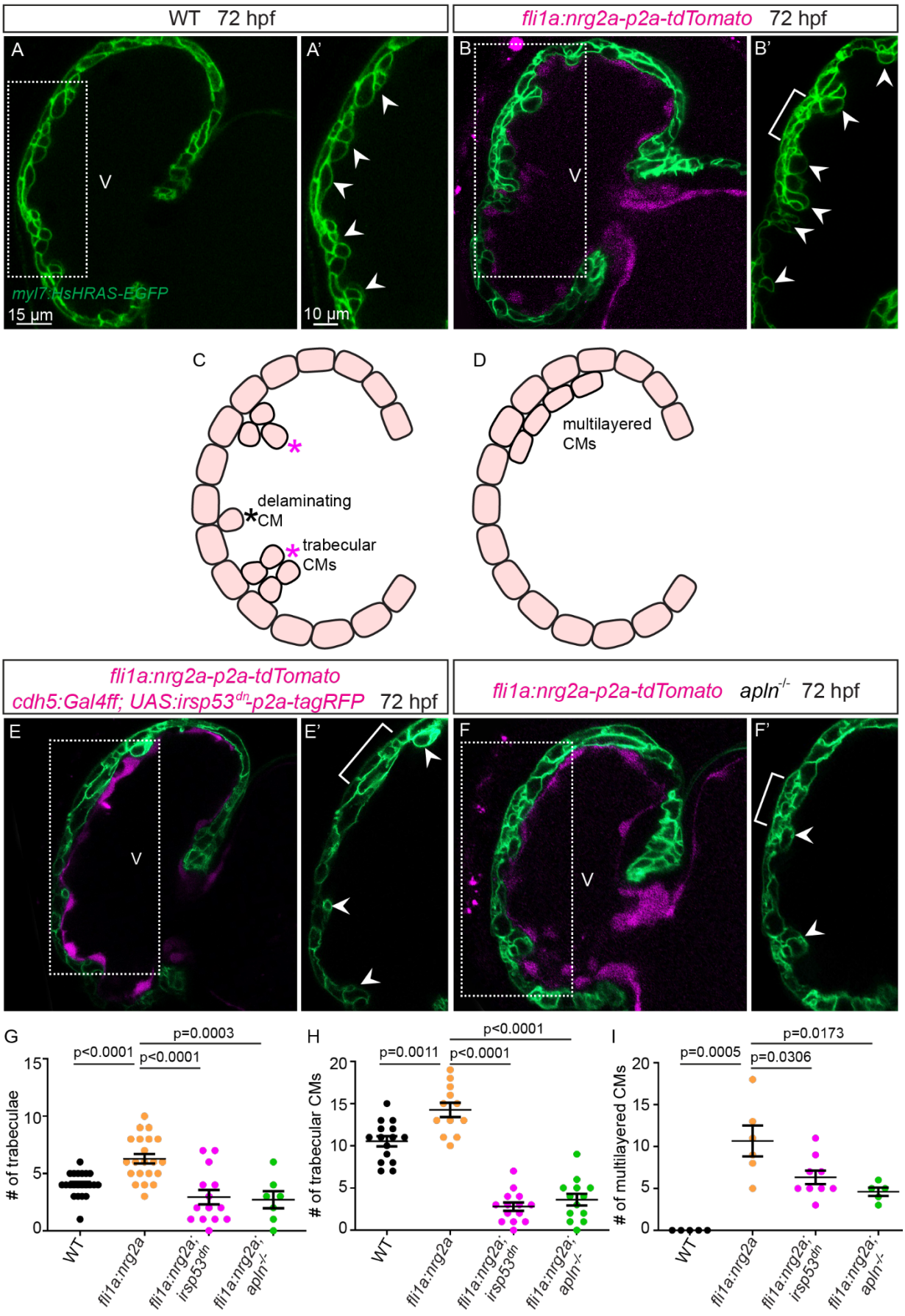
WT 72 hpf
fli1a:nrg2a-p2a-tdTomato 72 hpf
A
A'
B
B'
V
myl7:HsHRAS-EGFP
15 μm
10 μm
C
D
delaminating CM
trabecular CMs
multilayered CMs
fli1a:nrg2a-p2a-tdTomato
cdh5:Gal4ff; UAS:irsp53dn-p2a-tagRFP 72 hpf
fli1a:nrg2a-p2a-tdTomato apln-/- 72 hpf
E
E'
F
F'
G
H
I
# of trabeculae
# of trabecular CMs
# of multilayered CMs
p<0.0001
p=0.0003
p=0.0011
p=0.0005
p=0.0306
p=0.0173
WT
fli1a:nrg2a
fli1a:nrg2a; irsp53dn
fli1a:nrg2a; apln-/-

Figure 19. Endocardial protrusions are required for *nrg2a* function.
(A-B, E-F) Confocal images of the heart of *Tg(myl7:HsHRAS-EGFP)* larvae at 72 hpf. Boxed area shown in **(A'-B', E'-F')**. **(A-B)** Compared with wild-type **(A),** overexpression of *nrg2a* in the endothelium **(B)** results in an increased number of trabeculae and the multilayered CMs. **(C-D)** Schematic illustration of demonstrating delaminating CMs and trabecular CMs versus multilayered CMs. **(E)** In contrast to the larvae with overexpressing of *nrg2a* in the endothelium **(B)**, larvae with overexpressing *nrg2a* and *irsp53^{dn}* in the endothelium show reduced trabeculation and multilayered CMs. **(F)** In contrast to the larvae with overexpressing *nrg2a* in the endothelium **(B)**, *apln* mutant larvae with overexpressing *nrg2a* in the endothelium show reduced trabeculation and multilayered CMs. **(G)** Graphic showing the number of trabeculae. **(H)** Graphic showing the number of trabecular CMs. **(I)** Graphic showing the number of multilayered CMs in the ventricle. Arrowheads point to trabeculae; brackets indicate multilayered CMs. All images are ventral views, anterior to the top. V, ventricle. Data in graphs expressed as mean ± SEM.

Additionally, compared with controls, expression level of *nrg2a* is not altered in the heart *apln* mutant at 48 hpf (Figure 20).

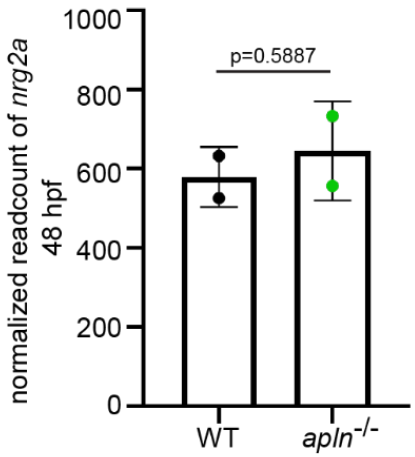

Figure 20. *nrg2a* expression is not affected in *apln* mutants.

Graphic showing the level of *nrg2a* mRNA from the extracted hearts of wild-type and *apln* mutant embryos at 48 hpf (from RNA-seq data). Data in graphs are expressed as mean ± SEM.

Overall, these data indicate that endocardial protrusions are required for Nrg-ErbB signaling.

4.6 Myocardial Erk signaling is attenuated via genetically blocking endocardial protrusion formation

4.6.1 Erk activity in CMs is repressed by Erk inhibitor

The extracellular signal-regulated kinase Erk is an essential molecule in the Nrg/ErbB signaling pathway (Lai et al., 2010). I utilized reporter lines *Tg(myl7:ERK-KTR-Clover-p2a-H2B-tagBFP)* and *Tg(myl7:ERK-KTR-Clover-p2a-H2B-mScarlet)* to visualize myocardial Erk activity in the CM of living zebrafish, as a readout of Nrg/ErbB signaling. When Erk is inactive, KTR is unphosphorylated and Clover is enriched in the nucleus of CM; in contrast, when Erk is active, KTR is phosphorylated and Clover is enriched in the cytoplasm of CM (de la Cova et al., 2017). To examine whether the Erk reporter functions, I treated this reporter with a MEK inhibitor and observed an increased number of ventricular CMs with nuclear Clover expression (i.e., inactive myocardial Erk signaling) compared with DMSO treated larvae (Figure 21), indicating that the reporter is functional.

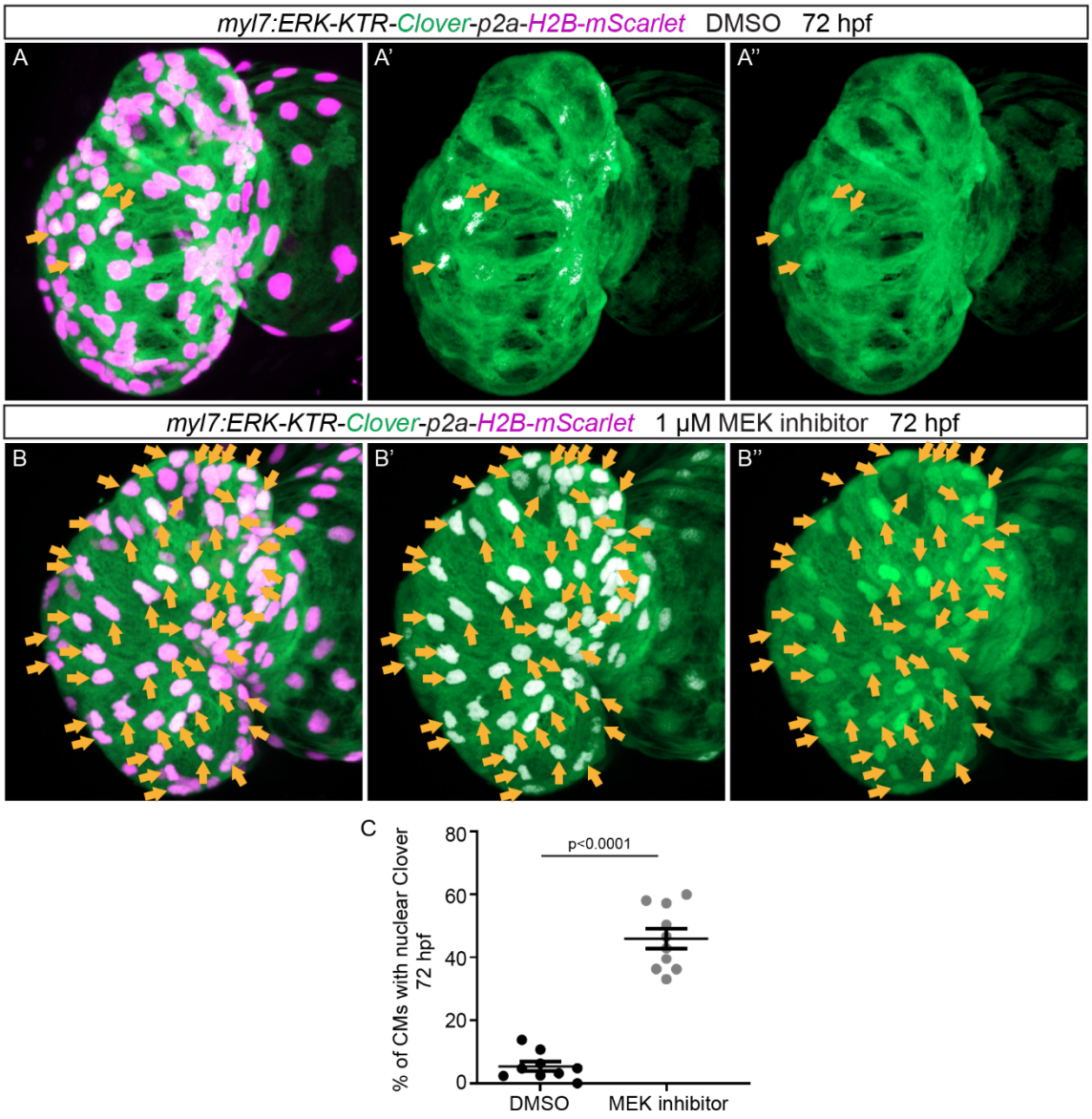

Figure 21. Validation of the Erk reporter line.

(A-B) Maximum intensity of confocal projection images of the heart of *Tg(myl7:ERK-KTR-Clover-p2a-H2B-mScarlet)* larvae at 72 hpf. **(A-B)** In contrast to DMSO treated larvae **(A)**, MEK inhibitor PD 0325901 treated larvae **(B)** (from 56 to 72 hpf) display an increased number of CMs with inactive Erk signaling. **(C)** Graphic showing the percentage of CMs with Clover enriched in nucleus of the ventricle. Arrows point to CMs with inactive Erk activity. All images are ventral views, anterior to the top. V, ventricle. Data in graphs expressed as mean ± SEM.

4.6.2 Blocking the formation of endocardial protrusion reduces myocardial Erk signaling activity

Next, I treated embryos of this reporter with an ErbB inhibitor and observed an increased number of CMs with nuclear Clover expression in the ventricle (Figure 22B). This observation assists that Erk acts as a downstream of Nrg/ErbB signaling pathway. To explore whether endocardial protrusions regulate myocardial Erk signaling activity, I genetically inhibited endocardial protrusion formation via overexpressing of *irsp53*^{dn} in the endothelium (Figure 22C). I found more CMs with nuclear Clover expression in the ventricle of larvae overexpressing *irsp53*^{dn} (Figure 22C and E) in contrast to control larvae (Figure 22A and E), suggesting more ventricular CMs with inactive Erk signaling in the larvae blocking the endocardial protrusion formation. Consistent with these findings, I found more CMs with inactive Erk signaling in the ventricle of *apln* mutants (Figure 22D and E) in contrast to *apln*$^{+/+}$ siblings (Figure 22A and E). Taken together, these observations indicate that Apelin signaling dependent endocardial protrusions modulate Nrg/ErbB/Erk signaling in CMs.

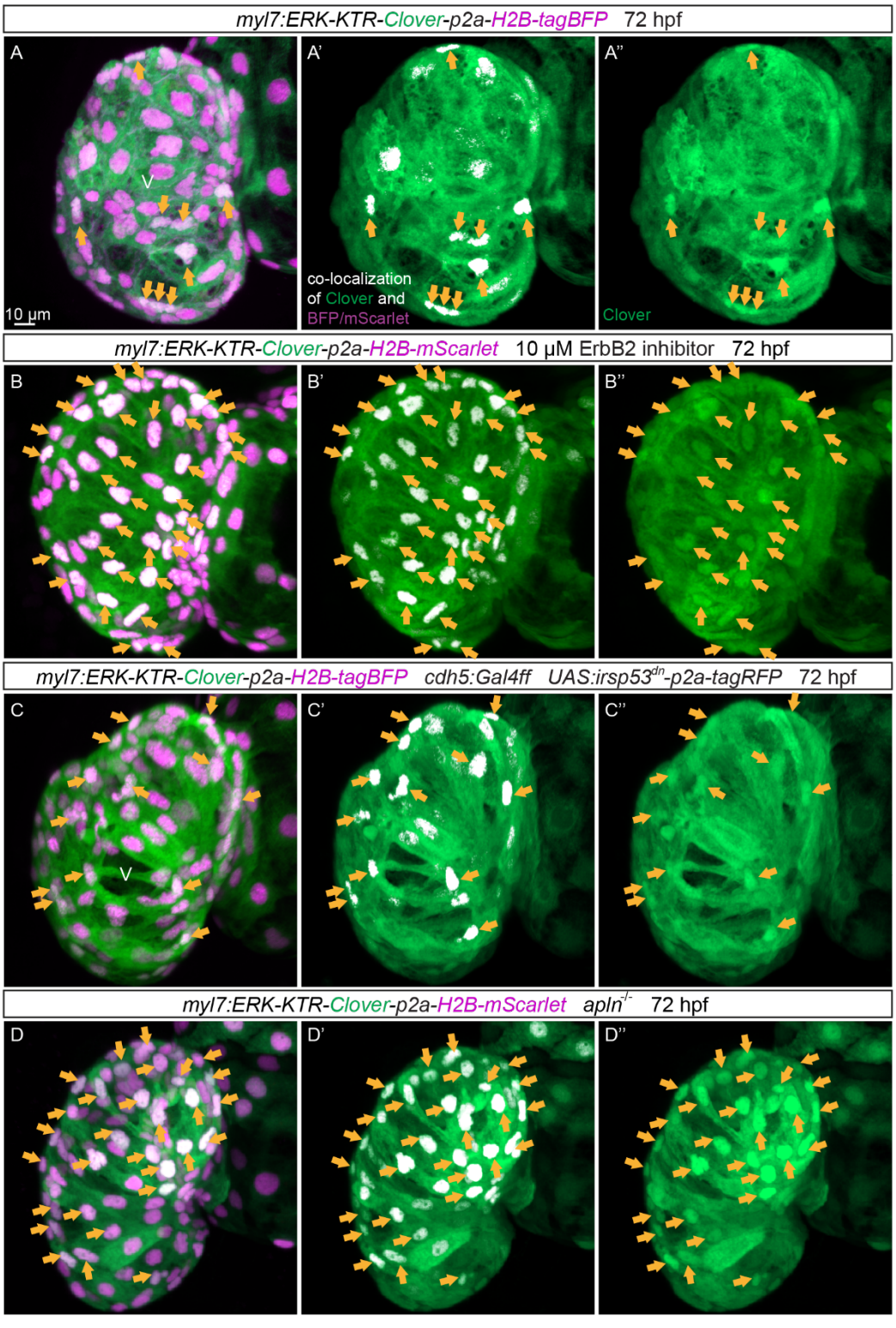
myl7:ERK-KTR-Clover-p2a-H2B-tagBFP 72 hpf
A
A'
A''
V
10 µm
co-localization of Clover and BFP/mScarlet
Clover
myl7:ERK-KTR-Clover-p2a-H2B-mScarlet 10 µM ErbB2 inhibitor 72 hpf
B
B'
B''
myl7:ERK-KTR-Clover-p2a-H2B-tagBFP cdh5:Gal4ff UAS:irsp53dn-p2a-tagRFP 72 hpf
C
C'
C''
V
myl7:ERK-KTR-Clover-p2a-H2B-mScarlet apln-/- 72 hpf
D
D'
D''

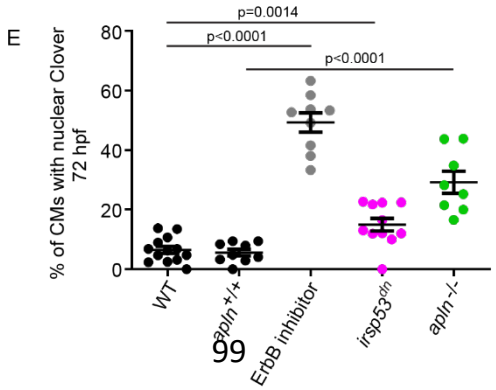
E
% of CMs with nuclear Clover 72 hpf
p=0.0014
p<0.0001
p<0.0001
80
60
40
20
0
WT
apln +/+
ErbB inhibitor
irsp53dn
apln -/-

Figure 22. Blocking the formation of endocardial protrusions represses Erk signaling activity in CMs.

(A-D) Maximum intensity confocal projection images of the heart of *Tg(myl7:ERK-KTR-Clover-p2a-H2B-tagBFP/mScarlet)* larvae at 72 hpf. In contrast to control larvae **(A)**, ErbB2 inhibitor treated larvae **(B)** exhibit an increased number of CMs with inactive Erk signaling in the ventricle. **(C)** In contrast to wild type larvae **(A)**, larvae with endothelial overexpression of $irsp53^{dn}$ display an increased number of ventricular CMs with inactive Erk signaling. **(D)** In contrast to $apln^{+/+}$ siblings, *apln* mutant larvae display an increased number of ventricular CMs with inactive Erk signaling. **(E)** Graphic showing the percentage of CMs with nuclear Clover expression in the ventricle. Arrows point to CMs with inactive Erk activity. All images are ventral views, anterior to the top. V, ventricle.

4.7 Proposed model

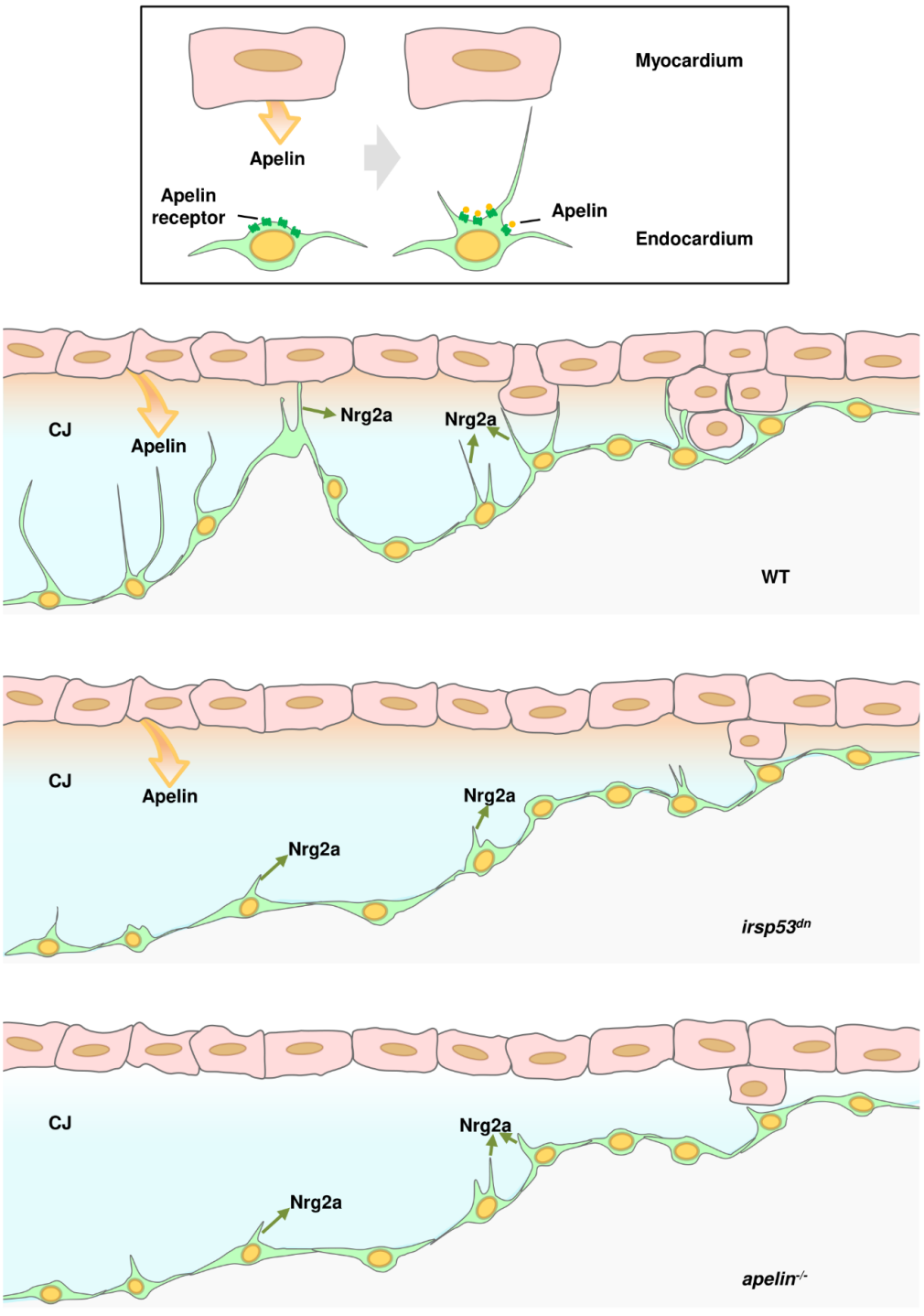

Figure 22. Schematic model.

Schematic model depicts that blocking endocardial protrusion formation leads to cardiac trabeculation defects via regulating Nrg/ErbB signaling.

5 Discussion

5.1 Cardiac trabeculation

In order to fulfill the requirements for development into a functional heart, the vertebrate heart undergoes a series of morphogenic progression including cardiac looping, chamber formation, and cardiac trabeculation etc. (Brown et al., 2016; Epstein et al., 2015). Cardiac trabeculation, which is crucial for heart contraction and conduction system formation, is one of the most important processes during cardiac development. To understand the function and biological mechanism of cardiac trabeculation, numerous of scientists dedicate themselves to this field in the last decades. Thanks to their works, we understand that cardiac trabeculation existing in various vertebrates, such as human, mouse, and zebrafish. In addition, the function of cardiac trabeculation in these species is conserved. Its defects often lead to severe consequences, such as heart failure, lethality (Gassmann et al., 1995; Lai et al., 2010; Lee et al., 1995; Liu et al., 2010; Rasouli & Stainier, 2017), left ventricular noncompaction (Claudia & Josef, 2004; Oechslin et al., 2000), and cardiomyopathy in human (Jenni et al., 1999). Many important relevant mechanisms have also been discovered.

Due to its importance, it is imperative to study cardiac trabeculation during early development in vertebrates. In 2018, Gonzalo and his colleagues reported the six phases of cardiac trabeculation in mouse from E8.0 to E14.5, endocardial sprouting, endocardial touchdown, ingression, assembly, trabecular extension, and termination. Although the first step of cardiac trabeculation is endocardial sprouting, this article mainly focused on the impacts of cardiac jelly on trabeculation (del Monte-Nieto et al., 2018). Shortly after this publication, Qu and his colleagues described the importance of angiopoietin 1/Tie2 signaling during heart development in mouse (Qu et al., 2019). They found that loss of *Tie2* in endocardium specifically impairs

endocardial sprouting, endocardial touchdown, and myocardial trabeculation. However, there are two aspects remaining largely unknown: 1) the morphogenetic event(s) of endocardial sprouting, and 2) the effect(s) of endocardial sprouting on cardiac morphogenesis including myocardial trabeculation.

As mentioned in section **1.2.3**, we aimed to address these two questions on zebrafish because of its transparency allows single-cell resolution imaging. Besides, the zebrafish is able to survive for a week under cardiac defects, which enables us the trace the cardiac phenotypes in the early developmental stages.

5.2 Endocardium-myocardium communication is essential for trabeculation

5.2.1 Endocardial protrusions contribute to myocardial trabeculation

In zebrafish, the onset of cardiac trabeculation begins with delamination of individual CMs from the myocardial monolayer, and these delaminated CMs protrude into the lumen (Jimenez-Amilburu et al., 2016; Liu et al., 2010; Peshkovsky et al., 2011; Priya et al., 2020; Staudt et al., 2014). In contrast to zebrafish, the mouse myocardium is multilayered at the initiation of cardiac trabeculation. Increasing studies have shown the importance of the endocardium during cardiac trabeculation (D'Amato et al., 2016; del Monte-Nieto et al., 2018; Grego-Bessa et al., 2007; Lai et al., 2010; Qu et al., 2019; Rasouli & Stainier, 2017). Similar to ECs, sprouting also occurs in EdCs (del Monte-Nieto et al., 2018). Endothelial sprouting, also known as angiogenesis, is a process that ECs break out from vessel wall and form new blood vessels. Growth factors play an important role in endothelial sprouting, and this process is fundamental to physiology and pathology. In contrast, it is unclear what morphogenetic events and molecular factors underlying endocardial sprouting, and what are the effects of endocardial sprouting on cardiac morphogenesis such as trabeculation.

It is known that endocardial sprouting and touchdown formation take place in the early phase during cardiac trabeculation in mouse (del Monte-Nieto et al., 2018). These findings are consistent with my data in zebrafish (Figure 8), suggesting that the cardiac trabeculation morphogenetic events are evolutionarily conserved. However, the structure of endocardial sprouts in mouse and endocardial protrusions in zebrafish appear to be different. In mouse, the endocardial sprouts seem to be cellular (del Monte-Nieto et al., 2018), while the endocardial protrusions in zebrafish are more closely resemble filopodia (Figure 8). One possible reason of these differences is that fixed heart tissue was used to study mouse trabeculation whereas live heart was used to study zebrafish trabeculation.

It has been reported that CM delamination and trabeculation in zebrafish mainly take place in the outer curvature of the ventricle (Jimenez-Amilburu et al., 2016; Liu et al., 2010; Rasouli & Stainier, 2017). Interestingly, my data show that endocardial protrusions are mostly also present in the outer curvature of the ventricle (Figure 9). Furthermore, the endocardial protrusions extend along delaminating CMs and trabecular CMs (Figure 9). The correlation between the timing and location of endocardial protrusions and CM delamination/trabeculation suggests that endocardial protrusions play a role in cardiac trabeculation.

5.2.2 Signaling pathways between the endocardium and the myocardium

Various signaling pathways are involved in the communication between the endocardium and myocardium, including Nrg/ErbB/Erk (del Monte-Nieto et al., 2018; Lai et al., 2010; Rasouli & Stainier, 2017), Notch (D'Amato et al., 2016; del Monte-Nieto et al., 2018; Grego-Bessa et al., 2007), angiopoetin 1/Tie2 (Qu et al., 2019), and Sema3E/plexinD1 (Sandireddy et al., 2019).

5.2.2.1 Nrg/ErbB/Erk signaling in cardiac trabeculation

Nrg/ErbB is a key signaling pathway during cardiac trabeculation. In mouse and zebrafish, the ligand Nrg is derived from the endocardium, and its receptor ErbB is

expressed in the myocardium (Gassmann et al., 1995; Liu et al., 2010; Meyer & Birchmeier, 1995; Rasouli & Stainier, 2017). In the late 20th century, scientists discovered that mouse lacking ErbB fail to form myocardial trabeculation (Gassmann et al., 1995; Lee et al., 1995; Meyer & Birchmeier, 1995). Later, scientists started studying the ligand Nrg in mouse. Nrg1 plays a crucial role in cardiac trabeculation (Lai et al., 2010). Zebrafish becomes a popular animal model in the cardiovascular field for its unique strengths (see section **1.2.3**). In the early 21st century, Liu et al. has shown that ErbB2 is required for cardiac trabeculation in zebrafish (Liu et al., 2010), indicating that the function of Nrg/ErbB signaling in trabeculation is evolutionarily conserved. Interestingly, unlike in mouse, *nrg1* is not required for cardiac trabeculation in zebrafish. Instead, *nrg2a* has be shown to be critical for trabeculation in zebrafish (Rasouli & Stainier, 2017). Selection of neuregulin during evolution is an interesting topic to study as well. In my study, I utilized transgenic line *Tg(fli1a:nrg2a-p2a-tdTomato)*^{bns199} overexpressing *nrg2a* in the endothelium and observed increased numbers of trabecular CMs and trabeculae (Figure 19), this result indicates that endocardial *nrg2a* is necessary and sufficient for cardiac trabeculation.

Notably, the function of *nrg2a* is compromised when the formation of endocardial protrusion is blocked (Figure 19), suggesting that endocardial protrusions are indispensable for the function of *nrg2a* during trabeculation. One question remains as to why *nrg2a* function needs endocardial protrusions. The molecular weight of the membrane-bound form of Nrg2a is 55 kilodaltons, and the presumed secreted form of Nrg2a is 22 kilodaltons. In comparison, the molecular weight of the most active form of Apelin is 1.52 kilodaltons. Hence, it is likely that Apelin can diffuse through the cardiac jelly due to its small size, whereas Nrg2a needs the assistance of endocardial protrusion to be transported to the myocardium.

Similar as other receptor tyrosine kinases, ErbB receptors simulate multiple signaling cascades upon ligand activation, such as the MAPK cascade, resulting in the phosphorylation of ERK1/2 (Wee & Wang, 2017). Accordingly, scientists observed attenuated ERK phosphorylation in CMs of mice with Nrg1/ErbB signaling deficient

(Lai et al., 2010). I analyzed a novel reporter of Erk activity in CMs, *Tg(-0.8myl7:ERK-KTR-Clover-p2a-Hsa.H2B-tagBFP/mScarlet)*^{bns565}, I observed that inhibition of endocardial protrusion formation via overexpression of Irsp53^{dn} particularly in endothelial cells by crossing *TgBAC(cdh5:Gal4ff)*^{mu101} line to *Tg(UAS: irsp53*^{dn}*-p2a-tagRFP)*^{bns440} line, as well as genetic Apelin signaling inactivation, results in attenuated Erk phosphorylation in zebrafish CMs (Figure 22). All these data suggest that endocardial protrusions regulate ErbB signaling in zebrafish CMs.

5.3 Molecular factors regulate endocardial sprouting

When the EC undergoes sprouting angiogenesis, the endothelial tip cells guide the new sprouts (Gerhardt et al., 2003). During this process, tip cells dynamically extend filopodia to read surrounding growth factors (Gerhardt et al., 2003). Apelin signaling and Notch signaling pathways are known to regulate the formation of endocardial filopodia (Helker et al., 2020; Hellstrom et al., 2007; Suchting et al., 2007). In comparison, the regulators of endocardial sprouting remain largely unknown. Tie2 signaling is the only one reported to regulate endocardial sprouting to date, and *Tie2* mutant mice have fewer endocardial touchdowns (Qu et al., 2019).

Recently, Apelin signaling pathway was shown to be required for the formation of filopodia in the zebrafish trunk vessels during sprouting angiogenesis (Helker et al., 2020). Consistence with this, I now show that Apelin is required for the formation of endocardial filopodia (Figure 23), revealing the role of Apelin signaling pathway is conserved in endothelial and endocardial sprouting.

Notch signaling pathway regulates endothelial sprouting angiogenesis in a negative manner (Hellstrom et al., 2007; Leslie et al., 2007; Siekmann & Lawson, 2007; Suchting et al., 2007). Consistent with these reported data, I discovered that inhibition of Notch signaling results in an increased number of endocardial protrusions as well (Figure 18). Remarkably, Notch signaling also negatively regulates CM delaminating and trabeculation (Priya et al., 2020). There may be a correlation between increased numbers of endocardial protrusions and of delaminated CMs and

trabeculae, although it is also possible that Notch signaling autonomously affects CM cell behavior (Han et al., 2016).

5.4 Future perspective

Proteolytic cleavage of Nrg1 is a key process for its function during cardiac trabeculation (Lai et al., 2010). Compared with Nrg1, little is known about Nrg2a in this process. For example, does proteolytic cleavage occur when Nrg2a moderates cardiac trabeculation? If proteolysis of Nrg2a is required for its function, when and where Nrg2a is cleaved. To investigate these questions, one can generate a transgenic zebrafish line in which two fluorescent proteins, e.g., mCherry and EGFP, are bound to the N- and C-termini of the wild type Nrg2a. Live imaging technology should allow us to see the putative secreted form of Nrg2a in red color. This experiment will reveal whether Nrg2a is proteolytically cleaved.

To understand whether proteolysis is required for the role of Nrg2a, two types of *nrg2a* mutants can be generated: one mutant expresses only the presumed secreted form of Nrg2a, and the other mutant blocks proteolysis by removing the cleavage sites. Whether proteolytic cleavage of Nrg2a is required during cardiac development will become apparent after analysis of the phenotypes of these two mutants.

6 Conclusion

In conclusion, I have identified new insights into the function of endocardial protrusion during myocardial trabeculation, as well as the underlying mechanisms. The aims were achieved as follows:

Aim 1: To investigate the role of endocardial protrusions during cardiac trabeculation.

First of all, I was able to find out the temporal and spatial correlation between endocardial protrusions and delaminating/trabeculation CMs by analyzing the location of endocardial protrusions and delaminating/trabecular CMs at different time points.

I then generated a *Tg(UAS: irsp53dn-p2a-RFP)* line and observed inhibition of endocardial protrusion formation at 48 hpf and impairment of cardiac trabeculation at 72 hpf by crossing this line to *TgBAC(cdh5:Gal4ff)*. In addition, I also studied the *apln* mutant which exhibits reduced endocardial protrusion formation at 24 and 48 hpf and impaired cardiac trabeculation at 72 hpf.

Aim 2: To identify the signaling pathway(s) that drive(s) the endocardial protrusion formation.

In *apln* mutant, I observed a fewer number of endocardial protrusions. Moreover, I also treated the embryos with Notch inhibitor and found an increased number of endocardial protrusions.

Aim 3: To understand how endocardial protrusions regulate cardiac trabeculation.

I found that the function of *nrg2a* is compromised during cardiac trabeculation while *nrg2a* is overexpressed in the endothelium and the formation of protrusion is blocked

in the endocardium. These data strongly suggest that endocardial protrusions regulate cardiac trabeculation via Nrg/ErbB signaling.

7 Summary

7.1 Zusammenfassung

7.1.1 Einleitung

Das Vertebratenherz durchläuft eine Reihe von morphogenetischen Ereignissen, darunter Herzschlingen, Kammerbildung, Herztrabekulation usw., um die Voraussetzungen für die Entwicklung zu einem reifen Organ zu erfüllen. Die Herztrabekulation ist ein Prozess, bei dem sich muskuläre, schwammartige Strukturen bilden, die eine Zunahme der Muskelmasse ermöglichen. Dieser Prozess ist für die Kontraktilität des Herzens und das Erregungsleitungssystem des Herzens erforderlich. Bei der Maus wurde die kardiale Trabekulation in sechs Phasen eingeteilt: endokardiale Sprossung, Touchdown-Bildung, Ingression, Aufbau, trabekuläre Ausdehnung und Abschluss (del Monte-Nieto et al., 2018). Es ist interessant zu wissen, dass die endokardialen Sprossen unter den Trabekeln hervorstehen, obwohl die Funktion der endokardialen Sprossen unklar bleibt. Das kompakte Myokard der Maus ist mehrschichtig, im Gegensatz dazu weist der Zebrafisch ein einschichtiges kompaktes Myokard auf (Liu et al., 2010; Priya et al., 2020). Bei Zebrafischen lösen sich die CM um 60 hpf vom kompakten Myokard ab, um die Trabekelschicht zum Lumen hin auszusäen, und die Trabekel sind bei 3 dpf vorhanden (Liu et al., 2010; Priya et al., 2020; Staudt et al., 2014).

Einer der bekannten Signalwege, der für die kardiale Trabekulierung erforderlich ist, ist der Nrg/ErbB-Signalweg. In der Maus wird der Ligand Nrg1 im Endokard exprimiert, während die Rezeptoren ErbB2 und ErbB4 im Myokard exprimiert werden (Gassmann et al., 1995; Grego-Bessa et al., 2007; Lee et al., 1995; Odiete et al., 2012). Das Fehlen von Nrg1, ErbB2 oder ErbB4 führt zu einem Mangel an kardialer Trabekulierung (Gassmann et al., 1995; Lai et al., 2010; Lee et al., 1995). Nrg1 enthält eine extrazelluläre rezeptorbindende Domäne, eine Spaltstelle, eine

Transmembrandomäne und eine zytoplasmatische Domäne (Kamezaki et al., 2016). Die extrazelluläre Domäne, die aus einer EGF-ähnlichen Domäne von Nrg1 besteht, wird nach proteolytischer Spaltung freigesetzt und bindet dann an den ErbB-Rezeptor (GrausPorta et al., 1997). In der Maus wird Nrg1 für die kardiale Trabekulierung benötigt, Nrg2 hingegen nicht (Britto et al., 2004; Rasouli & Stainier, 2017; Samsa et al., 2016). Im Gegensatz dazu ist Nrg2a für die kardiale Trabekelbildung im Zebrafisch erforderlich, Nrg1 hingegen nicht.

Es wurde über mehrere endokardiale Signalwege berichtet, die für die kardiale Trabekulation unverzichtbar sind, wie die Notch- und Angiopoietin 1/Tie2-Signalübertragung. Die Deletion von Notch1, einem im Endokard exprimierten Notch-Rezeptor, führt zu Defiziten bei der kardialen Trabekelation (D'Amato et al., 2016; del Monte-Nieto et al., 2018; Grego-Bessa et al., 2007). Angiopoietin 1 wird im Myokard und Tie2 im Endokard exprimiert, und das Fehlen eines der beiden führt zu schweren kardialen Trabekeldefekten (Qu et al., 2019; Suri et al., 1996; Tachibana et al., 2005). All diese Berichte deuten darauf hin, dass das Endokard für die Entwicklung des Herzmuskels wesentlich ist.

In den letzten Jahren ist das Thema Zytoneme in aller Munde. Zytoneme sind filopodienartige Ausstülpungen, die in verschiedenen Organismen wie *Drosophila* (Huang et al., 2019; Ramirez-Weber & Kornberg, 1999; Roy et al., 2011), Küken (Sanders et al., 2013), Zebrafischen (Stanganello et al., 2015), und Mäusen (Fierro-Gonzalez et al., 2013) aktiv Moleküle transportieren können.

Bei Säugetieren besteht der Apelin-Signalweg aus zwei Liganden, *Apelin* und *Apela*, und einem Rezeptor *Aplnr*. Beim Zebrafisch gibt es aufgrund einer Genomverdoppelung zwei Rezeptoren für den Apelin-Signalweg, *aplnra* und *aplnrb*. Fehlt die Funktion von Apln oder Aplnr, führt dies zu einem Rückgang der endothelialen Angiogenese. Die Rolle der Apelin-Signalübertragung im Endokard ist jedoch noch nicht untersucht worden.

In meiner Studie zeige ich zunächst, dass (1) die Bildung endokardialer Ausstülpungen von Apelin-Signalen abhängt und (2) endokardiale Ausstülpungen die kardiale Trabekulierung durch die Regulierung von Nrg/ErbB/Erk-Signalen fördern.

7.1.2 Ergebnisse

7.1.2.1 Interaktionen zwischen Endokard und Myokard während der Trabekulierung im Zebrafisch

Del Monte-Nieto et al. haben die Stadien der kardialen Trabekulation in der Maus in endokardiale Sprossung, Touchdown-Bildung, endokardiale Ingression, Aufbau, trabekuläre Ausdehnung und Abschluss definiert (del Monte-Nieto et al., 2018). Um die Stadien der kardialen Trabekulierung im Zebrafisch zu untersuchen, habe ich die In-vivo-Bildgebungstechnologie eingesetzt. Ich entdeckte, dass sich endokardiale Ausstülpungen bei 24 (Figure 8A-A'') und 48 hpf (Figure 8B-B'') in Richtung Myokard ausdehnen. Ähnlich wie bei der Maus beobachtete ich auch, dass die ventrikulären endokardialen Ausstülpungen mit dem Myokard in Berührung kommen (Figure 8B-B''), und diese Berührungen sind auch dann stabil, wenn sich das Herz zusammenzieht (Figure 8E-H). Die CM beginnen, sich vom einschichtigen, kompakten Myokard in Richtung Kammerhöhle zu lösen, um die trabekuläre Schicht um 60 hpf auszusäen (Figure 8C, C' und C''''), was mit einem früheren Bericht übereinstimmt (Priya et al., 2020). Nach diesem Schritt beginnen die trabekulären CMs um 72 hpf, sich zu "fingerähnlichen" multizellulären Fortsätzen, den Trabekeln, zusammenzusetzen (Figure 8D, D' und D''''). Zusammenfassend habe ich die Phasen der Trabekulierung bei Zebrafischen in endokardiale Ausstülpungen, endokardiale Touchdown-Bildung, CM-Delamination und trabekuläre Expansion unterteilt.

Außerdem stellte ich fest, dass es im Ventrikel mehr endokardiale Ausstülpungen gibt als im Atrium, und dass sich die endokardialen Ausstülpungen hauptsächlich in

Richtung Myokard erstrecken (Figure 9A und B). Als Nächstes untersuchte ich die Korrelation zwischen den endokardialen Ausstülpungen und den delaminierenden/trabekulären CMs, indem ich die Lage dieser beiden Strukturen analysierte. Es ist bereits bekannt, dass die kardiale Trabekulierung hauptsächlich in der äußeren Ventrikelkrümmung auftritt (Liu et al., 2010). In ähnlicher Weise befinden sich die meisten endokardialen Ausstülpungen in der ventrikulären Außenkrümmung bei 48, 60 und 72 hpf (Figure 9C-F). Interessanterweise befinden sich in der ventrikulären Außenkrümmung 69 % und 91 % der endokardialen Ausstülpungen in unmittelbarer Nähe zu delaminierenden CMs bei 60 hpf bzw. zu trabekulären CMs bei 72 hpf (Figure 9D, E und G). 98 % der delaminierenden CM liegen bei 60 hpf in der Nähe von endokardialen Ausstülpungen, und 93 % der trabekulären CM liegen bei 72 hpf in der Nähe von endokardialen Ausstülpungen (Figure 9D, E und H). Die zeitlichen und räumlichen Korrelationen deuten darauf hin, dass endokardiale Ausstülpungen bei der kardialen Trabekulierung eine Rolle spielen.

7.1.2.2 Genetische Blockierung der Bildung endokardialer Ausstülpungen beeinträchtigt das Herzwachstum

Um die Funktion endokardialer Ausstülpungen während der Herzentwicklung zu untersuchen, habe ich eine transgene Linie *Tg(UAS: irsp53^{dn}-p2a-RFP)* (Figure 10A) erzeugt, die die Bildung endokardialer Ausstülpungen durch Kreuzung mit *TgBAC(cdh5:Gal4ff)* spezifisch hemmt. Die Embryonen mit *irsp53^{dn}*-Überexpression in den ECs weisen nach 48 hpf eine um 70 % verringerte Anzahl endokardialer Ausstülpungen auf (Figure 10B-D), während die Verteilung der endokardialen Ausstülpungen unverändert bleibt (Figure 10E-E'). Nach 72 hpf zeigen die Larven mit *irsp53^{dn}*-Überexpression in ECs einen Mangel an myokardialer Trabekulierung (Figure 11) und CM-Proliferation (Figure 12) im Ventrikel. Zusammengenommen zeigen diese Daten, dass endokardiale Ausstülpungen für die myokardiale Trabekulierung und CM-Proliferation erforderlich sind.

7.1.2.3 Apelin-Signalisierung reguliert die Bildung endokardialer Ausstülpungen und die Myokardtrabekulierung

Es wurde gezeigt, dass der Apelin-Signalweg die Bildung von Endothelausstülpungen während der Angiogenese in Zebrafischen fördert (Helker et al., 2020). Um die Rolle der Apelin-Signalübertragung bei der Bildung der endokardialen Protrusion aufzudecken, untersuchte ich zunächst die Expression von *apln* und *aplnrb* und stellte fest, dass *apln* im Myokard und *aplnrb* im Endokard bei 48 und 72 hpf exprimiert wird (Figure 13).

Als nächstes untersuchte ich die *aplnra*-Mutante (Helker et al., 2015), *aplnrb*-Mutante (Helker et al., 2015), und *apln*-Mutante (Helker et al., 2015). Da die *apela*-Mutanten kein Herz bilden (Chng et al., 2013), habe ich sie nicht analysiert. Nur eine kleine Anzahl von *aplnrb*-Mutanten ist in der Lage, ein Herz zu bilden. Ich analysierte sie und stellte fest, dass sie eine geringere Anzahl von Endokardausstülpungen bei 48 hpf (Figure 14A und B) und eine geringere Trabekulierung bei 72 hpf (Figure 14C und D) aufweisen. Außerdem weisen die *aplnrb*-Mutanten im Vergleich zu ihren Wildtyp-Geschwistern dickere CJ in der äußeren Krümmung des Ventrikels auf (Figure 14C und D). Darüber hinaus zeigen *aplnra*-Mutanten auch eine Verringerung der Trabekulierung bei 72 hpf (Figure 14E und F).

Anschließend habe ich mich auf die Untersuchung der *apln*-Mutanten konzentriert, da die meisten *apln*-Mutanten ein normal aussehendes Herz bilden und die Herzfunktion nicht beeinträchtigt ist (Figure 17). *apln*-Mutanten zeigen eine signifikante Verringerung der Bildung von Endokardvorwölbungen bei 24 und 48 hpf (Figure 15A-F) und Endokardaufsetzer bei 48 hpf (Figure 15D, E, und G). Darüber hinaus analysierte ich die *apln*-Mutante nach 72 hpf und stellte ähnliche Defekte bei der kardialen Trabekulierung und der CM-Proliferation fest, wie ich sie bei den Larven mit überexprimiertem *irsp53*^{dn} in den ECs beobachtete. Zusammengenommen deuten alle diese Daten darauf hin, dass der Verlust der endokardialen

Ausstülpungen zu Defekten der Myokardtrabekulierung führt und nicht die sekundäre Folge einer Herzfehlfunktion ist.

7.1.2.4 Die Notch-Signalübertragung reguliert die Bildung endokardialer Ausstülpungen negativ

Viele Berichte haben gezeigt, dass die Notch-Signalisierung die Bildung von endothelialen Ausstülpungen negativ beeinflusst (Hellstrom et al., 2007; Leslie et al., 2007; Siekmann & Lawson, 2007; Suchting et al., 2007). Daher habe ich den γ-Sekretase-Inhibitor RO4929097 verwendet, um die Notch-Signalübertragung in Zebrafischembryonen zu hemmen, und konnte eine verringerte Expression der Notch-Signalübertragung im Endokard feststellen (Figure 18A und B). Darüber hinaus ist die Anzahl der ventrikulären endokardialen Ausstülpungen in Embryonen, die mit dem Notch-Inhibitor behandelt wurden, erhöht (Figure 18C, D und G). Insgesamt zeigen diese Daten, dass der Notch-Signalweg die Bildung von endokardialen Ausstülpungen auf negative Weise vermittelt.

7.1.2.5 Endokardiale Ausstülpungen orchestrieren die myokardiale Trabekulierung über Nrg/ErbB/Erk-Signalisierung

Als nächstes wollte ich die zugrunde liegenden Mechanismen herausfinden. Nrg/ErbB ist einer der wichtigsten Signalwege bei der kardialen Trabekulierung. Wie bereits erwähnt (Abschnitt 1.2.5), ist *nrg2a* für die kardiale Trabekelbildung erforderlich. Ich habe zunächst *nrg2a* im Endothel überexprimiert und eine Hypertrabekulierung sowie mehrschichtige CMs im Ventrikel beobachtet (Figure 19A und B, 19G-I). Dann überexprimierte ich *nrg2a* im Endothel, während ich die Bildung der endokardialen Ausstülpung blockierte, und beobachtete weniger Trabekel sowie weniger mehrschichtige CMs im Vergleich zur Kontrollgruppe (Figure 19E-I).

Da Erk ein wichtiges Molekül der Nrg/ErbB-Signalübertragung ist, beschloss ich, die myokardiale Erk-Aktivität mit Hilfe einer Erk-Reporterlinie zu untersuchen. Zunächst testete ich die Funktionalität des Erk-Reporters, indem ich die Embryonen des Erk-

Reporters mit einem MEK-Inhibitor behandelte und eine erhöhte Anzahl von ventrikulären CMs mit inaktiver Erk-Aktivität beobachtete (Figure 21). Die Daten weisen auf die Funktion des Reporters hin. Wenn die Embryonen des Erk-Reporters mit einem ErbB-Inhibitor behandelt wurden, gibt es mehr ventrikuläre CMs mit inaktiver Erk-Aktivität (Figure 22B). Diese Beobachtung weist darauf hin, dass Erk dem Nrg/ErbB-Signalweg nachgeschaltet ist. Um zu untersuchen, ob endokardiale Ausstülpungen für die myokardiale Erk-Signalaktivität erforderlich sind, habe ich die Bildung endokardialer Ausstülpungen blockiert und festgestellt, dass im Vergleich zu den Kontrollen mehr CMs im Ventrikel eine inaktive Erk-Aktivität aufweisen (Figure 22A und C-E). Zusammengenommen deuten diese Ergebnisse darauf hin, dass endokardiale Ausstülpungen die myokardiale Trabekulierung über Nrg/ErbB/Erk-Signale in CMs modulieren.

7.1.3 Schlussfolgerung

In dieser Studie habe ich mit Hilfe der Methode des genetischen Funktionsverlusts zur Blockierung der Bildung von Endokardprotrusionen herausgefunden, dass Endokardprotrusionen für die Herztrabekulation erforderlich sind und dass die Bildung von Endokardprotrusionen von der Apelin-Signalisierung abhängt. Auf mechanischer Ebene zeige ich, dass der Beitrag von *nrg2a* und der Erk-Aktivität während der Herztrabekulation beeinträchtigt wird, wenn die Bildung der endokardialen Protrusion blockiert ist. Diese Daten deuten darauf hin, dass endokardiale Ausstülpungen die kardiale Trabekulierung durch Nrg/ErbB/Erk-Signale fördern.

7.2 Summary

7.2.1 Introduction

The vertebrate heart undergoes a series of morphogenetic events, including cardiac looping, chamber formation, cardiac trabeculation, etc., to meet the requirements for developing into a mature organ. Cardiac trabeculation is a process in which muscular, sponge-like structure is formed, allowing an increase in muscle mass. This process is required for cardiac contractility and the cardiac conduction system. In mouse, cardiac trabeculation has been divided into six phases: endocardial sprouting, touchdown, ingression, assembly, trabecular extension, and termination (del Monte-Nieto et al., 2018). It is interesting to note that the endocardial sprouts protrude below the trabeculae, although the function of the endocardial sprouts remains unclear. The compact myocardium in mouse is multilayered, in contrast to zebrafish, which has a mono-layered compact myocardium (Liu et al., 2010; Priya et al., 2020). In zebrafish, CMs delaminate from the compact myocardium at around 60 hpf to seed the trabecular layer toward the lumen, and trabeculae are present at 3 dpf (Liu et al., 2010; Priya et al., 2020; Staudt et al., 2014).

One of the known signaling pathways which is required for cardiac trabeculation is the Nrg/ErbB signaling pathway. In mouse, the ligand Nrg1 is expressed in the endocardium, whereas the receptors ErbB2 and ErbB4 are expressed in the myocardium (Gassmann et al., 1995; Grego-Bessa et al., 2007; Lee et al., 1995; Odiete et al., 2012). The absence of Nrg1, ErbB2, or ErbB4 leads to cardiac trabeculation deficiency (Gassmann et al., 1995; Lai et al., 2010; Lee et al., 1995). Nrg1 contains an extracellular receptor-binding domain, cleavage site, a transmembrane domain, and a cytoplasmic domain (Kamezaki et al., 2016). The extracellular domain consisting of an EGF-like domain of Nrg1 is released after proteolytic cleavage and then binds to ErbB receptor (GrausPorta et al., 1997). In mouse, Nrg1 is needed for cardiac trabeculation whereas Nrg2 is not (Britto et al., 2004; Rasouli & Stainier, 2017; Samsa

et al., 2016). In contrast, Nrg2a is required for cardiac trabeculation in zebrafish whereas Nrg1 is not.

Several endocardial signaling pathways have been reported to be indispensable for cardiac trabeculation, such as Notch and Angiopoietin 1/Tie2 signaling. Depletion of Notch1, a Notch receptor expressed in the endocardium, leads to cardiac trabeculation deficits (D'Amato et al., 2016; del Monte-Nieto et al., 2018; Grego-Bessa et al., 2007). Angiopoietin 1 is expressed in the myocardium and Tie2 in the endocardium; absence of either results in severe cardiac trabeculation defects (Qu et al., 2019; Suri et al., 1996; Tachibana et al., 2005). All these reports suggest that the endocardium is essential for myocardial development.

In recent years, cytoneme has become a hot topic. Cytonemes are filopodia-like protrusions that can actively transport molecules in different organisms such as *Drosophila* (Huang et al., 2019; Ramirez-Weber & Kornberg, 1999; Roy et al., 2011), chick (Sanders et al., 2013), zebrafish (Stanganello et al., 2015), and mouse (Fierro-Gonzalez et al., 2013).

In mammals, Apelin signaling consists of two ligands, *Apelin* and *Apela*, and one receptor *Aplnr*. There are two receptors of Apelin signaling in zebrafish, *aplnra* and *aplnrb*, because of genome duplication. Lack of function of Apln or Aplnr results in a decrease in endothelial angiogenesis. However, the role of Apelin signaling in the endocardium has not been examined.

In my study, I first show that – (1) formation of endocardial protrusion is Apelin signaling dependent and (2) endocardial protrusions promote cardiac trabeculation through regulating Nrg/ErbB/Erk signaling.

7.2.2 Results

7.2.2.1 Interactions between the endocardium and myocardium during trabeculation in zebrafish

Del Monte-Nieto et al. have defined the cardiac trabeculation stages into endocardial sprouting, touchdown formation, endocardial ingression, assembly, trabecular extension, and termination in mouse (del Monte-Nieto et al., 2018). To investigate the cardiac trabeculation stages in zebrafish, I utilized *in vivo* imaging technology. I discovered that endocardial protrusions extend towards the myocardium at 24 (Figure 8A-A'') and 48 hpf (Figure 8B-B''). Similar to the finding in mouse, I also observed that the ventricular endocardial protrusions form touchdowns and come into contact with the myocardium (Figure 8B-B''), and these touchdowns are stable even when the heart contracts (Figure 8E-H). The CMs begin to delaminate from the mono-layer compact myocardium toward the chamber cavity to seed the trabecular layer at around 60 hpf (Figure 8C, C', and C''''), consistent with a previous report (Priya et al., 2020). Following this step, trabecular CMs begin to assemble into "finger-like" multicellular projections, named trabeculae, at 72 hpf (Figure 8D, D', and D''''). In summary, I defined the phases of zebrafish trabeculation into endocardial protrusions, endocardial touchdowns, CM delamination, and trabecular expansion.

Moreover, I found that there were more endocardial protrusions in the ventricle than in the atrium, and endocardial protrusions extended mainly toward the myocardium (Figure 9A and B). Next, I studied the correlation between the endocardial protrusions and the delaminating/ trabecular CMs by analyzing the location of these two structures. It is already known that cardiac trabeculation mainly occurs in the ventricular outer curvature (Liu et al., 2010). Similarly, most endocardial protrusions are located in the ventricular outer curvature at 48, 60, and 72 hpf (Figure 9C-F). Interestingly, in the ventricular outer curvature, 69% and 91% of endocardial protrusions are in close proximity to delaminating CMs at 60 hpf and to trabecular

CMs at 72 hpf respectively (Figure 9D, E, and G). 98% of delaminating CMs are close to endocardial protrusions at 60 hpf, and 93% of trabecular CMs are close to endocardial protrusions at 72 hpf (Figure 9D, E, and H). The temporal and spatial correlations indicate that endocardial protrusions play a role during cardiac trabeculation.

7.2.2.2 Genetically blocking the formation of endocardial protrusion impairs cardiac growth

In order to examine the function of endocardial protrusions during myocardial development, I generated a transgenic line *Tg(UAS: irsp53^{dn}-p2a-RFP)* (Figure 10A), which specifically inhibits the formation of endocardial protrusion by crossing to *TgBAC(cdh5:Gal4ff)*. Embryos with *irsp53^{dn}* overexpression in ECs have 70% fewer endocardial protrusions at 48 hpf (Figure 10B-D), whereas the distribution of endocardial protrusions remains unaltered (Figure 10E-E'). At 72 hpf, larvae with *irsp53^{dn}* overexpression in ECs show a deficiency of myocardial trabeculation (Figure 11) and CM proliferation (Figure 12) in the ventricle. Taken together, these data show that endocardial protrusions are required for myocardial trabeculation and CM proliferation.

7.2.2.3 Apelin signaling regulates endocardial protrusion formation and myocardial trabeculation

It has been reported that Apelin signaling promotes the formation of endothelial protrusion during angiogenesis in zebrafish (Helker et al., 2020). To uncover the role of Apelin signaling in endocardial protrusion formation, I first studied the expression of *apln* and *aplnrb* and discovered that *apln* is expressed in the myocardium and *aplnrb* is expressed in the endocardium at 48 and 72 hpf (Figure 13).

Next, I studied the *aplnra* mutant (Helker et al., 2015), *aplnrb* mutant (Helker et al., 2015), and *apln* mutant (Helker et al., 2015). Since the *apela* mutants are unable to form a heart (Chng et al., 2013), I did not analyze them. Only a small number of

aplnrb mutants are able to form a heart, I analyzed them and found that they exhibit fewer number of endocardial protrusions at 48 hpf (Figure 14A and B) and reduced trabeculation at 72 hpf (Figure 14C and D). Besides, the *aplnrb* mutants display thicker CJ in the outer curvature of the ventricle compared with their wild-type siblings (Figure 14C and D). In addition, *aplnra* mutants exhibit a reduction of trabeculation at 72 hpf as well (Figure 14E and F).

I then focused on studying the *apln* mutant, because most of the *apln* mutants form a normal-looking heart and the cardiac function is not impaired (Figure 17). *apln* mutants exhibit a significant reduction of endocardial protrusion formation at 24 and 48 hpf (Figure 15A-F) and endocardial touchdowns at 48 hpf (Figure 15D, E, and G). Furthermore, I analyzed the *apln* mutant at 72 hpf and observed similar cardiac trabeculation and CM proliferation defects as I observed in larvae with overexpressing *irsp53*^{dn} in ECs. Taken together, all these data suggest that loss of endocardial protrusions leads to myocardial trabeculation defects and is not the secondary effect of heart dysfunction.

7.2.2.4 Notch signaling negatively regulates endocardial protrusion formation

Many reports have shown that Notch signaling negatively moderates the formation of endothelial protrusions (Hellstrom et al., 2007; Leslie et al., 2007; Siekmann & Lawson, 2007; Suchting et al., 2007). I am interested to know if Notch signaling also moderates the formation of endocardial protrusion, so I used the γ–secretase inhibitor RO4929097 to inhibit Notch signaling in zebrafish embryos and discovered decreased expression of Notch signaling in the endocardium (Figure 18A and B). Furthermore, the number of ventricular endocardial protrusions is increased in embryos treated with Notch inhibitor (Figure 18C, D, and G). Altogether, these data show that Notch signaling mediates the endocardial protrusion formation in a negative manner.

7.2.2.5 Endocardial protrusions orchestrate myocardial trabeculation via Nrg/ErbB/Erk signaling

Next, I wanted to find out the underlying mechanisms. Nrg/ErbB is one of the most important signaling pathways during cardiac trabeculation. As mentioned previously (section **1.2.5**), *nrg2a* is required for cardiac trabeculation. I first overexpressed *nrg2a* in the endothelium and observed hypertrabeculation as well as multilayered CMs in the ventricle (Figure 19A and B, 19G-I). Then I overexpressed *nrg2a* in the endothelium while blocking the formation of endocardial protrusion and observed fewer trabeculae as well as fewer multilayered CMs compared with control group (Figure 19E-I).

Since Erk is an important molecule in Nrg/ErbB signaling, I decided to study myocardial Erk activity using an Erk reporter line. First, I tested the functionality of the Erk reporter by treating the embryos of the Erk reporter with an MEK inhibitor and observing an increased number of ventricular CMs with inactive Erk activity (Figure 21). These data indicate the reporter functions. When the Erk reporter embryos were treated with an ErbB inhibitor, there are more ventricular CMs with inactive Erk activity (Figure 22B). This observation indicates that Erk is downstream of Nrg/ErbB signaling pathway. To explore whether endocardial protrusions are required for myocardial Erk signaling activity, I blocked the formation of endocardial protrusions and found more CMs in the ventricle exhibit inactive Erk activity compared with controls (Figure 22A, and C-E). Taken together, these findings suggest that endocardial protrusions modulate myocardial trabeculation via Nrg/ErbB/Erk signaling in CMs.

7.2.3 Conclusion

In this study, I used the genetic loss of function method to block the formation of endocardial protrusion and discovered that endocardial protrusions are required for

cardiac trabeculation, and that the formation of endocardial protrusion depends on Apelin signaling. Mechanistically, I showed that the contribution of *nrg2a* and Erk activity are compromised during cardiac trabeculation when the formation of endocardial protrusion is blocked. These data indicate that endocardial protrusions promote cardiac trabeculation through Nrg/ErbB/Erk signaling.

8 References

Alastalo, T. P., Li, M., Perez Vde, J., Pham, D., Sawada, H., Wang, J. K., Koskenvuo, M., Wang, L., Freeman, B. A., Chang, H. Y., & Rabinovitch, M. (2011). Disruption of PPARgamma/beta-catenin-mediated regulation of apelin impairs BMP-induced mouse and human pulmonary arterial EC survival. *J Clin Invest*, *121*(9), 3735–3746. https://doi.org/10.1172/JCI43382

Britto, J. M., Lukehurst, S., Weller, R., Fraser, C., Qiu, Y., Hertzog, P., & Busfield, S. J. (2004). Generation and characterization of neuregulin-2-deficient mice. *Mol Cell Biol*, *24*(18), 8221–8226. https://doi.org/10.1128/MCB.24.18.8221-8226.2004

Brown, D. R., Samsa, L. A., Qian, L., & Liu, J. D. (2016). Advances in the Study of Heart Development and Disease Using Zebrafish. *Journal of Cardiovascular Development and Disease*, *3*(2). https://doi.org/ARTN 13 10.3390/jcdd3020013

Bussmann, J., & Schulte-Merker, S. (2011). Rapid BAC selection for tol2-mediated transgenesis in zebrafish. *Development*, *138*(19), 4327–4332. https://doi.org/10.1242/dev.068080

Chandra, S. M., Razavi, H., Kim, J., Agrawal, R., Kundu, R. K., de Jesus Perez, V., Zamanian, R. T., Quertermous, T., & Chun, H. J. (2011). Disruption of the apelin-APJ system worsens hypoxia-induced pulmonary hypertension. *Arterioscler Thromb Vasc Biol*, *31*(4), 814–820. https://doi.org/10.1161/ATVBAHA.110.219980

Charo, D. N., Ho, M., Fajardo, G., Kawana, M., Kundu, R. K., Sheikh, A. Y., Finsterbach, T. P., Leeper, N. J., Ernst, K. v, Chen, M. M., Ho, Y. D., Chun, H. J., Bernstein, D., Ashley, E. A., & Quertermous, T. (2009). Endogenous regulation of cardiovascular function by apelin-APJ. *Am J Physiol Heart Circ Physiol*, *297*(5), H1904-13. https://doi.org/10.1152/ajpheart.00686.2009

Chi, N. C., Shaw, R. M., de Val, S., Kang, G., Jan, L. Y., Black, B. L., & Stainier, D. Y. (2008). Foxn4 directly regulates tbx2b expression and atrioventricular canal formation. *Genes Dev*, *22*(6), 734–739. https://doi.org/10.1101/gad.1629408

Chng, S. C., Ho, L., Tian, J., & Reversade, B. (2013). ELABELA: a hormone essential for heart development signals via the apelin receptor. *Dev Cell*, *27*(6), 672–680. https://doi.org/10.1016/j.devcel.2013.11.002

Chun, H. J., Ali, Z. A., Kojima, Y., Kundu, R. K., Sheikh, A. Y., Agrawal, R., Zheng, L., Leeper, N. J., Pearl, N. E., Patterson, A. J., Anderson, J. P., Tsao, P. S., Lenardo, M. J., Ashley, E. A., & Quertermous, T. (2008). Apelin signaling antagonizes Ang II effects in mouse models of atherosclerosis. *J Clin Invest*, *118*(10), 3343–3354. https://doi.org/10.1172/JCI34871

Claudia, S., & Josef, F. (2004). Left ventricular hypertrabeculation/noncompaction. *Journal of the American Society of Echocardiography*, *17*, 91–100.

Cox, C. M., D'Agostino, S. L., Miller, M. K., Heimark, R. L., & Krieg, P. A. (2006). Apelin, the ligand for the endothelial G-protein-coupled receptor, APJ, is a potent angiogenic factor required for normal vascular development of the frog embryo. *Developmental Biology*, *296*(1), 177–189. https://doi.org/10.1016/j.ydbio.2006.04.452

D'Amato, G., Luxan, G., del Monte-Nieto, G., Martinez-Poveda, B., Torroja, C., Walter, W., Bochter, M. S., Benedito, R., Cole, S., Martinez, F., Hadjantonakis, A. K., Uemura, A., Jimenez-Borreguero, L. J., & de la Pompa, J. L. (2016). Sequential Notch activation regulates ventricular chamber development. *Nat Cell Biol*, *18*(1), 7–20. https://doi.org/10.1038/ncb3280

D'Amico, L., Scott, I. C., Jungblut, B., & Stainier, D. Y. (2007). A mutation in zebrafish hmgcr1b reveals a role for isoprenoids in vertebrate heart-tube formation. *Curr Biol*, *17*(3), 252–259. https://doi.org/10.1016/j.cub.2006.12.023

de la Cova, C., Townley, R., Regot, S., & Greenwald, I. (2017). A Real-Time Biosensor for ERK Activity Reveals Signaling Dynamics during C. elegans Cell Fate Specification. *Dev Cell*, *42*(5), 542-553 e4. https://doi.org/10.1016/j.devcel.2017.07.014

del Monte-Nieto, G., Ramialison, M., Adam, A. A. S., Wu, B., Aharonov, A., D'Uva, G., Bourke, L. M., Pitulescu, M. E., Chen, H., de la Pompa, J. L., Shou, W., Adams, R. H., Harten, S. K., Tzahor, E., Zhou, B., & Harvey, R. P. (2018). Control of cardiac jelly dynamics by NOTCH1 and NRG1 defines the building plan for trabeculation. *Nature*, *557*(7705), 439–445. https://doi.org/10.1038/s41586-018-0110-6

del Toro, R., Prahst, C., Mathivet, T., Siegfried, G., Kaminker, J. S., Larrivee, B., Breant, C., Duarte, A., Takakura, N., Fukamizu, A., Penninger, J., & Eichmann, A. (2010). Identification and functional analysis of endothelial tip cell-enriched genes. *Blood*, *116*(19), 4025–4033. https://doi.org/10.1182/blood-2010-02-270819

Epstein, J. A., Aghajanian, H., & Singh, M. K. (2015). Semaphorin Signaling in Cardiovascular Development. *Cell Metabolism*, *21*(2), 163–173. https://doi.org/10.1016/j.cmet.2014.12.015

Fierro-Gonzalez, J. C., White, M. D., Silva, J. C., & Plachta, N. (2013). Cadherin-dependent filopodia control preimplantation embryo compaction. *Nat Cell Biol*, *15*(12), 1424–1433. https://doi.org/10.1038/ncb2875

Gassmann, M., Casagranda, F., Orioli, D., Simon, H., Lai, C., Klein, R., & Lemke, G. (1995). Aberrant neural and cardiac development in mice lacking the ErbB4 neuregulin receptor. *Nature*, *378*(6555), 390–394. https://doi.org/10.1038/378390a0

Gerhardt, H., Golding, M., Fruttiger, M., Ruhrberg, C., Lundkvist, A., Abramsson, A., Jeltsch, M., Mitchell, C., Alitalo, K., Shima, D., & Betsholtz, C. (2003). VEGF guides angiogenic sprouting utilizing endothelial tip cell filopodia. *The Journal of Cell Biology*, *161*(6), 1163–1177. https://doi.org/10.1083/JCB.200302047

Goetze, J. P., Rehfeld, J. F., Carlsen, J., Videbaek, R., Andersen, C. B., Boesgaard, S., & Friis-Hansen, L. (2006). Apelin: a new plasma marker of cardiopulmonary disease. *Regul Pept*, *133*(1–3), 134–138. https://doi.org/10.1016/j.regpep.2005.09.032

GrausPorta, D., Beerli, R. R., Daly, J. M., & Hynes, N. E. (1997). ErbB-2, the preferred heterodimerization partner of all ErbB receptors, is a mediator of lateral signaling. *Embo Journal*, *16*(7), 1647–1655. https://doi.org/DOI 10.1093/emboj/16.7.1647

Grego-Bessa, J., Luna-Zurita, L., del Monte, G., Bolos, V., Melgar, P., Arandilla, A., Garratt, A. N., Zang, H., Mukouyama, Y. S., Chen, H. Y., Shou, W. N., Ballestar, E., Esteller, M., Rojas, A., Perez-Pomares, J. M., & de la Pompa, J. L. (2007). Notch signaling is essential for ventricular chamber development. *Developmental Cell*, *12*(3), 415–429. https://doi.org/10.1016/j.devcel.2006.12.011

Guerra, A., Germano, R. F., Stone, O., Arnaout, R., Guenther, S., Ahuja, S., Uribe, V., Vanhollebeke, B., Stainier, D. Y., & Reischauer, S. (2018). Distinct myocardial lineages break atrial symmetry during cardiogenesis in zebrafish. *Elife*, *7*. https://doi.org/10.7554/eLife.32833

Han, P., Bloomekatz, J., Ren, J., Zhang, R., Grinstein, J. D., Zhao, L., Burns, C. G., Burns, C. E., Anderson, R. M., & Chi, N. C. (2016). Coordinating cardiomyocyte interactions to direct ventricular chamber morphogenesis. *Nature*, *534*(7609), 700–704. https://doi.org/10.1038/NATURE18310

Hashimoto, T., Kihara, M., Imai, N., Yoshida, S., Shimoyamada, H., Yasuzaki, H., Ishida, J., Toya, Y., Kiuchi, Y., Hirawa, N., Tamura, K., Yazawa, T., Kitamura, H., Fukamizu, A., & Umemura, S. (2007). Requirement of apelin-apelin receptor system for oxidative stress-linked atherosclerosis. *Am J Pathol*, *171*(5), 1705–1712. https://doi.org/10.2353/ajpath.2007.070471

Helker, C. S., Eberlein, J., Wilhelm, K., Sugino, T., Malchow, J., Schuermann, A., Baumeister, S., Kwon, H. B., Maischein, H. M., Potente, M., Herzog, W., & Stainier, D. Y. (2020). Apelin signaling drives vascular endothelial cells toward a pro-angiogenic state. *Elife*, *9*. https://doi.org/10.7554/eLife.55589

Helker, C. S., Schuermann, A., Karpanen, T., Zeuschner, D., Belting, H. G., Affolter, M., Schulte-Merker, S., & Herzog, W. (2013). The zebrafish common cardinal veins develop by a novel mechanism: lumen ensheathment. *Development*, *140*(13), 2776–2786. https://doi.org/10.1242/dev.091876

Helker, C. S., Schuermann, A., Pollmann, C., Chng, S. C., Kiefer, F., Reversade, B., & Herzog, W. (2015). The hormonal peptide Elabela guides angioblasts to the midline during vasculogenesis. *Elife*, *4*. https://doi.org/10.7554/eLife.06726

Hellstrom, M., Phng, L. K., Hofmann, J. J., Wallgard, E., Coultas, L., Lindblom, P., Alva, J., Nilsson, A. K., Karlsson, L., Gaiano, N., Yoon, K., Rossant, J., Iruela-Arispe, M. L., Kalen, M., Gerhardt, H., & Betsholtz, C. (2007). Dll4 signalling through Notch1 regulates formation of tip cells during angiogenesis. *Nature*, *445*(7129), 776–780. https://doi.org/10.1038/nature05571

Ho, L., van Dijk, M., Chye, S. T. J., Messerschmidt, D. M., Chng, S. C., Ong, S., Yi, L. K., Boussata, S., Goh, G. H., Afink, G. B., Lim, C. Y., Dunn, N. R., Solter, D., Knowles, B. B., & Reversade, B. (2017). ELABELA deficiency promotes preeclampsia and cardiovascular malformations in mice. *Science*, *357*(6352), 707–713. https://doi.org/10.1126/science.aam6607

Huang, H., Liu, S. M., & Kornberg, T. B. (2019). Glutamate signaling at cytoneme synapses. *Science*, *363*(6430), 948-+. https://doi.org/10.1126/science.aat5053

Inui, M., Fukui, A., Ito, Y., & Asashima, M. (2006). Xapelin and Xmsr are required for cardiovascular development in Xenopus laevis. *Dev Biol*, *298*(1), 188–200. https://doi.org/10.1016/j.ydbio.2006.06.028

Jenni, R., Rojas, J., & Oechslin, E. (1999). *Isolated Noncompaction of the Myocardium*. https://doi.org/10.1056/NEJM199903253401215

Jimenez-Amilburu, V., Rasouli, S. J., Staudt, D. W., Nakajima, H., Chiba, A., Mochizuki, N., & Stainier, D. Y. R. (2016). In Vivo Visualization of Cardiomyocyte Apicobasal Polarity Reveals Epithelial to Mesenchymal-like Transition during Cardiac Trabeculation. *Cell Reports*, *17*(10), 2687–2699. https://doi.org/10.1016/j.celrep.2016.11.023

Kalin, R. E., Kretz, M. P., Meyer, A. M., Kispert, A., Heppner, F. L., & Brandli, A. W. (2007). Paracrine and autocrine mechanisms of apelin signaling govern embryonic and tumor angiogenesis. *Dev Biol*, *305*(2), 599–614. https://doi.org/10.1016/j.ydbio.2007.03.004

Kamezaki, A., Sato, F., Aoki, K., Asakawa, K., Kawakami, K., Matsuzaki, F., & Sehara-Fujisawa, A. (2016). Visualization of Neuregulin 1 ectodomain shedding reveals its local processing in vitro and in vivo. *Scientific Reports*, *6*. https://doi.org/10.1038/SREP28873

Kidoya, H., Kunii, N., Naito, H., Muramatsu, F., Okamoto, Y., Nakayama, T., & Takakura, N. (2012). The apelin/APJ system induces maturation of the tumor vasculature and improves the efficiency of immune therapy. *Oncogene*, *31*(27), 3254–3264. https://doi.org/10.1038/onc.2011.489

Kimmel, C. B., Ballard, W. W., Kimmel, S. R., Ullmann, B., & Schilling, T. F. (1995). Stages of embryonic development of the zebrafish. *Dev Dyn*, *203*(3), 253–310. https://doi.org/10.1002/aja.1002030302

Kojima, Y., Kundu, R. K., Cox, C. M., Leeper, N. J., Anderson, J. A., Chun, H. J., Ali, Z. A., Ashley, E. A., Krieg, P. A., & Quertermous, T. (2010). Upregulation of the apelin-APJ pathway promotes neointima formation in the carotid ligation model in mouse. *Cardiovasc Res*, *87*(1), 156–165. https://doi.org/10.1093/cvr/cvq052

Krugmann, S., Jordens, I., Gevaert, K., Driessens, M., Vandekerckhove, J., & Hall, A. (2001). Cdc42 induces filopodia by promoting the formation of an IRSp53:Mena complex. *Curr Biol*, *11*(21), 1645–1655. https://doi.org/10.1016/s0960-9822(01)00506-1

Lai, D., Liu, X. F., Forrai, A., Wolstein, O., Michalicek, J., Ahmed, I., Garratt, A. N., Birchmeier, C., Zhou, M., Hartley, L., Robb, L., Feneley, M. P., Fatkin, D., & Harvey, R. P. (2010). Neuregulin 1 Sustains the Gene Regulatory Network in Both Trabecular and Nontrabecular Myocardium. *Circulation Research*, *107*(6), 715-U74. https://doi.org/10.1161/Circresaha.110.218693

Lee, K. F., Simon, H., Chen, H., Bates, B., Hung, M. C., & Hauser, C. (1995). Requirement for neuregulin receptor erbB2 in neural and cardiac development. *Nature*, *378*(6555), 394–398. https://doi.org/10.1038/378394a0

Leslie, J. D., Ariza-McNaughton, L., Bermange, A. L., McAdow, R., Johnson, S. L., & Lewis, J. (2007). Endothelial signalling by the Notch ligand Delta-like 4 restricts angiogenesis. *Development*, *134*(5), 839–844. https://doi.org/10.1242/dev.003244

Lim, K. B., Bu, W. Y., Goh, W. I., Koh, E., Ong, S. H., Pawson, T., Sudhaharan, T., & Ahmed, S. (2008). The Cdc42 effector IRSp53 generates filopodia by coupling membrane protrusion with actin dynamics. *Journal of Biological Chemistry*, *283*(29), 20454–20472. https://doi.org/10.1074/jbc.M710185200

Lin, Y. F., Swinburne, I., & Yelon, D. (2012). Multiple influences of blood flow on cardiomyocyte hypertrophy in the embryonic zebrafish heart. *Dev Biol*, *362*(2), 242–253. https://doi.org/10.1016/j.ydbio.2011.12.005

Liu, J., Bressan, M., Hassel, D., Huisken, J., Staudt, D., Kikuchi, K., Poss, K. D., Mikawa, T., & Stainier, D. Y. (2010). A dual role for ErbB2 signaling in cardiac trabeculation. *Development*, *137*(22), 3867–3875. https://doi.org/10.1242/dev.053736

Meyen, D., Tarbashevich, K., Banisch, T. U., Wittwer, C., Reichman-Fried, M., Maugis, B., Grimaldi, C., Messerschmidt, E. M., & Raz, E. (2015). Dynamic filopodia are required for chemokine-dependent intracellular polarization during guided cell migration in vivo. *ELife*, *4*(4), 1–25. https://doi.org/10.7554/ELIFE.05279

Meyer, D., & Birchmeier, C. (1995). Multiple essential functions of neuregulin in development. *Nature*, *378*(6555), 386–390. https://doi.org/10.1038/378386a0

Millard, T. H., Bompard, G., Heung, M. Y., Dafforn, T. R., Scott, D. J., Machesky, L. M., & Futterer, K. (2005). Structural basis of filopodia formation induced by the IRSp53/MIM homology domain of human IRSp53. *EMBO J*, *24*(2), 240–250. https://doi.org/10.1038/sj.emboj.7600535

Nakagawa, H., Miki, H., Nozumi, M., Takenawa, T., Miyamoto, S., Wehland, J., & Small, J. v. (2003). IRSp53 is colocalised with WAVE2 at the tips of protruding lamellipodia and filopodia independently of Mena. *Journal of Cell Science*, *116*(12), 2577–2583. https://doi.org/10.1242/jcs.00462

Nobes, C. D., & Hall, A. (1995). Rho, rac, and cdc42 GTPases regulate the assembly of multimolecular focal complexes associated with actin stress fibers, lamellipodia, and filopodia. *Cell*, *81*(1), 53–62. https://doi.org/10.1016/0092-8674(95)90370-4

Odiete, O., Hill, M. F., & Sawyer, D. B. (2012). Neuregulin in cardiovascular development and disease. *Circ Res*, *111*(10), 1376–1385. https://doi.org/10.1161/CIRCRESAHA.112.267286

Oechslin, E. N., Attenhofer Jost, C. H., Rojas, J. R., Kaufmann, P. A., & Jenni, R. (2000a). Long-term follow-up of 34 adults with isolated left ventricular noncompaction: a distinct cardiomyopathy with poor prognosis. *J Am Coll Cardiol*, *36*(2), 493–500. https://doi.org/10.1016/s0735-1097(00)00755-5

Oechslin, E. N., Attenhofer Jost, C. H., Rojas, J. R., Kaufmann, P. A., & Jenni, R. (2000b). Long-term follow-up of 34 adults with isolated left ventricular noncompaction: a distinct cardiomyopathy with poor prognosis. *Journal of the American College of Cardiology*, *36*(2), 493–500. https://doi.org/10.1016/S0735-1097(00)00755-5

Parsons, M. J., Pisharath, H., Yusuff, S., Moore, J. C., Siekmann, A. F., Lawson, N., & Leach, S. D. (2009). Notch-responsive cells initiate the secondary transition in larval zebrafish pancreas. *Mech Dev*, *126*(10), 898–912. https://doi.org/10.1016/j.mod.2009.07.002

Pauli, A., Norris, M. L., Valen, E., Chew, G. L., Gagnon, J. A., Zimmerman, S., Mitchell, A., Ma, J., Dubrulle, J., Reyon, D., Tsai, S. Q., Joung, J. K., Saghatelian, A., & Schier, A. F. (2014). Toddler: An Embryonic Signal That Promotes Cell Movement via Apelin Receptors. *Science*, *343*(6172), 746-+. https://doi.org/ARTN 1248636 10.1126/science.1248636

Peshkovsky, C., Totong, R., & Yelon, D. (2011). Dependence of cardiac trabeculation on neuregulin signaling and blood flow in zebrafish. *Dev Dyn*, *240*(2), 446–456. https://doi.org/10.1002/dvdy.22526

Pitkin, S. L., Maguire, J. J., Kuc, R. E., & Davenport, A. P. (2010). Modulation of the apelin/APJ system in heart failure and atherosclerosis in man. *Br J Pharmacol*, *160*(7), 1785–1795. https://doi.org/10.1111/j.1476-5381.2010.00821.x

Priya, R., Allanki, S., Gentile, A., Mansingh, S., Uribe, V., Maischein, H. M., & Stainier, D. Y. R. (2020). Tension heterogeneity directs form and fate to pattern the myocardial wall. *Nature*, *588*(7836), 130–134. https://doi.org/10.1038/s41586-020-2946-9

Prols, F., Sagar, & Scaal, M. (2016). Signaling filopodia in vertebrate embryonic development. *Cell Mol Life Sci*, *73*(5), 961–974. https://doi.org/10.1007/s00018-015-2097-6

Qi, J., Rittershaus, A., Priya, R., Mansingh, S., Stainier, Y. R., & Sm Helker, C. (2022). Apelin signaling dependent endocardial protrusions promote cardiac trabeculation in zebrafish. *ELife*. https://doi.org/10.7554/eLife

Qu, X., Harmelink, C., & Baldwin, H. S. (2019). Tie2 regulates endocardial sprouting and myocardial trabeculation. *JCI Insight*, *5*. https://doi.org/10.1172/jci.insight.96002

Ramirez-Weber, F. A., & Kornberg, T. B. (1999). Cytonemes: Cellular processes that project to the principal signaling center in Drosophila imaginal discs. *Cell*, *97*(5), 599–607. https://doi.org/Doi 10.1016/S0092-8674(00)80771-0

Rasouli, S. J., & Stainier, D. Y. R. (2017). Regulation of cardiomyocyte behavior in zebrafish trabeculation by Neuregulin 2a signaling. *Nature Communications*, *8*. https://doi.org/10.1038/ncomms15281

Roy, S., Hsiung, F., & Kornberg, T. B. (2011). Specificity of Drosophila cytonemes for distinct signaling pathways. *Science*, *332*(6027), 354–358. https://doi.org/10.1126/science.1198949

Roy, S., Huang, H., Liu, S., & Kornberg, T. B. (2014). Cytoneme-mediated contact-dependent transport of the Drosophila decapentaplegic signaling protein. *Science*, *343*(6173), 1244624. https://doi.org/10.1126/science.1244624

Sagar, Prols, F., Wiegreffe, C., & Scaal, M. (2015). Communication between distant epithelial cells by filopodia-like protrusions during embryonic development. *Development*, *142*(4), 665–671. https://doi.org/10.1242/dev.115964

Saint-Geniez, M., Masri, B., Malecaze, F., Knibiehler, B., & Audigier, Y. (2002). Expression of the murine msr/apj receptor and its ligand apelin is upregulated during formation of the retinal vessels. *Mechanisms of Development*, *110*(1–2), 183–186. https://doi.org/Doi 10.1016/S0925-4773(01)00558-5

Samsa, L. A., Ito, C. E., Brown, D. R., Qian, L., & Liu, J. (2016). IgG-Containing Isoforms of Neuregulin-1 Are Dispensable for Cardiac Trabeculation in Zebrafish. *Plos One*, *11*(11), e0166734. https://doi.org/10.1371/journal.pone.0166734

Sanders, T. A., Llagostera, E., & Barna, M. (2013). Specialized filopodia direct long-range transport of SHH during vertebrate tissue patterning. *Nature*, *497*(7451), 628–632. https://doi.org/10.1038/nature12157

Sandireddy, R., Cibi, D. M., Gupta, P., Singh, A., Tee, N., Uemura, A., Epstein, J. A., & Singh, M. K. (2019). Semaphorin 3E/PlexinD1 signaling is required for cardiac ventricular compaction. *JCI Insight*, *4*(16). https://doi.org/ARTN e125908 10.1172/jci.insight.125908

Scimia, M. C., Hurtado, C., Ray, S., Metzler, S., Wei, K., Wang, J. M., Woods, C. E., Purcell, N. H., Catalucci, D., Akasaka, T., Bueno, O. F., Vlasuk, G. P., Kaliman, P., Bodmer, R., Smith, L. H., Ashley, E., Mercola, M., Brown, J. H., & Ruiz-Lozano, P. (2012). APJ acts as a dual receptor in cardiac hypertrophy. *Nature*, *488*(7411), 394–398. https://doi.org/10.1038/nature11263

Scita, G., Confalonieri, S., Lappalainen, P., & Suetsugu, S. (2008). IRSp53: crossing the road of membrane and actin dynamics in the formation of membrane protrusions. *Trends Cell Biol*, *18*(2), 52–60. https://doi.org/10.1016/j.tcb.2007.12.002

Scott, I. C., Masri, B., D'Amico, L. A., Jin, S. W., Jungblut, B., Wehman, A. M., Baier, H., Audigier, Y., & Stainier, D. Y. (2007). The g protein-coupled receptor agtrl1b regulates early development of myocardial progenitors. *Dev Cell*, *12*(3), 403–413. https://doi.org/10.1016/j.devcel.2007.01.012

Siekmann, A. F., & Lawson, N. D. (2007). Notch signalling limits angiogenic cell behaviour in developing zebrafish arteries. *Nature*, *445*(7129), 781–784. https://doi.org/10.1038/nature05577

Stanganello, E., Hagemann, A. I., Mattes, B., Sinner, C., Meyen, D., Weber, S., Schug, A., Raz, E., & Scholpp, S. (2015). Filopodia-based Wnt transport during vertebrate tissue patterning. *Nature Communications*, *6*, 5846. https://doi.org/10.1038/ncomms6846

Staudt, D. W., Liu, J., Thorn, K. S., Stuurman, N., Liebling, M., & Stainier, D. Y. (2014). High-resolution imaging of cardiomyocyte behavior reveals two distinct steps in ventricular trabeculation. *Development*, *141*(3), 585–593. https://doi.org/10.1242/dev.098632

Suchting, S., Freitas, C., le Noble, F., Benedito, R., Breant, C., Duarte, A., & Eichmann, A. (2007). The Notch ligand Delta-like 4 negatively regulates endothelial tip cell

formation and vessel branching. *Proc Natl Acad Sci U S A*, *104*(9), 3225–3230. https://doi.org/10.1073/pnas.0611177104

Suri, C., Jones, P. F., Patan, S., Bartunkova, S., Maisonpierre, P. C., Davis, S., Sato, T. N., & Yancopoulos, G. D. (1996). Requisite role of angiopoietin-1, a ligand for the TIE2 receptor, during embryonic angiogenesis. *Cell*, *87*(7), 1171–1180. https://doi.org/10.1016/s0092-8674(00)81813-9

Tachibana, K., Jones, N., Dumont, D. J., Puri, M. C., & Bernstein, A. (2005). Selective role of a distinct tyrosine residue on Tie2 in heart development and early hematopoiesis. *Mol Cell Biol*, *25*(11), 4693–4702. https://doi.org/10.1128/MCB.25.11.4693-4702.2005

Tatemoto, K., Hosoya, M., Habata, Y., Fujii, R., Kakegawa, T., Zou, M. X., Kawamata, Y., Fukusumi, S., Hinuma, S., Kitada, C., Kurokawa, T., Onda, H., & Fujino, M. (1998). Isolation and characterization of a novel endogenous peptide ligand for the human APJ receptor. *Biochem Biophys Res Commun*, *251*(2), 471–476. https://doi.org/10.1006/bbrc.1998.9489

Uribe, V., Ramadass, R., Dogra, D., Rasouli, S. J., Gunawan, F., Nakajima, H., Chiba, A., Reischauer, S., Mochizuki, N., & Stainier, D. Y. R. (2018). In vivo analysis of cardiomyocyte proliferation during trabeculation. *Development*, *145*(14). https://doi.org/10.1242/dev.164194

Uribesalgo, I., Hoffmann, D., Zhang, Y., Kavirayani, A., Lazovic, J., Berta, J., Novatchkova, M., Pai, T. P., Wimmer, R. A., Laszlo, V., Schramek, D., Karim, R., Tortola, L., Deswal, S., Haas, L., Zuber, J., Szucs, M., Kuba, K., Dome, B., … Penninger, J. M. (2019). Apelin inhibition prevents resistance and metastasis associated with anti-angiogenic therapy. *EMBO Mol Med*, *11*(8), e9266. https://doi.org/10.15252/emmm.201809266

Wee, P., & Wang, Z. (2017). *cancers Epidermal Growth Factor Receptor Cell Proliferation Signaling Pathways*. https://doi.org/10.3390/cancers9050052

Yamagishi, A., Masuda, M., Ohki, T., Onishi, H., & Mochizuki, N. (2004). A novel actin bundling/filopodium-forming domain conserved in insulin receptor tyrosine kinase substrate p53 and missing in metastasis protein. *J Biol Chem*, *279*(15), 14929–14936. https://doi.org/10.1074/jbc.M309408200

Zeng, X. X., Wilm, T. P., Sepich, D. S., & Solnica-Krezel, L. (2007). Apelin and its receptor control heart field formation during zebrafish gastrulation. *Dev Cell*, *12*(3), 391–402. https://doi.org/10.1016/j.devcel.2007.01.011

Zhao, H., Tian, X., He, L., Li, Y., Pu, W., Liu, Q., Tang, J., Wu, J., Cheng, X., Liu, Y., Zhou, Q., Tan, Z., Bai, F., Xu, F., Smart, N., & Zhou, B. (2018). Apj(+) Vessels Drive Tumor Growth and Represent a Tractable Therapeutic Target. *Cell Reports*, *25*(5), 1241-1254 e5. https://doi.org/10.1016/j.celrep.2018.10.015